Use of Nanoparticles and Tunable Resistive Pulse Sensing Technology for Biosensing and Nanoflowers for Transfection

YANG, Kar Lai Alice

A Thesis Submitted in Partial Fulfillment

of the Requirements for the Degree of

Doctor of Philosophy

in

Biochemistry

The Chinese University of Hong Kong

September 2013

Thesis/Assessment Committee

Professor KWAN, Yiu Wa (Chair)

Professor KONG, Siu Kai (Thesis Supervisor)

Professor HO, Ho Pui (Committee Member)

Professor MAK, Nai-ki (External Examiner)

Publications List

Papers included in the thesis

This thesis is based on the following papers, which are referred to in the text by their roman numerals.

I **Yang, A.K.L.**; Kwan, P.; Ho, H.P.; Wu, S.Y.; Kong, S.K. (2013). SYBR Green I inhibits DNA Amplification of the MRSA Panton-Valentine Leukocidin toxin by LAMP (Loop-mediated Isothermal DNA Amplification). *Journal of Biochemistry and Molecular Biology in the post genomic era, (in press)*

II **Yang, A.K.L.**; Lu, H.; Wu, S.Y.; Kwok, H.C.; Ho, H.P.; Yu, S.; Cheung, A.K.L.; Kong, S.K. (2013). Detection of Panton-Valentine Leukocidin DNA from Methicillin-Resistant *Staphylococcus aureus* by Resistive Pulse Sensing and Loop-mediated Isothermal Amplification (LAMP) with Gold Nanoparticles. *Analytic Chimica Acta*, 782(11), 46-53.

III Cheung, A.K.L.; **Yang, A.K.L.**; Yu, S.; Gao, M.; Lau, P.M.; Kong, S.K. Quantitative Tunable Resistive Pulse Sensing Assay for Human Erythrocytes Toxicity Study. *Submitted to Biosensor and Bioelectronics.*

Acknowledgements

I would like to express my sincere gratitude to my supervisor, Professor Kong Siu Kai, for his patient guidance, advice, constant encouragement and care throughout the period of my final year project and PhD. study.

I would like to thank Professor Ho Ho Pui, Professor Kwan Yiu Wa and Professor Mak Nai Ki as my thesis committee. I would like to thank Dr. S.Y. Wu, Dr. H.F. Lu, Dr. Q.L. Chen, Dr. G.H. Wang and Mr. H.C. Kwok from Prof. Ho's group, who give me a lot of technical help. Also, I would like to thank my dearest labmates and colleagues from BMSB 514 and MMW 610, especially Ms. Irene Lau, Mr. Anthony Cheung, Ms. Jennifer Gao and Ms. Choi Pui Wah for their support and care.

Thanks for all my friends from BCH and SBS. Thank you Dr. Sam Yu from the Izon Science Ltd., who provides a lot for support in my research project and teaching me how to handle the qNano machine.

Last but not least, I would like to thank my mom for her love and care throughout my life.

Abstract

Infection with pathogens such as influenza virus or methicillin-resistant *Staphylococcus aureus* (MRSA) is a threat of public heath and economic burden. Thus, it is an urgent matter to develop a fast yet simple detection method with high sensitivity and selectivity for disease diagnosis. Loop-mediated isothermal amplification (LAMP) is a powerful technique without using thermal cycles to amplify target DNA from pathogens. LAMP is a highly sensitive and rapid detection method working at one temperature at 60 - 65 ^{0}C. With appropriate primers, target genes can be amplified by LAMP within 30 minutes. The specificity of LAMP is very high since four primers are utilized to amplify one DNA template. Another advantage is that LAMP can also be used to measure cDNA or RNA quantitatively, similar to that of the real-time PCR (qPCR).

Nowadays, SYBR Green I (SGI) is a commonly used DNA binding probe to report qPCR signals. According to work from Gudnason et al (2007)., SGI has effect in increasing the Ct value in qPCR in a dose dependent manner. However, due to the short history of LAMP, no or not too many studies using SGI for real-time LAMP (RT-LAMP) is available in the literature. In the first part of this thesis, the inhibitory effect of SGI and another DNA binding dye, SYTO-9 (ST9) on RT-LAMP for the detection of the panton-valentine leukocidin (*PVL*) gene of MRSA was confirmed. According to the RT-LAMP results, SGI blocked the *PVL* DNA amplification by

LAMP in a dose-dependent manner. Also, this inhibition was confirmed using the RT-PCR tools, the amplification efficiency and threshold cycle value, for the analysis. On the contrary, ST9 showed less inhibitory effect on LAMP when similar concentration was used. Results from our study indicated that ST9 is more compatible with the RT-LAMP for fast and sensitive biosensing if fluorescence-based system is the only choice.

To avoid this negative effect, we tried to combined LAMP and gold nanoparticles (AuNPs) for biosensing. Through funcationalization, DNA were conjugated to the AuNPs which acted as carriers or probes for biosensing. We reported here that AuNPs coated with DNA were used to detect the *PVL* gene by LAMP. After DNA amplification at single temperature (65 ^{0}C), the Lamplicons (amplicons from LAMP) were mixed with the DNA probes on the surface of AuNPs. As a result of DNA-DNA hybridization, AuNPs formed aggregations and the changes were measured by the tunable resistive pulse sensing (TRPS) technology. Using the TRPS technique, the agglomerated AuNPs were allowed to pass through a size-tunable fluidic nanopore to give blockade events which provided information of the size and dynamic of the agglomerated AuNPs. The TRPS technique was sensitive and could achieve a detection limited of 208 copies of MRSA templates and the detction could be completed within a short period of time (2 hours). Therefore, the LAMP-based AuNP TRSP is a sensitive yet simple platform for detecting different

kinds of antigens.

Nanoflowers (NF) are the flower-like structure with the core in the middle and branches extended. It is made of Fe3O4@SiO2@γ-AlOOH@Au, which is able to be attached with nucleic acids for gene transfer and delivery. We confirmed here the low cytotoxicity feature of the NFs by AlamarBlue assay in the huamn basophils (KU812 cells) and human embryonic kidney cells (HEK293T cells). NFs were functionalized with the pEGFP-N1 and pDsRed1-C1 vectors with the green fluorescent protein (GFP) or red fluorescent protein (RFP) gene, respectively, for transfection by incubating the KU812 cells or HEK293T cells with the functionalized NFs in culture medium at 37 ^{0}C for 48 hr. From the results of flow cytometry, the expression rate of GFR or RFP in the KU812 and HEK293T cells was found to be high, approximately 50 % and 78 % respectively. Our expreiments therefore indicated that NFs is a biocompatible nanomaterial which is safe and a good carrier of DNA transfection in human cell lines.

On the other hand, TRPS, originally used in the field of nanotechnology, was employed to determine cell death in human red blood cells (RBCs) for toxicity studies. The death process in the RBCs is called eryptosis which is characterized by the phosphatidylserine (PS) externalization, apoptotic body formation and cell shrinkage, akin to the features of the classical apoptosis. RBCs were treated with a potential anti-cancer agent polyphyllin D (PD) or the silver nanoparticles (AgNPs)

for 24 hr, followed by the cell death detection with the TRPS. With the externalization of PS on the cell surface, PS-binding probe Annexin V was used to detect the death in the RBCs. In this connection, magnetic beads were functionalized with Annexin V-RFP (Bead-Annexin V-RFP) and mixed with the PD- or AgNPs-treated RBCs. The Bead-Annexin V-RFP could conjugate with the dead RBCs and formed aggregates, which increased the volumnetric size and could be detected by the TRPS device. Results from confocal imaging also confirmed this change - formation of assemblies. The data in our study thus demonstrated that the TRPS technique was able to detect the number of assemblies of different size. After subtracted from the background populations, more and larger positive populations bigger than 85 fL were found in the PD (2.5 and 1.25 μM)-treated RBCs when compared with the negative control. The combination of the TRPS technique and modified beads can therefore be used as a good sensing tool for cell death analysis. Taken together, the work in this thesis shows a key how to integrate and refine different technologies to provide a good platform for biosensing and other biomedical applications.

論文摘要

在現今社會，傳染病是一個威脅公眾健康和引致醫療負擔的公共衞生問題。其中的表表者有流感病毒及耐甲氧西林金黃色葡萄球菌（MRSA）。因此，有迫切性去開發一種快速而簡單的檢測方法，以提高診斷傳染病的效率，選擇性及靈敏度。環介導等溫擴增（LAMP）是一個功能強大的去氧核醣核酸(DNA)擴增技術。有別於一般的聚合酶鏈鎖反應(PCR), LAMP 省卻了熱循環擴增步驟。LAMP 是一個高度敏感和快速檢測方法，其參與反應的酶的最適溫度是介乎 60 - 65 ^{0}C。利用四至六條引物，就可以在 30 分鐘內利用完成擴增，而且擁有極高的特異性。LAMP 亦有另一個優點，就是其適用於 cDNA 或 RNA 的檢測，而且與實時熒光定量 PCR（qPCR）的相似。

SYBR Green I（SGI）是一種常用的 DNA 結合染料，主要用於 qPCR。據居德納松等人的報告（2007 年），當 SGI 的濃度上升時, qPCR 的 Ct 值亦會上升。換而言之, SGI 對於 qPCR 是有抑制作用。然而，由於 LAMP 的歷史很短，現時並沒有太多研究文獻記錄利用 SGI 進行實時環介導等溫擴增（RT-LAMP）的數據。因此，在這篇論文中，我們會探討 SGI 在 RT-LAMP 的抑制作用。同時，另一種 DNA 結合染料, SYTO-9 (ST9）亦會使用。而在此研究中，我們會利用到 MRSA 的 *PVL* 基因作為示範。根據 RT-LAMP 的結果, SGI 會中止 *PVL* DNA 的擴增，而且抑制效用與濃度成正比關係。.另一方面，在使用與 SGI 相同濃度的 ST9 時，其中抑制效果明顯較 SGI 的低。 因此, ST9 會是比較合適的染料以發出熒光信號。

為了避免有如 SGI 的負面影響，我們試圖結合 LAMP 和黃金納米粒子（納米金）作生物傳感器。DNA 透過與納米金粒子的表面結合去修飾成為 DNA 探針。在經過 DNA 擴增後, Lamplicons（LAMP 擴增產物）可與納米金粒子上的 DNA 探針互補，出現 DNA-DNA 雜交。隨後，納米金粒子會凝聚成聚合物並可以透過可調電阻脈衝傳感技術（TRPS）進行測定。使用 TRPS 技術，凝聚的金納米粒子在通過一個可調納米孔膜時會阻斷電流，其大小和動態信息因此被紀錄。 根據我們的實驗數據，這個結合 TRPS, LAMP 及納米金的基因檢測技術是十分敏感，可以在兩小時內完成實現檢測，而其最低檢測限值為 208 對 MRSA *PVL* 模板。 因此，這個簡單的生物傳感器是具潛力去發展成為檢驗不同種抗原的檢測方法。

納米花（NF）是在花狀結構的納米粒子，其結構是透過四氧化三鐵@二氧化矽@γ-AlOOH 而組成有一個核心及其他延伸的分支。納米花能夠與核酸用以用作基因轉移和轉染。透過 AlamarBlue 檢測，我們發現納米花對人類嗜鹼性白細胞（KU812 細胞）及人胚腎細胞（HEK293T 細胞）的呈現低度的細胞毒性。同時，我們將納米花與 pEGFP-N1 及 pDsRed1-C1 質粒結合成質粒載體，並將其轉染至細胞中。利用流式細胞儀，我們檢測到 KU812 細胞及 HEK293T 細胞在轉染 48 小時後有很高的綠色熒光蛋白（GFP）或紅色熒光蛋白（RFP）基因表達，兩種細胞的蛋白表達率分別為 50 % 及 78 %。 因此，納米花是一種安全而具生物相容性的納米材料，可以在用作人類細胞 DNA 轉染的良好載體。

另一方面，TRPS 在納米技術領域之中，除了可以檢測納米粒子的大小及聚

合，亦可以用來確定人類紅血細胞(紅細胞)凋亡，以作毒性研究。紅細胞的死亡過程被稱為 eryptosis，其中的表現型與一般的細胞凋亡很相似，包括磷脂酰絲氨酸（PS）外化，凋亡小體的形成，以及細胞皺縮。皂苷 D（PD）是經研究文獻証實的一種潛在抗癌藥，紅細胞在加入 PD 或納米銀粒子的培養液中培養 24 小時後,呈現細胞死亡。在細胞表面外的 PS 可以與膜聯蛋白 V 這探針結合，從而可檢測出紅細胞的死亡。我們利用膜聯蛋白 V-RFP 去修飾磁性小珠，並混合經 PD 或納米銀粒子處理的紅細胞，令膜聯蛋白 V-RFP 磁性小珠與死亡中的紅細胞聚合，從而令紅細胞的容量增加。透過共軛焦顯微鏡，我們可以看紅細胞與磁性小珠結合並凝聚。 同時, TRPS 可以檢測到聚合物的大小及數量: 與陰性對照組作比較，紅細胞在 2.5 及 1.25 μM PD 處理後會有較多群組大於 85 fL。 總括而言，我們將 TRPS 技術及納米粒子作結合，從而整合出新的技術以完善現有的生物傳感器及應用於各項醫學診斷。

Table of Content

List of Figures

List of Tables

Abbreviations

^{0}C	Celsius degree
µg	Microgram
µL	Microliter
µM	Mircomolarity
mL	Milliliter
mm	Millimeter
mM	Millimolarity
mg	Milligram
Ag	Silver
Au	Gold
BSA	Bovine serum albumin
Bst	Bst DNA Polymerase
DNA	Deoxyribonucleic acid
DMED	Dulbecco's Modified Eagle Medium
dNTP	Deoxynucleic triphosphate
dsDNA	Double-stranded DNA
EDC	1-Ethyl-3-(3-dimethylaminopropyl) carbodiimide
Edx	Energy Dispersive X-Ray Analysis
fL	Femtoliter
FSC	Forward Scatter
GFP	Green Fluoresence Protein
Hb	Hemoglobin
HAD	Helicase-dependent Amplification
HEPES	N-[2-Hydroxyethl]piperazine-N'-[2-Ethanesulfonic Aicd]
hr	Hour
LAMP	Loop-mediated isothermal amplification
MRSA	Methicillin-Resistant *Staphylococcus aureus*
miRNA	Micro RNA
min	Minute
ms	Millisecond
nA	Nanoampere
ng	Nanogram
nm	Nanometer
nM	Nanomolarity
NAC	N-acetylcysteine
NF	Nanoflower
nm	Nanometer

NP	Nanoparticle
p	p-value
PBS	Phosphate buffered saline
PCR	Polymerase Chain Reaction
PD	Polyphyllin D
PS	Phosphatidylserine
PVL	Panton-Valentine Leukocidin toxin
q	Quantitative
qPCR	Real-time PCR/ quantitative PCR
RBC	Human erythrocyte
RCA	Rolling-circle Amplification
RFP	Red Fluoresence Protein
ROS	Reactive Oxygen Species
RPA	Recombinase Polymerase Amplification
rpm	Revolution Per Minute
RPMI	Roswell Park Memorial Institue Tissue Culture Medium
RPS	Resistive Pulse Sensing
RT	Real-time
RU	Response Unit
s	Second
SDA	Strand-displacement Amplifcation
SGI	SYBR Green I
SPR	Surface Plasmon Resonance
SSC	Side Scatter
ssDNA	Single-stranded DNA
ST9	SYTO-9
TBE	Tris-Borate-EDTA
TEM	Transmitted Eletron Microscopy
TRPS	Tunable Resistive Pulse Sensing
UV	Ultra Violet
v/v	Volume per volume
w/v	Weight per volume

Chapter 1 General Introduction

The objectives of this project tried to develop various techniques for biosensing. Nanomaterials and electrochemical sensors, Tunable Resistive Pulse Sensing (TRPS), were utilized for DNA sensing, in order to provide accurate, rapid and novel medical diagnosis biosensors. To extend the utility of TRPS, an alternative application of TRPS on cell biological study was investigated.

This thesis will be divided into four parts: Isothemal DNA amplification and its application on pathogen DNA detection (Chapter 2 & 3); Transfection of eukaryotic cells with nanomaterials carried plasmids (Chapter 4); and detection and analysis of death of human erythrocytes with electrochemical methods (Chapter 5).

In chapter 2, we focus on the discussion of the technique of real-time loop-mediated isothermal amplification (LAMP) on pathogens DNA detection [Yang et al., 2013], as described in Paper I. To date, people are threatening by different kinds of infectious diseases. The outbreaks of Avian influenza and Severe Acute Respiratory Syndrome (SARS) happened in this decade are lethal, which took only a few days to spread out the infections in the society. Hence, a fast and accurate confirmation of the types of pathogens may stop the infections. Molecular-based detection method is more accurate and time saving than the traditional pathogen culturing method. For example, it takes 21 days for culturing the *Mycobacterium*

tuberculosis for drug-resistance testing. In comparison, it takes only a few hours to do a quantitative polymerase chain reaction (qPCR) in checking the drug-resistance of the pathogen. The usage of molecular based detection method becomes more and more popular in the medical laboratories.

Methicillin-resistant *Staphylococcus aureus* (MRSA) is the pathogen being studied in this chapter. MRSA was reported in the first time in the UK in 1961, which was found in the long-term hospitalization individuals. Different from the hospital-associated MRSA (HA-MRSA), community-associated MRSA (CA-MRSA) infection cases are happened in the community, with different molecular characteristics, clinical presentation, risk of contact and infection, and the presence or absence of exotoxins [Center of health protection, 2007]. To compare with the HA-MRSA, CA-MRSA is more susceptible to different kinds of antibiotics. Many CA-MRSA isolates are resistant to beta-lactams, macrolides and azalides antibiotics. In Hong Kong, the first case of CA-MRSA was reported in 2004 [Ho et al., 2004]. The symptoms of the CA-MRSA infection are mainly found on the skin and soft tissues, associated with necrotizing pneumonia, empyema, sepsis syndrome, fever and others. According to the report from Centre of Health Protection (CHP) of Department of Health, HKSAR (2007), there were 112 notifications of CA-MRSA infection during 2005 to 2007, and two patients died. Eighty-two cases (73 %) were

found to have *Staphylococcal cassette* chromosome *mec* (SCC*mec*) type IV or V and the presence of Panton-Valentine leucocidin (*PVL*) gene. Due to the presence of toxin genes, microbiological characteristics, and drug-resistant genes, molecular based detection is suitable to distinguish the HA-MRSA from the CA-MRSA. Also, it can help us to trace the source of CA-MRSA infections. To monitoring the infection of MRSA, CHP encourages all the Hong Kong hospital microbiologists to report the cases, in order to have effective public health prevention and control measures. It has been shown that MRSA is one of the infectious diseases that Department of Health seriously concerns.

To shorten the time for diagnosis and obtaining more information on drug resistance, molecular based detection method, PCR or qPCR are widely used in clinical laboratories. In the past few decades, there are a number of amplification methods developed. These include the strand-displacement amplification (SDA), helicase-dependent amplification (HAD), rolling-circle amplification (RCA) or ramification amplification (RAM), and loop-mediated isothermal amplification (LAMP) etc. (Table 1.1) To compare with the traditional DNA amplification by the PCR, the isothermal amplification techniques have a major advantage that the reaction can be executed in a water bath at a single temperature without the need of thermo-cycling (Table 1.2). Also, the reaction can be finished within an hour, with

high sensitivity. For example, RCA allows amplification of the input circular DNA up to 10,000-fold [Detter et al., 2002]. LAMP is able to detect a few copies of template [Hill et al., 2008].

Due to the low cost and dramatic high scale of target gene amplifying ability, LAMP was chosen as the DNA amplification method for the real-time monitoring and novel biosensor development. In Chapter 2, we firstly demonstrated the real-time LAMP assay by using fluorescence reporter, such as SYBR Green I dye (SGI) and SYTO-9 dye (ST9), which were used to monitor the result of DNA amplification in a way similar to that of the qPCR [Yang et al., 2013]. Also, we discussed the fluorescence based RT-LAMP for the detection of the MRSA *PVL* target gene and the results were published [Yang et al., 2013].

Table 1.1 Comparison of different common isothermal amplification methods.

SDA: Strand-displacement Amplification; RCA: Rolling-circle Amplification; HDA: Helicase-dependent Amplification; RPA: Recombinase Polymerase Amplification

Method	Enzyme(s)	Efficiency *	Advantages	Disadvantages	Applications *
SDA	*Φ29* DNA polymerase; DNA polymerase I	Can amplify >10kb gDNA segment; Amplifies gDNA in several hours from ng, at RT	Strong proofreading; Accurate shotgun genome sequencing	Involve initial heating step to denature DNA and fluorescent-labeled probe binding in nicking-initiated SDA	Whole genome amplification (WGA)
LAMP	*Bst* DNA polymerase	Can amplify >200 bp DNA; detection limit as a few copies; Amplifies up to $>10^9$ X in 15-60 min	High specificity due to 4-6 primers for one single gene; Small amount input DNA provides large amount of loop-shape lamplicon; Not require special reagents and equipment → lower cost; Can be detected by nake-eye → convenient	High reaction temperature (65^0C), require heating system in point-of-care; Difficult to quantify; Difficult to study structure of lamplicon due to the cauliflower-like stem loop shape; Difficult for multiplex LAMP and multiplexing SNP	SNP detection by involving mismatching nucleotide on 5'-end of inner primer; Intergraded with detection system into a micro-fluidic chip
RCA	*Φ29* DNA polymerase	High, repeated copies of template amplification; Amplifies up to 10,000 X than input	Range of DNA size is board: form miRNA to 100kb; Smaller template size gives higher amplification efficiency and lower probability for strand breakdown; Flexible to couple with different detection module; High	Amplification of padlock probes is usually done by PCR;	Widely used for strictly required amplification condition; Small size genome, eg. Viruses, bacteriophages, plasmids; miRNA amplification; RCA-based protein assay

			specificity due to the padlock probe consisting two-target complementary segment for circular DNA sysnthesis		
HDA	Helicase and DNA polymerase, together with ssDNA-binding proteins (SSB) and ATP	3 x 10^3 X after an hour in 37^0C for primerase-based HAD for WGA	Share similar advantages as PCR: Relatively simple primer design; High sensitivity; Relatively easier to have multiplex detection among isothermal amplifications; Adopts to PCR detection method	Require numbers of protein factor for amplification; For target-HAD, the amplicon size is relatively small, within 80-120bp	Primerase-based HDA for WGA; HDA microarray
RPA	Recombinase proteins, creatine kinase, *Bsu* DNA polymerase and ATP	Allows to detect 100 copies DNA within 30 min	Compares with other isothermal amplification, no need to heat up (reaction temperature lower than 37 ^{0}C)	Require numbers of protein factors for amplification; Reagents are easily oxidized that increasing difficulty of handling; Reaction initialed by adding magnesium acetate at RT that carefully handling is needed; Failed to amplify large size of targets (< 1500 bp)	Micro-fluid combined RPA and Lab-on-a-chip

*[Kim and Easley 2011]

Table 1.2 Comparison of LAMP, Traditional PCR and Real-time PCR.

	LAMP	Traditional PCR	Real-time PCR
Time	30-60 min	Usually 2.5 hr (for 35 cycles)	30 min – 2 hr
Thermal cycles	No; Optimal temperature at 60-65 °C	Yes, including denature, annealing, elongation	Yes
Amplicons	Variable, can be very large *; dsDNA with stem-loop; The concentration of amplicons can be 400-800 ug/ml *	Exact size, usually 100-1000 bp **; dsDNA; the concentration of amplicons can be 4-40 ug/ml **	Not less than 50bp, 100-150bp is optimal; dsDNA
Specificity and Sensitivity	As sensitive as qPCR, 10 copies can be detected	Low sensitivity	High specificity and sensitivity
Detection	Immediately by naked eyes (+ve or –ve result)	Gel electrophoresis	Real-time; DNA dinging dye; TaqMan; Molecular Beacons

The readout platform described in Paper II is reported in Chapter 3. DNA-surface interactions draw more and more attention due to two reasons. Firstly, some techniques require the immobilization of nucleotides, including DNA for the DNA microarray and miRNA microarray. In terms of signal acquisition and device design, surface plasmon resonance (SPR) and mass-base detection with gold surface are commonly used for label-free detection [Liu 2012]. Secondly, gold nanoparticles

(AuNPs) and other NPs provide a new dimension to study DNA-DNA interactions for biosensors development, and drug- and DNA-delivery for different biomedical applications. As an excellent fluorescence quencher, AuNPs enable fluorescence signaling due to the absorption or desorption of DNA [Dubertret et al., 2001; Ray et al., 2007]. Also, the AuNPs SPR effect and the surface chemistry for DNA immobilization give a new technique for DNA detection without using traditional DNA reporting dyes. At the same time, the assembly of AuNPs after DNA absorption provides a good measure to detect the amount of target DNA in a highly specific manner [Li and Rothberg et al., 2004a, b; Wang et al., 2010; Xu et al., 2011]. Moreover, AuNPs-DNA can be internalized by cells for transfection whereas the free DNA cannot [Rosi et al., 2006].

In this connection, Tunable Resistive Pulse Sensing (TRPS) can be used to non-optically to characterize and quantify the aggregation dynamics of AuNPs in solution in a label-free manner.TRPS is an electrochemical analysis technique that allows the monitoring of target analyte-induced nanoparticles aggregation. Similar to flow cytometry, the size of particles can be measured one-by-one in the solution. Besides the size, other parameters, such as the surface charge and concentration of particles can be analyzed [Billinge et al., 2013]. The integration of the use of LAMP, AuNPs and TRPS is firstly demonstrated in Chapter 3 for the detection and

quantification of the MRSA DNA.

In Chapter 4, we are going to discuss something different from the previous chapters. As mentioned, the usage of NPs in biological and medical studies becomes more and more common. Besides using NPs for DNA detection as demonstrated in Chapter 3, one of the applications is the NP-mediated nucleic acid delivery for the gene therapy. NPs are tiny particles small enough to pass through the cell membrane as DNA carriers to bring DNA into cells efficiently. Existing in a variety of sizes, shapes and materials, NPs have been frequently applied in biomedical applications for the delivery of drug [De Jong and Borm 2008] and nucleic acids [Schins et al., 2002].

Now, there are many types of NPs different in shape and size. Among different kinds of NPs, flowers-like NPs, also known as Nanoflowers (NFs) are of particular interests due to the high surface areas. The technique of DNA transfection using NFs is described in Chapter 4. In general, NFs are composed of a nano-sized core, which is usually a metal oxide, covered a shell made up of large quantities of nanosheets of 5-10 nm thick and 100-300 nm wide. Our collaborators have previously reported the fabrication of a hierarchical core/shell Fe_3O_4@SiO2@γ-AlOOH@Au NFs and the potential use for protein immobilization (Xuan et al., 2011). Owing to the exceptionally high surface area of the extensive

nanosheets on the surface, and the large void nano-space in between the nanosheets, the NFs allow the immobilization of bovine serum albumin (BSA) up to 369.3 mg per gram of NFs. To further increase the use of the NFs, we suggested that the NFs could be used for nucleic acid delivery by making use of its unique features for targeted-drug/gene delivery and therapeutic purposes. We aim to show the feasibility of plasmid-functionalized NFs as a non-cytotoxic tool for targeted gene delivery for biomedical purposes.

In Chapter 5, it is going to report the application of TRPS on cell biology in addition to the nanotechnology. As presented in Paper III, the death of mature human erythrocytes (RBCs) induced by Polyphyllin D (PD), the anti-cancer drug was studied. In our pervious study, it was confirmed that PD can induce the apoptosis of drug-resistant human liver cancer cells (R-HepG2) through the mitochondrial apoptotic pathway, leading to the phosphatidylserine (PS) externalization and DNA fragmentation [Cheung et al., 2005; Ong et al., 2008]. Based on the fact that RBCs are devoid of nuclei and mitochondria, it is believe that PD would not lead to the death of RBCs, due to the lacking in elements for mitochondrial apoptotic pathways. However, out of the expectation, we found that PD can trigger the death of RBCs.

The death program of mature human erythrocytes (RBCs), eryptosis, is characterized by cell shrinkage, membrane blebbing, activation of protease, and

exposure of phosphatidylserine (PS) on the cell surface [Lang et al., 2006].The exposing of PS is a signal for equipping macrophages to engulf RBCs. It is believed that eryptosis is a process to removedefective RBCs to avoid hemolysis. Different from apoptosis, eryptosis is triggered by oxidative stress, formation of prostaglandin E_2 leading to the activation of Ca^{2+}-permeable cation channels, and the phospholipase A_2-mediated release of platelet-activating factor activating sphingomyelinase, leading to the formation of ceramide [Lang et al., 2006]. In Chapter 5, we studied the effect of PD on the induction of eryptosis by using TRPS. In this chapter, we reported the usage of TRPS in cell death analysis for the first time.

On the other hand, due to the increase number of new resistance strains of bacteria to current antibiotics, the study of anti-bacterial nanomaterials becomes more and more important [Sotiriou and Pratsinis 2010]. The anti-bacterial activities of silver ions and silver-based materials have been confirmed in a wide range of mirco-organisms. Silver nanoparticles (AgNPS) can affect the tyrosine phosphorylation in bacteria, leading to the decrease of bacterial growth. Hence, the silver-based materials have been extensively used in treating a variety of infections such as burns and wound-healing purposes. As the rapidly development of nanomedicine, the safety issues of using nanomaterials has been concerned. Due to

the chemical composition, surface structure, surface functional groups, surface area to volume ratio, nanomaterials share different levels of toxicity. A wide range of surface coating methods provides countless possibility of conjugation of any biomolecules interested to the nanomaterials. For example, polyethylene glycol (PEG), which is commonly used as surface coating for AuNPs, serves as a stable anchor for biomolecule conjugation [Holpuch et al., 2010]. However, health and safety issues of using NPs in human and animals are also greatly concerned. Our previous studies showed that the surface coating is crucial to the biocompatibility of AuNPs to human erythrocytes and basophils [Lau et al., 2011; Cheung et al., 2012]. In addition, the shape of NPs also determines the toxicity [Kulamarva et al., 2008]. Therefore the choice for the type of NPs and their surface treatment are of most important for biomedical applications.

The toxicity of nanomaterials can be caused by the production of reactive oxygen species (ROS), which may lead to inflammation, damage of cell membranes and DNA [Nel et al., 2006; Holsapple et al., 2005]. The safety, environmental and health issues of nanomaterials are still under investigation. In Chapter 5, we tried to briefly demonstrated the effect of silver nanoparticle (AgNPs) on human erythrocytes (RBCs) by TRPS, supported by confocal image.

References:

Billinge, E.R., Muzard, J. and Platt, M. (2013). Tunable resistive pulse sensing as a tool to monitor analyte induced particle aggregation. *Nanomater. Nano. Sci.*, 1(1), http://dx.doi.org/10.7243/2053-0927-1-1

Cheung, J.Y., Ong, R.C. et al. (2005). Polyphyllin D is a potent apoptosis inducer in drug-resistant HepG2 cells. *Cancer Lett.*, 217(2), 203-11.

Cheung, K.L., Chen, Q.L. et al. (2012). CTAB-coated gold nanorods elicit allergic response through degranulation and cell death in human basophils. *Nanoscale*, 4(15), 4447-49.

De Jong, W.H. and Borm, P.J.A. (2008). Drug delivery and nanoparticles: Applications and hazards. *Int. J. Nanomedicine*, 3(2), 133-49.

Detter, J. C., Jett, J. M., Arellano, A. R., & al., e. (2002). Isothermal strand-displacement amplification applications for high-throughput genomics. *Genomics, 80*(6), 691-698.

Dubertret, B., Calame, M. and Libchaber, A.J. (2001). Single-mismatch detection using gold-quenched fluorescent oligonucleotides. *Nat. Biotechnol.*, 19(4), 365-70.

Hill, J., Beriwal, S. et al. (2008). Loop-mediated isothermal amplification assay for rapid detection of common strains of *Escherichia coli*. *J. Clin. Microbiol.*, 46(8), 2800-04.

Ho, P.L., Tse, C.W. et al. (2004). Community-acquired methicillin-resistant *Staphylococcus aureus* arrives in Hong Kong. *J. Antimicrob. Chemother.*, 54, 845-846.

Holpuch, A.S., Hummel, G.J. et al. (2010). Nanoparticles for local drug delivery to the oral mucosa: proof of principle studies. *Pharm. Res.*, 27(7), 1224-36.

Holsapple, M.P., Farland, W.H. et al. (2005). Research Strategies for Safety Evaluation of Nanomaterials, Part II: Toxicological and Safety Evaluation of Nanomaterials, Current Challenges and Data Needs. *Toxicol. Sci.,* 88(1), 12–7.

Kim, J., & Easley, C. J. (2011). Isothermal DNA Amplification in Bioanalysis: Strategies and Applications. *Bioanalysis, 3*(2), 227-239.

Kulamarva, A., Bhathena, J. et al. (2008). In vitro cytotoxicity of functionalized single walled carbon nanotubes for targeted gene delivery applications. *Nanotoxicology*, 2(4), 184–88.

Lang, F., Lang, K.S. et al. (2006). Mechanisms and significance of Eryptosis. *Antioxid. Redox. Signaling*, 8, 1183-92.

Lau, I.P., Chen, H. et al. (2011). *In vitro* effect of CTAB- and PEG-coated gold nanorods on the induction of eryptosis/erythroptosis in human erythrocytes. *Nanotoxicology*, 6, 847-56.

Li, H. and Rothberg, L. (2004). Label-free colorimetric detection of specific sequences in genomic DNA amplified by the polymerase chain reaction. *J. Am. Chem. Soc.*, 126, 10958-61. (2004a)

Li, H. and Rothberg, L. (2004). Colorimetric detection of DNA sequences based on electrostatic interactions with unmodified gold nanoparticles. *PNAS.*, 101(39), 14036-39. (2004b)

Liu, J.W. (2012). Adsorption of DNA onto gold nanoparticles and grapheme oxide: surface science and applications. *Phys. Chem. Chem. Phys.*, 14, 10485-96.

Nel, A., Xia, T. et al. (2006). Toxic potential of materials at nanolevel. *Science*, 311(5761), 622-27.

Ong, R.C., Lei, J. et al. (2008). Polyphyllin D induces mitochondrial fragmentation

and acts directly on the mitochondria to induce apoptosis in drug-resistant HepG2 cells. *Cancer Lett*., 261(2), 158-64.

Ray, P.C., Darbha, G.K. et al. (2007). Gold nanoparticle based FRET for DNA detection. *Plasmonics*, 2, 173-83.

Rosi, N.L., Giljohann, D.A. et al. (2006). Oligonucleotide-modified gold nanoparticles for intracellular gene regulation. *Science*, 312, 1027-1030.

Schins, R.P., Duffin, R. et al. (2002). Surface modification of quartz inhibits toxicity, particle uptake, and oxidative DNA damage in human lung epithelial cells. *Chem. Res. Toxicol.*, 15, 1166–73.

Scientific Committee on Emerging and Zoonotic Disease. (2007). A review of community-associated methicillin resistant *Staphylococcal aureus* (CA-MRSA) cases in Hong Kong. Centre for Health Protection.

Sotiriou, G.A. and Pratsinis, S.E. (2010). Antibacterial activity of nanosilver ions and particles. *Environ. Sci. Technol.*, 44, 5649-54.

Wang, Z., Zhang, J. et al. (2010). DNA-mediated control of metal nanoparticle shape: one-pot synthesis and cellular uptake of highly stable and functional gold nanoflowers. *Nano Letters*, 10, 1886–91.

Xuan, S., Wang, F. et al. (2011). Hierarchicalcore/shell Fe3O4@SiO2@γ-AlOOH@Au micro/nanoflowers for protein immobilization. *Chem. Commun. (Camb.)*, 47(9), 2514-16.

Xu, L., Zhu, Y. et al. (2011). New synthesis strategy for DNA functional gold nanoparticles. *J. Phys. Chem. C.,* 115, 3243-49.

Chapter 2 Fluorescence-based and Optical-based Loop-mediated Isothermal Amplification

2.1 Introduction

In this chapter, the Lamplicons (products of LAMP reaction) monitoring method and the effect of DNA dyes, SYBR Green I (SGI) and SYTO-9 (ST9), in LAMP reaction were investigated. At the same time, the non-fluorescent based monitoring method was also introduced, in order to improve the technology of nowadays Lamplicons detection methods.

At present, detection of pathogens relies on the amplification of DNA. This is based on the fact that pathogen carries unique DNA signature that can differentiate it from other organisms. Also, the pathogen genetic make-up provides information on drugs resistance and mutation. Recently, in Hong Kong and Europe, both Scarlet fever and enterohemorrhagic *E. coli* (EHEC) are found carrying drug resistance and mutations. The epidemics spread rapidly and are fatal. The traditional identification method by aseptic culturing is not efficient enough to study the bacterial characters. It is an urgent matter to understand the characteristics of bacteria or novel virus as infections from these microorganisms may be lethal within a few days. In Hong Kong, when a patient is suspected to have been infected by unknown pathogen, samples are collected for further detection by sample culturing, DNA detection or sequencing. In this regard, polymerase chain reaction (PCR) is the most widely used DNA amplification method. It exponentially amplifies a fragment of interest DNA through thermo-cycling enzymatic reactions. PCR starts with 95 ^{0}C heat-treatment to denature the double-stranded DNA template. Two ssDNA strands then cool down to 55 ^{0}C to be hybridized with primers with complementary

sequences (annealing). Subsequently, the primers-DNA complex is heated to 72 ^{0}C to allow the heat-stable DNA polymerase to add nucleotides from 5' to 3' end according to the Watson and Crick base pairing with reference to the DNA template sequence (extension). By repeating the above three steps, a single DNA template can be amplified into millions of identical copies.

To monitor the PCR amplification in a real-time (RT) manner is regarded to be a rapid and specific detection method to identify pathogens (qPCR or real-time PCR (RT-PCR)). There are four different chemistries for the qPCR. Namely, they are the TaqMan, SYBR Green, Molecular Beacons and Scorpions design which are available as reporters for the qPCR detection. All of the above techniques allow PCR products to be detected by fluorescent signals during thermo-cycles. However, there are disadvantages using these approached to detect target DNA. First of all, labeling of molecules or synthesis of specific reporters is expensive. Secondly, fluorescence is easily to have photo-bleaching. Additionally, the machine for qPCR is expensive and energy-demanding.

Isothermal amplification methods, similar to the qPCR, can be monitored in RT during the process of DNA amplification by different means or immerged with different detection platforms. In our project, LAMP was chosen for target DNA amplification. The reasons for choosing LAMP are as follows: First of all, the reagents and materials for LAMP reactions are simple and easily obtained, compared with the other isothermal methods. Besides, the enzymes and other protein factors are not needed. The cost of the reaction is low and the setup for LAMP is simple. Second, the potential to determine the LAMP products (Lampilcons) as a result of the complicate structures of the products is high. For example, RT detection of

LAMP products can be easily executed using fluorescence or turbidity [Aoi et al., 2006; Mori et al., 2001, 2004]. Also, the application of LAMP on chips and NPs is not yet developed.

LAMP has been developed for an era by the researchers of Eiken Chemicals Company, Tokyo, Japan. The specificity of LAMP is very high. Four to six primers are utilized for amplifying one single gene. Two long primers, FIP and BIP can recognize two positions at forward and backward of a dsDNA template respectively. Another two short primers, F3 and B3, help the FIP and BIP to recognize the specific position (Figure2.1.1). During the amplification process, Bst DNA polymerase has the strand displacement and the 5' to 3' DNA polymerization ability at 60 - 65 ^{0}C [Zhang et al., 2009]. After the elongation process, cauliflower-like DNA loops are formed. As the incubation time increased, the quantity and length of DNA loop would be increased [Mori and Notomi 2009; Parida et al., 2008]. Hence, a small amount of DNA template can be amplified to a very large amount of DNA loop shape products, Lamplicons.

For the detection of Lamplicons, similar to the case of PCR, gel electrophoresis can be applied for checking the relative amount of target genes. Also, due to the incubation temperature at 65 ^{0}C, the pyrophosphate ions produced by dNTP during the DNA amplification form precipitates in the reaction mixture. Whereas the precipitates disappear in high denature temperature in the PCR thermal cycles. Investigators can use naked eye to observe the result of LAMP immediately after reaction [Mori et al., 2004]. To make the result more easily to be observed, some dyes including SGI and calcein can be added into the reaction mixture after amplification. These dyes give fluorescence signal under UV irradiation. Yet, the

end-point methods mentioned above cannot monitor or quantify the target genes by LAMP in a RT manner. Therefore, it will be nice to employ DNA binding dyes to report fluorescence signal in a RT fashion for LAMP reactions in a way similar to the qPCR. To date, no literature is found to report the fluorescence-based real-time LAMP (RT-LAMP or qLAMP) reaction. One of the reasons may be due to the unknown inhibitory effect of the DNA dyes to LAMP reaction. Previous studies suggested that SGI dyes inhibit the amplification efficiency in the qPCR [Gudnason et al., 2007]. The GC content of target genes is one of the factors decreasing the binding affinity of SGI to DNA, thus lowering the efficiency of DNA amplification. However, the inhibitory effect of SGI and other DNA molecular probes in LAMP remains unknown.

To detect target genes, surface plasmon resonance (SPR) is a highly sensitive label-free optical system when compared with qPCR. It can be used to measure different bimolecular interactions such as DNA-DNA, RNA-DNA, nucleotides-protein, protein-protein, aptamers-protein and antibodies-antigens etc. in a RT manner [Scarano et al., 2010]. The molecules binding on gold surface in SPR can lead to light phase shift for biosensing. It is a highly sensitive and specific detection method. In this study, we are going to use SPR to detect the pathogen DNA or RNA in a RT manner. Unfortunately, SPR is a temperature sensitive optical system that cannot be used with PCR thermo-cycles to amplify DNA. Hence, the isothermal DNA amplification, LAMP, was applied. The advantage of using isothermal amplification instead of traditional PCR is that less time consuming for temperature change. Also, our data show that LAMP has higher sensitivity than PCR. Hence, by combining SPR and LAMP (SPR-LAMP), the biosensor would be very sensitive and efficient. Having the above advantages, it is believed that the SPR-LAMP will be a

good system for disease diagnosis and prognosis, toxin and contamination detection, as well as for pollution monitoring and forensic investigation. To proof the concept for the SPR-LAMP system, a particular pathogen is chosen as the model. The criteria of choosing the model are the convenience for obtaining samples, low risk of infectious and the prospective of drugs resistance. It is expected that SPR-LAMP is a fluorescence-label free, high sensitivity, quantitative and low cost system for target DNA detection. In our project, one of the major works is to obtain a standard curve for the conversion between SPR light phase change signal and the pathogen amount or its DNA copy number. In addition, multi-gene amplification is needed for point-of-care diagnosis purpose. The ideal SPR-LAMP is not only suitable for the model chosen, but also can be applied on the sensing with pathogens, genetic diseases, or even food contaminants.

SPR technique has been used as a power alternative for studying bimolecular interactions. In fact, SPR is not only for protein-protein interaction detection, but also for the detection of DNA [Goodrich, Lee & Corn 2004]. One of the advantages using SPR as a tool for genomic DNA or RNA assay is that SPR can provide direct analysis in an array format. It is expected to be useful for viral and bacterial identification, gene expression analysis and biological warfare detection. However, the extensively application on DNA and RNA detection is limited, due to its nanomolar detection limit [Nelson et al., 2001]. Normally, the quantification of gene expression and disease marker is in the femtomolar level, especially the assay only using a drop of blood or body fluid. This means we still have difficulties in using conventional SPR for point-of-care application.

To improve SPR measurement, different means were published within this

decade, for example, incorporation of fluorescent spectroscopy into SPR to push the detection sensitivity to attomolar level; incorporation of bi-cell photodiode detector; modifying SPR Au-surface by coating gold-capped nanoparticle layer or porous substrate allowing DNA to hybridize [Kim et al., 2007]. Also, some research groups focused on incorporating additional chemical reactions and using external labels to raise the DNA detection sensitivity, for example, performing SPR detection after amplifying DNA by PCR [Wang et al., 2004]. In particular, the amplicon obtained from PCR was heat denatured, followed by hybridization with short oligonucleotide to avoid re-annealing. The hybridized ssDNA was flown into Biacore XTM SPR. The sensor chip was coated with oligonucleotide probes which are complementary with the amplicons. The probes were conjugated with thiol group for attaching to Au surface. By this approach, the amplified-DNA hybridized with oligonucleotide had 4-fold larger RU compared with the one without hybridization. The purpose of involving DNA amplification was that enhancing the number of DNA copies. The hybridization of oligonucleotide to denatured DNA not only avoided re-annealing, but also elevated the sensitivity. Hence, a significant difference of RU could be observed for different amount of DNA. However, the denature step in PCR includes a heating step at 95 ^{0}C, which is not compatible with the SPR platform for simultaneous target DNA amplification and detection step. Therefore, the combination of LAMP with, SPR seems to be a good integration to speed up the analytic process.

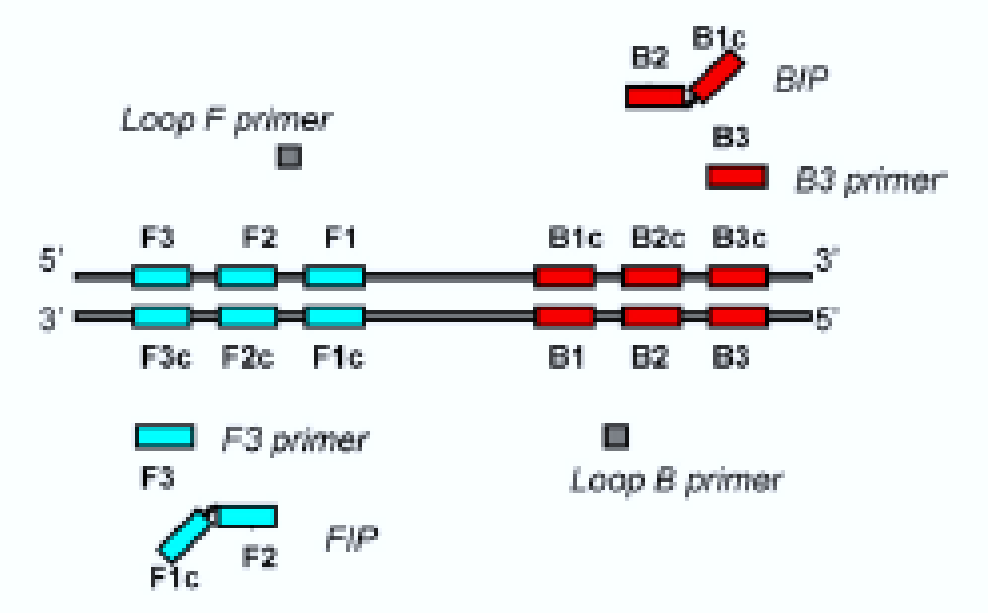

Fig. 2.1.1 Position of primer set binding on target gene in LAMP reaction. The essential primers, including FIP, BIP, F3 and B3 primers. FIP primer hybridizes to F2c and F1 regions. BIP primer hybridizes to B2c and B1 regions. F3 and B3 primers are located at F3c and B3c regions respectively. The non-essential primers, Loop F and Loop B primers are complemented with the regions between F2c and F1c or B1 and B2. [Curtis et al., 2008]

2.2 Materials and Methods

2.2.1 Materials

45 nm thick Gold sensor chips and white light LED spectrum-SPR were obtained from Prof. H.P. Ho's group, Department of Electronic Engineering, CUHK.

All the buffers and reagents were prepared by dissolving chemicals into double distilled water (ddH_2O). The pH value was adjusted with HCl or NaOH.

Phosphate buffered saline (PBS) was composed of 136 mM NaCl, 2.7 mM KCl, 1.5 mM KH_2PO_4 and 8 mM Na_2HPO_4. PBS is titrated to pH 7.4, and then

sterilized by autoclave. PBS was stored at room temperature. Filtration and degassing were done before used.

5X TBE Buffer was composed of 57 g Tris base, 27.5 g boric acid and 20 mL 0.5 M EDTA (pH 8.0), dissolved in 1 L of ddH_2O.

2.2.2 Methods

2.2.2.1 Preparation of MRSA DNA template

The MRSA *PVL* toxin gene was synthesized by overlapping PCR using the information from the database at NCBI GenBank (Accession AB488779, from codon 604 to 943, 340 bp long). Overlapping PCR reaction was performed in a 50μL reaction mixture, containing 0.2 μM each of primers (Sangon Biotech); 1 X Pfu DNA polymerase reaction buffer (Promega) (20 mM Tris-HCl, 10 mM KCl, 10 mM$(NH_4)_2SO_4$, 2 mM $MgSO_4$, 0.1 % Triton X-100 and 0.1 mg/mL nuclease-free BSA); 200 μM dNTP mixture; 0.5 unit Pfu DNA polymerase (Promega) and the volume was adjusted by nuclease-free ddH_2O. The mixture was placed in a thermal cycler for PCR reaction: initial denature at 95 ^{0}C, 3 min; thermal cycle starting from denature at 95 ^{0}C, 30 sec; annealing at 58 ^{0}C, 30 sec, extension at 72 ^{0}C, 1 min 20 sec, for 35 cycles; and final extension at 72 ^{0}C, 10 min. The schematic diagram showing the overlapping PCR is below (Figure 2.2.1):

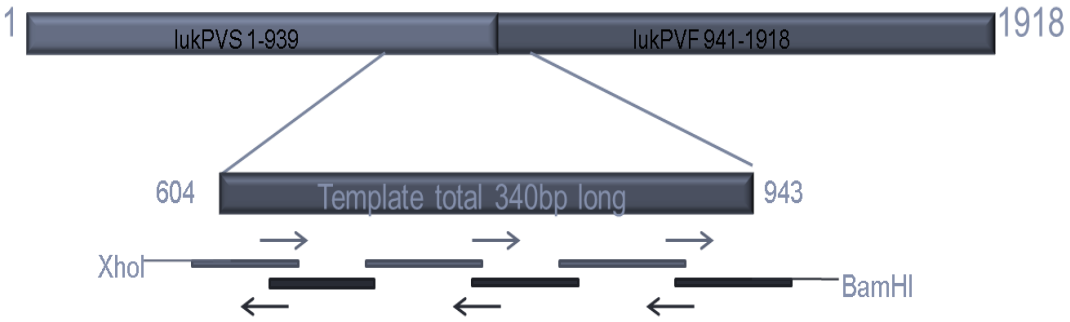

Fig. 2.2.1 Schematic diagram showing the construction of MRSA *PVL* DNA

template by overlapping PCR.

The final DNA product was sequenced (Tech Dragon) and it was confirmed that the sequence was 100 % identical to the *PVL* DNA sequence in the GenBank.

2.2.2.2 LAMP reaction and PCR reaction

LAMP primers (2 outer primers (F3, B3) and 2 inner primers (FIP, BIP)) specific to the *PVL* gene was designed using the Primer Explorer software, version 4.0 (http://primerexplorer.jp/elamp4.0.0/index.html) (Table 2.2.1). All primers were in ultra-PAGE grade and the 5'-end of the FIP primer was biotinylated (Sangon Biotech). LAMP reactions were performed according to procedures as described [Tomita et al., 2008]. Briefly, the reaction was performed in a 25 μL reaction mixture, containing 1.5 μM of BIP and 5'-biotin-FIP; 0.4 μM each of F3 and B3; 1 X ThermoPol reaction buffer with 2 mM $MgSO_4$ (20 mMTris-HCl, 10 mM $(NH_4)_2SO_4$, 10 mMKCl, 2 mM $MgSO_4$, 0.1 % Triton X-100, pH 8.8) (New England BioLabs); 0.8 M Betaine (Affymetrix USB); 10 mMdNTP; 0.8 μL of 8 units Bst DNA polymerase (New England BioLabs); 1 μL of MRSA template (10^8 copies); additional with 6 mM $MgSO_4$ and the volume of reaction mix was adjusted by nuclease-free ddH_2O. The mixture was incubated at 65 ^{0}C for 30 min.

Table 2.2.1 LAMP Primers for MRSA *PVL* target DNA

Primer Name	**Sequence (5' → 3')**	**Locus**
F3	AGACAATGAATTACCCCCATT	666-686
B3	CGTTGTGTATTCTAGATCCTTCT	859-837
FIP*	GTATCTCCTGAGCCTTTTTCATGAGAATTCTACACAGTGG TTTCAATCCT	F2: 689-708; F1c: 752-729

BIP*	TAACGTATGGCAGAAATATGGATGTGAATTCACTATTGCC ATAGTGTGTTGTT	B1c: 767-791 B2: 831-810
B2-LB	5'C6(SH)-*ATAT*-ACTATTGCCATAGTGTGTTGTTCTTCTAGT AGCATGAGTA	831-798, 44 nucleotides

*FIP and BIP primers were composed of short primers F2, F1c, and B2, B1c, respectively. The sequence and loci of all primers, including F2, F1c, B1c and B2 were shown. F2 and B1c were located on the target strand, whereas F1c and B2 on the complementary strand. The orientation of the construction of the FIP and BIP were from 5'-F2-F1c-3' and 5'-B1c-B2-3' respectively. The *EcoRI* restriction site was underlined.

2.2.2.3 RT-LAMP reactions

RT-LAMP reactions were conducted in MicroAmp Fast Optical 96-Well Reaction Plate, 0.1 mL (Applied Biosystems) and monitored using MyiQ^{TM}2 two-color RT-PCR detection system (Bio-Rad). Reaction mixture was prepared as described above. The sample was initially heated at 50 ^{0}C for 1 min, followed by 50 cycles of 65 ^{0}C for 1 min each (including fluorescence detection step) in the RT-PCR machine, followed with termination at 80 ^{0}C for 5 min. After amplification, the melting curves were acquired by heating the sample with the following dissociation program: 95 ^{0}C for 1 min; 55 ^{0}C for 1 min; and 55 to 90 ^{0}C by 0.5 ^{0}C with a hold of 10 sec each step. The threshold was set at 400 relative fluorescence units. The threshold cycles (Ct values) of RT-LAMP with either SGI or ST9 were compared.

2.2.2.4 Gold chip modification

Gold sensor chips of 45nm thick were cleaned by absolute ethanol twice, followed by 10mM 11-mercapto-undecanoic acid (MUA)/ethanol (Sigma-Aldrich) overnight incubation at room temperature. The incubation medium then changed to aqueous by washing with phosphate buffered saline (PBS). Freshly prepared 0.4M N-(3-dimethylaminopropyl)-N-ethylcarbodiimide (EDC) and 0.15 M *N*-Hydroxysuccinimide (NHS) (both in PBS) were mixed and injected to the chips,

and incubated for 15 min. Streptavidin (1mg/mL) in PBS was subsequently injected to chips. After 15 min incubation, the non-specific binding on the gold surface was blocked by ethanolamine (1 M, pH 8.5, 10 min). Between each of the incubation steps, the chips were washed twice by PBS. After washing, the chips can be stored at 4 ^{0}C in PBS until use.

2.2.2.5 End-point Spectral-Surface Plasmon Resonance (SPR)-LAMP detection

The white light LED spectrum-SPR was utilized in our SPR-LAMP system. Samples (Lamplicons) were 5 X diluted with nuclease-free ddH_2O before detection. The surface prepared gold sensor chip was connected to injection tubes. 0.2 X LAMP reaction buffer (0.2 X ThermoPol reaction buffer, 1.2 mM $MgSO_4$, 0.16 M betaine) was used as SPR running buffer. After obtaining a stable baseline, 40 μL diluted sample was flowed into the chamber of chip. Signals were detected for 30 min. The chamber was then flowed with 100 μL running buffer, followed by regeneration with 60 μL 25 mM NaOH. Running buffer (50 μL) was used for washing after regeneration. The spectrum was recorded every two seconds.

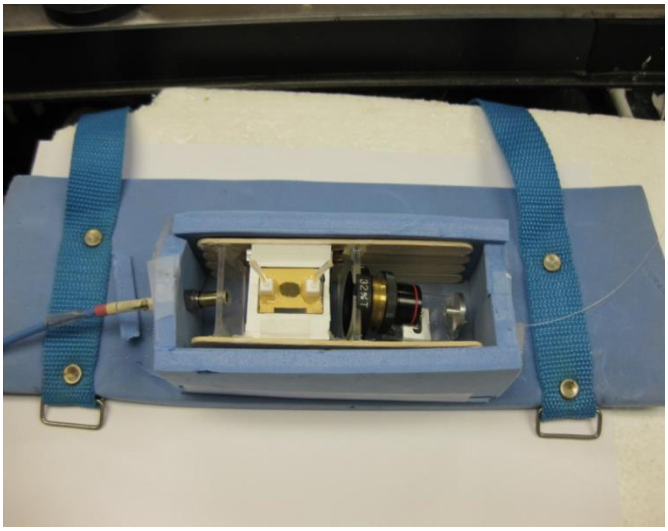

Fig. 2.2.2 Setup of spectral-SPR-LAMP system.

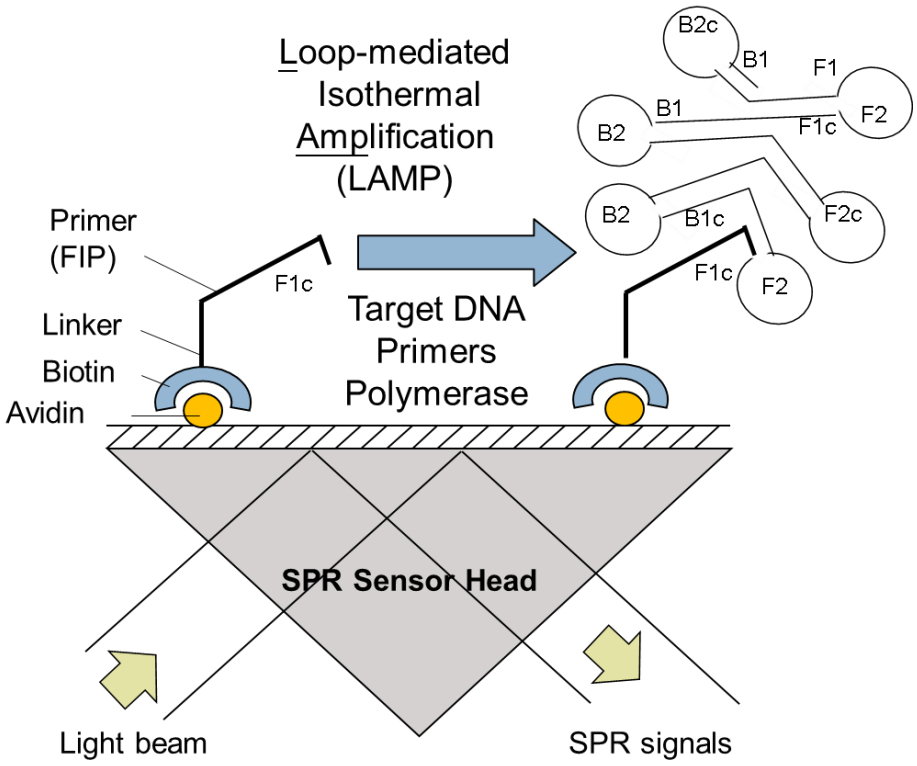

Fig. 2.2.3 Schematic diagram of spectral SPR-LAMP for detecting target DNA. Biotinylated FIP primers were allowed to bind to the SPR gold layer coated with SA. When amplification occurred, target gene on the SPR surface was detected by phase change.

2.2.2.6 Calculation

Curve fitting and finding dip of the spectrum were done by using the MATLAB software. Histogram and standard curve were plotted as mean ± SD (n=3), and *p*-values less than 0.05 were considered statistically significant. Data were compared with student t-test.

2.3 Results

2.3.1 Fluorescence-based visualization for Lamplicons detection

End-point fluorescence-based visualization is widely used as Lamplicons observation. By adding 2.5 μM of calcein solution, which could capture the magnesium pyrophosphate salt in LAMP reaction mixture with Lamplicons, exhibited fluorescence under UV irradiation (Figure 2.3.1). For the reaction mixture without target DNA template or before DNA amplification, the calcein in the mixtures could not exhibit fluorescence under UV light.

A Traditional DNA dye, SGI can also been utilized as end-point visible observation in LAMP. In the time-dependent LAMP assay, the Lamplicons were drawn out after incubating at 65 ^{0}C for 0, 10, 20, 30, 45 and 60 min respectively, followed by gel electrophoresis to check the formation of Lamplicons (DNA ladder bands) (Figure 2.3.2a). At the same time, 1 X SGI dye was added into each of the corresponding tube, followed by exposing UV light (Figure 2.3.2b). In the gel photo, there were enough Lamplicons produced after 30, 45 or 60 min of amplification (Figure 2.3.2a, Lane 4 - 6). However, the DNA ladder was absence in 0, 10 and 20 min amplification (Lane 1 - 3). For the SGI end-point visualization, only the reaction mixtures with 30 and 45 min amplification could exhibit green fluorescence under UV

light. The SGI end-point visualization result matched with the gel electrophoresis result.

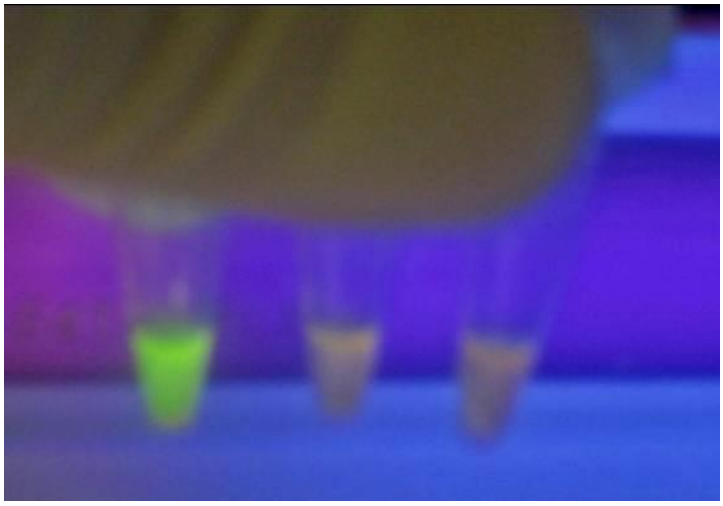

Fig. 2.3.1 Naked-eye visible end-point detection of Lamplicons by using calcein. 2.5 μM of calcein solution was added into each of the 25 μL reaction mixture, followed by UV irradiation. Tubes from left to right were positive sample, negative sample and reaction mixture at time before incubation at 65 ^{0}C respectively.

(a)

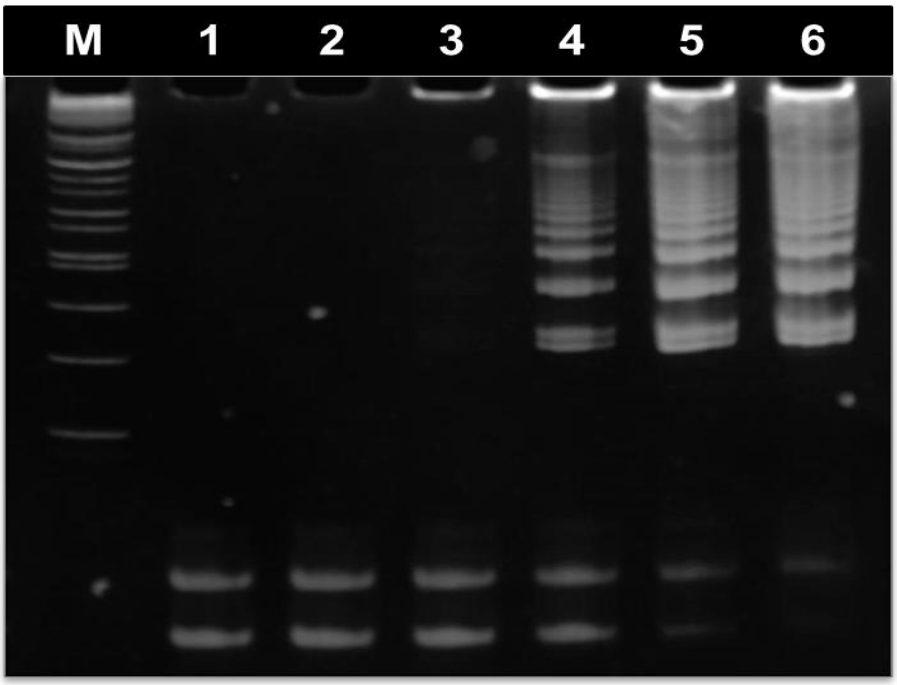

(b)

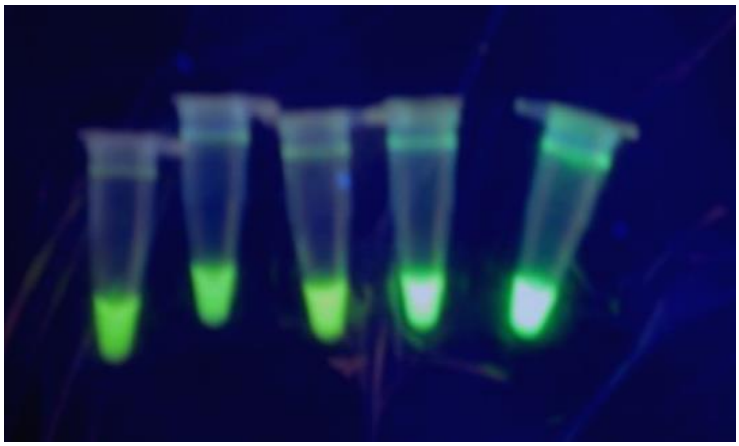

Fig. 2.3.2 Traditional end-point detection method to detect Lamplicons after different time-interval of LAMP reaction. (**a**) 12 % PA gel electrophoresis was done by loading 10 μL of Lamplicons, post-stained with 3 X GelRed^{TM} dye. M: 1kb

plus DNA ladder marker; Lamplicons were produced after 1: 0 min; 2: 10 min; 3: 20 min; 4: 30 min; 5: 45 min or 6: 60 min of LAMP reaction. (**b**) The gel electrophoresis corresponding reaction tubes were detected by using Fluorescent-based visual method. 1 X SGI dye was added into each reaction tube, exposing to UV light. The reaction tubes, from left to right, were referred 0 min, 10 min, 20 min, 30 min 45 min and 60 min LAMP reactions. The amount of DNA was 1,000 copies per 25 μL reaction mixture.

2.3.2 RT-LAMP detection by using DNA dye

Figure 2.3.3 compares the efficiency of DNA amplification of MRSA *PVL* toxin using LAMP and PCR through the conventional end-point agarose electrophoresis assay. As can be seen in the agarose gel, PCR required 10^6 copies of DNA templates to report the presence of MRSA *PVL* (Lane 13) (Figure 2.3.3). On the contrary, LAMP only required 100 copies and used a shorter incubation time (LAMP 30 min vs. PCR 75 min) to provide strong signals (Lane 1), while the negative controls in the absence of template showed nothing (Figure 2.3.3). These results indicate that LAMP has a lower detection limit than PCR to probe the MRSA.

To test the utility of SGI for the RT-LAMP, we put SGI into a reaction mix and evaluated its effect on DNA amplification first by conventional gel electrophoresis. After performing LAMP for 30 min, DNA fragments were separated by

polyacrylamide gel electrophoresis to give better resolution. PCR products were run simultaneously in the polyacrylamide gel. After electrophoresis, DNAs were stained by GelRed^{TM} solution for comparison. As shown in Figure 2.3.4a, when the MRSA template was included in the reaction mix in the absence of SGI, LAMP produced a series of DNA bands (Lane 5) while PCR generated one single band (193 bp) (Lane 11), indicating the nature of LAMP. Different from PCR, LAMP did not give a single band but a DNA smear indicating the formation of cauliflower-like DNA structures of different molecular size. Although LAMP could not synthesize amplicons of the same size to the target DNA template, the DNA smear provided an advantage to increase assay sensitivity if bulk fluorescence was determined from a reaction tube. A second finding of note in Figure 2.3.4a is that when SGI was added into the reaction mix, it blocked both the DNA amplification using LAMP (Lanes 3 & 4) or PCR (Lanes 9 & 10) when its concentration was greater than 1 μM. In fact, SGI has been previously shown to exert inhibitory effects on PCR [Gudnason et al., 2007].

The binding affinity of SGI to dsDNA is affected by the ionic strength of reaction buffer [Zipper et al., 2004]. A tight binding affinity may impose an inhibitory effect on LAMP. Also, Mg^{2+} is required for the Bst-mediated DNA polymerization [Wang et al., 2004; Li et al., 1988] and the DNA double-helix stability [Notcovich et

al., 2000; Owczaray et al., 2008]. We therefore investigated the effect of the concentration of Mg^{2+} on the SGI-mediated LAMP inhibition. In Figure 2.3.4b, the final concentration of Mg^{2+} ions was increased from 6 to 10 mM for LAMP. As can be seen, SGI again inhibited the LAMP in a concentration dependent manner. For the effect of Mg^{2+}, it can be seen that 8 mM was the optimal concentration for LAMP. These observations are consistent with the previous findings that 4 to 8 mM is the optimal Mg^{2+} concentration for LAMP [Notomi et al., 2000; Saiki et al., 1988]. However, further increase in the Mg^{2+}concentration could not eliminate the SGI inhibitory effect (Figure 2.3.4b).

In view of the SGI inhibitory effect on LAMP, we tried another DNA intercalating dye for RT DNA biosensing. Similar to SGI, ST9 is non-fluorescent by itself too, but it becomes highly fluorescent upon binding to dsDNA. As shown in Figure 2.3.5, LAMP again gave a series of DNA bands. Pre-loading of ST9 up to 2μM in the LAMP reaction mix (Lane 1) only showed a small inhibition (weaker fluorescence) when compared to that with a lower ST9 concentration (e.g. Lanes 3, 5 and 7). On the other hand, SGI once more blocked the LAMP reaction (e.g. Lanes 9 and 11).

Next, we tested the use of ST9 for the RT-LAMP using a RT-PCR machine but set the temperature at 65 ^{0}C all the time. As shown in Figure 2.3.6a, significant ST9 fluorescence above threshold was obtained 20 min after the LAMP reaction. The more the ST9 in the reaction mix, the stronger the fluorescence was obtained. On the other hand, when SGI was used as the fluorescent reporter, 2 μM of the dye totally blocked the LAMP reaction (signals overlapped with the baseline). When the concentration of SGI was reduced to 1μM, significant fluorescence above threshold was observed 30 min after LAMP reaction. Further reduction of the SGI concentration gave an earlier start of the rising phase but signals reached its plateau before 30 min. Also, the log-linear range in the exponential phase of DNA amplification was very narrow (Figure 2.3.6a).

To investigate the correlation of dye concentration and LAMP, we conducted RT-LAMP assays with a constant amount of input of MRSA template (10^5 or 10^8 copies) with various dye concentrations. In Figure 2.3.6a, we employed the PCR tools for data analysis by plotting the threshold value (Ct, the number of cycles (or time in LAMP) required for the fluorescent signal to cross the threshold) against the logarithmic dye concentration. As can be seen, a linear realtionship was observed in the mixtures with ST9 (Figure 2.3.6b, solid line, R^2 = 0.93). However, the systems

with SGI did not show a linear realtionship (Figure 2.3.6b, dotted line, R^2 = 0.89 and 0.84). The Ct value of the reation mix with 2 μM SGI was undetecable and therefore no data point was shown in Figure 2.3.6b. When the SGI concentration was decreased from 1 (log value = 0) to 0.25 (log value = -0.6) μM, the Ct value dropped substantially. It is thus confirmed that SGI not only had a negative impact to PCR [Gudnason et al., 2007] but also on LAMP and the RT-LAMP. On the contrary, ST9 showed less inhibitory effect on LAMP.

A standard curve plotting the Ct value against log starting copy numberwas also obtained (Figure 2.3.6c). The amplification efficiency was calculated by the following formula ($E = [10^{(-1/slope)} - 1] \times 100$ %, where E = Efficiency) [Pfaffl 2001] and slopes were obtained from line fitting (R^2 between 0.963 to 0.995). Theoretically, the ideal amplification efficiency should be 90-110 % depending on the length of amplicon, its secondary structure and primer design. In Figure 2.3.6c, the effeciency of LAMP amplification was in the following order: 0.5 μM ST9 (E=92.4 %) > 1 μM ST9 (E=64.1 %) > 0.5 μM SGI (E=56.7 %) > 1 μM SGI (E=19.3 %). These observations again were consistent with our findings in Figures 2.3.4 and 2.3.5.

According to Figure 2.3.4a, 1 μM or above of SGI could inhibit the PCR reaction.

To investigate the inhibitory effect of ST9 in PCR at high concentration (2 μM or above), PCR assays were repeated by adding various concentraions of ST9 into reaction mixture, followed by 35 cycles reactions. 12 % PA gel electrophoresis was done to detect the amplicons. The signal under UV irridiation may be due to the high concentration of ST9 in reaction mixture, or the GelRed™ staining after gel electrophoresis, it was necessary to take photos before and after GelRed™ stainig. In Figure 2.3.7, there were light DNA bands in the lands with 2 and 3 μM of ST9 before GelRed™ staining. After GelRed™ staining, all the lanes with *PVL* templates gave significant DNA bands. However, to compare with gel photos before and after staining, we cannot see an obvious inhibitory effect of ST9 at high concentraion. The result indicates that ST9 shows a low inhibitory effect in both RT-PCR and RT-LAMP to compare with the traditional fluoresence reporter, SGI.

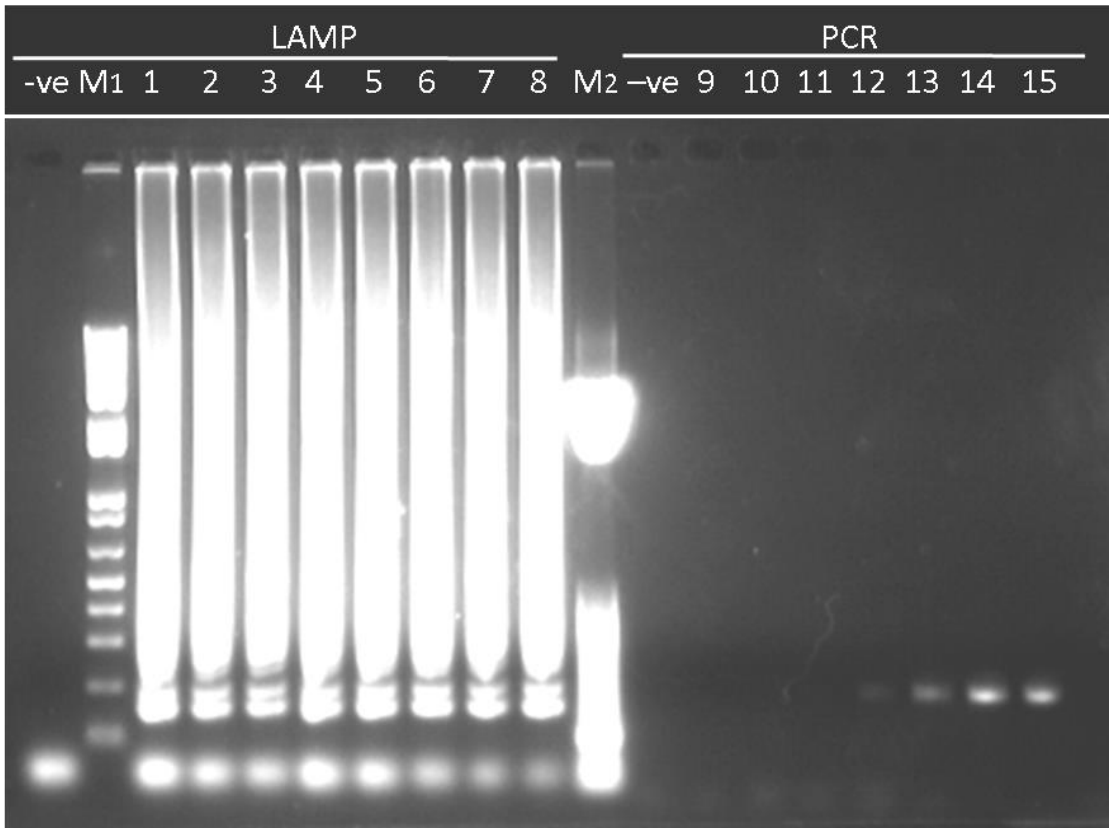

Fig. 2.3.3 Detection limit for MRSA from LAMP and PCR. The initial *PVL* DNA templates were in a range from 10^2 to 10^9 copies (10-fold increase for LAMP) (Lane 1-8); Lanes 9-15: 10^2 to 10^8 copies (10-fold increase for PCR). M1: 1 kb plus DNA markers; M2: 25 bp DNA ladder. Negative: no MRSA template. LAMP and PCR amplicons were obtained after incubating the reaction mix at 65 ^{0}C for 30 min and 30 PCR cycles (2.5 min/cycle), respectively. Agarose gel was then stained with 3X GelRed^{TM}dye after electrophoresis to show the DNA bands.

(a)

Lane	M	1	2	3	4	5	6	7	8	9	10	11	12
Reaction	-	LAMP						PCR					
MRSA	-	+	+	+	+	+	-	+	+	+	+	+	-
SGI (mM)	-	0.25	0.5	1	2	-	-	0.25	0.5	1	2	-	-

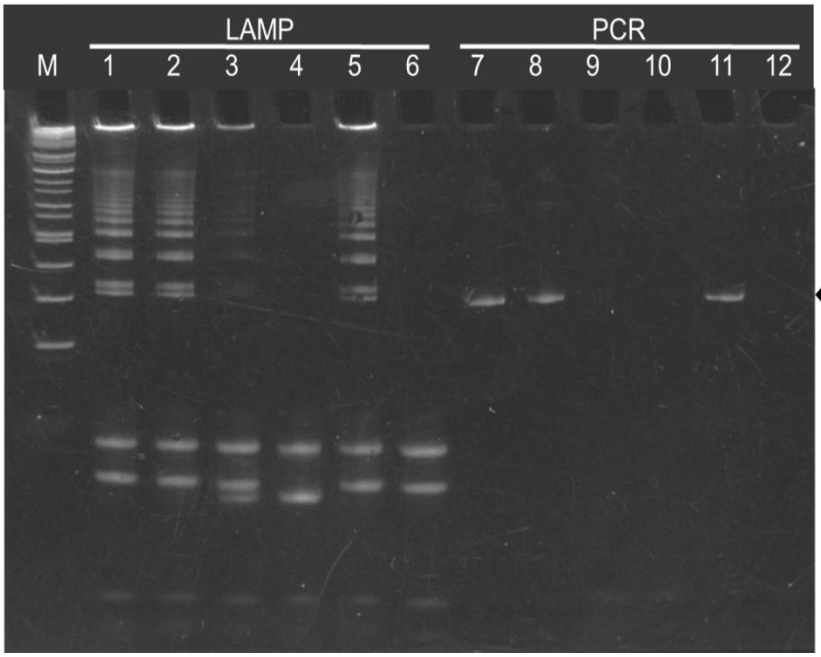

(b)

Lane	M	1	2	3	4	5	6	7	8	9	10	11	12	13
SGI (mM)	-	2	2	2	1	1	1	0.5	0.5	0.5	0	0	0	0
$MgSO_4$ (mM)	-	6	8	10	6	8	10	6	8	10	6	8	10	8

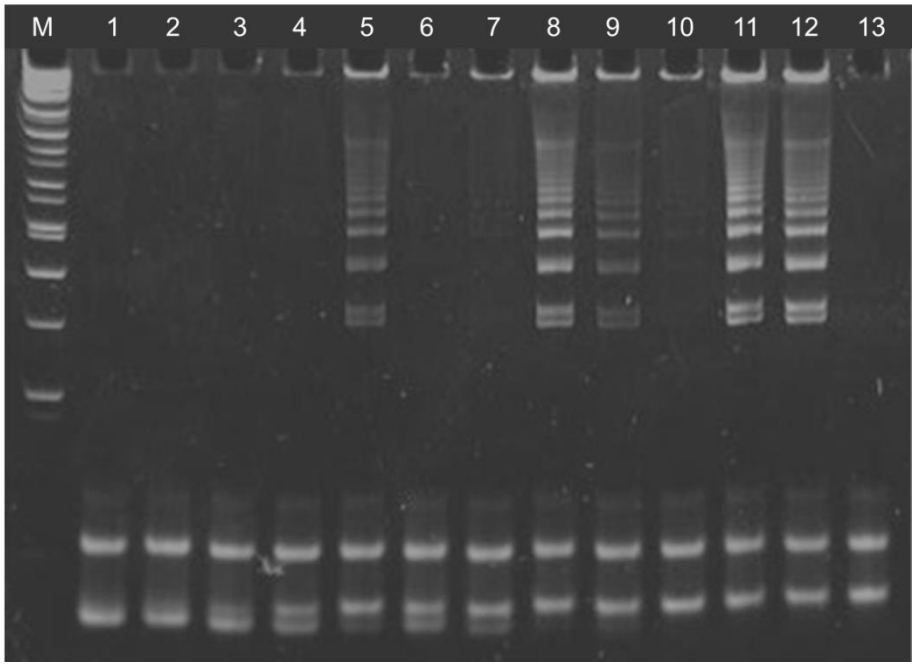

Fig. 2.3.4 Effects of SGI and Mg^{2+} on PCR and LAMP to probe MRSA. Reaction mix containing 10^5 copies MRSA template or water as the starting material was pre-mingled with SGI (**a, b**) and Mg^{2+} ion (**a**: 8 mM) at the concentration as indicated. LAMP and PCR were performed as mentioned in Fig. 2.3.3. Negative controls were shown in lane 6 and 12 (a), and lane 13(b). The post-staining procedure was performed with 3 X GelRed^{TM} dye to show the DNA bands. M: 1 kb plus DNA ladder markers.

Lane	M	1	2	3	4	5	6	7	8	9	10	11	12	13	14
MRSA	-	+	-	+	-	+	-	+	-	+	-	+	-	+	-
ST9 (mM)	-	2		1		0.5		0 (DMSO)		-		-		-	
SGI (mM)	-	-		-		-		0 (DMSO)		2		1		0.5	

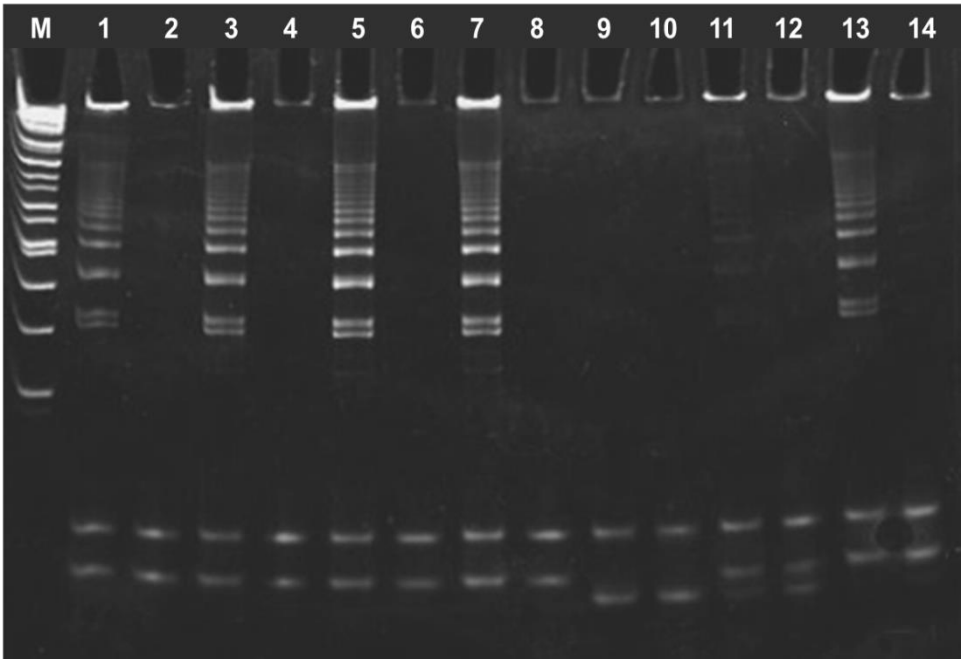

Fig. 2.3.5 Effects of SGI and ST9 on LAMP in the detection of MRSA. Reaction mix containing 10^5 copies MRSA template (odd number lane) or water (even number lane) as the starting material was pre-mingled with SGI or ST9 at the concentration as indicated. In some tests, DMSO (4 %) was included as the solvent control. The post-staining procedure was done with 3 X GelRed™ dye to show the DNA bands. M: 1 kb plus DNA ladder markers.

(a)

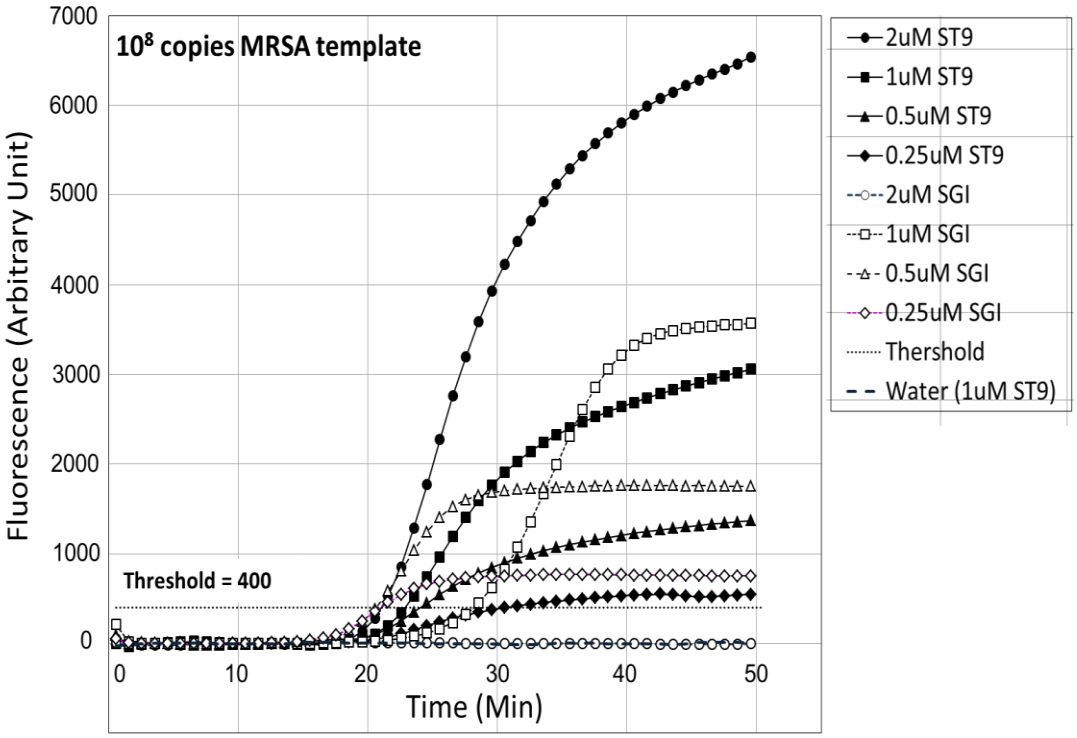
10^8 copies MRSA template
Fluorescence (Arbitrary Unit)
Time (Min)
Threshold = 400
0
1000
2000
3000
4000
5000
6000
7000
0
10
20
30
40
50
2uM ST9
1uM ST9
0.5uM ST9
0.25uM ST9
2uM SGI
1uM SGI
0.5uM SGI
0.25uM SGI
Thershold
Water (1uM ST9)

(b)

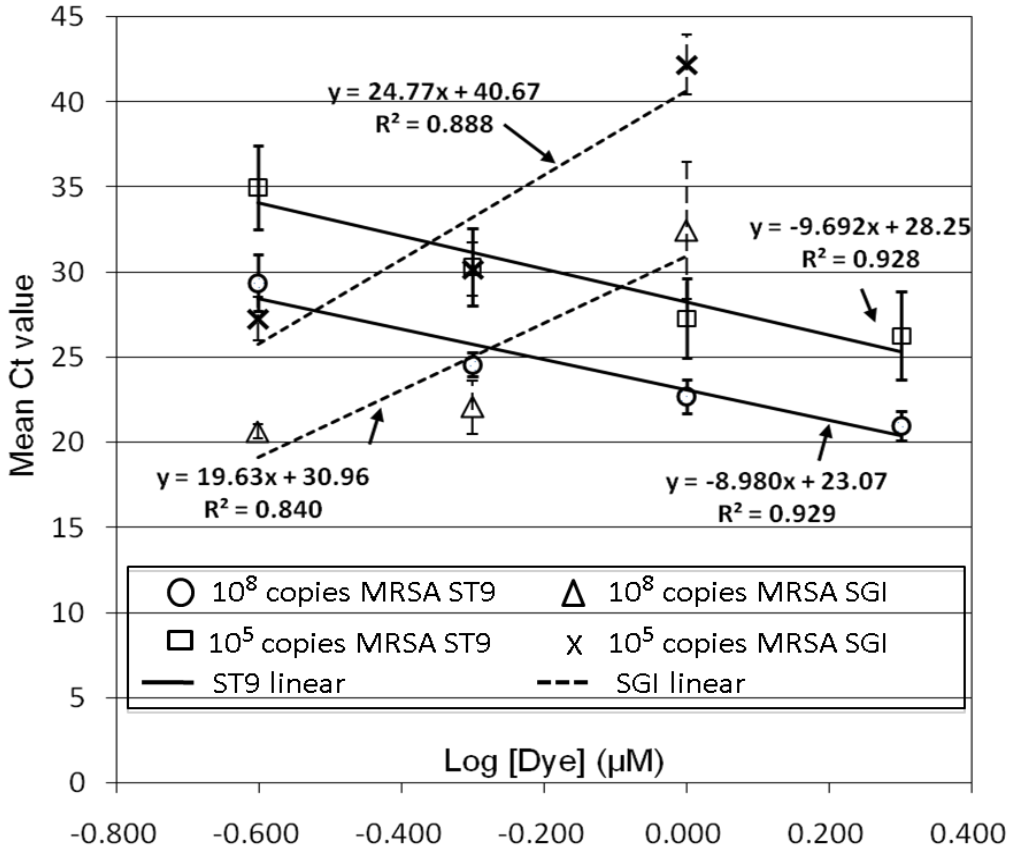
y = 24.77x + 40.67
R² = 0.888
y = -9.692x + 28.25
R² = 0.928
y = 19.63x + 30.96
R² = 0.840
y = -8.980x + 23.07
R² = 0.929
10⁸ copies MRSA ST9
10⁸ copies MRSA SGI
10⁵ copies MRSA ST9
10⁵ copies MRSA SGI
ST9 linear
SGI linear
Mean Ct value
Log [Dye] (µM)
45
40
35
30
25
20
15
10
5
0
-0.800
-0.600
-0.400
-0.200
0.000
0.200
0.400

(c)

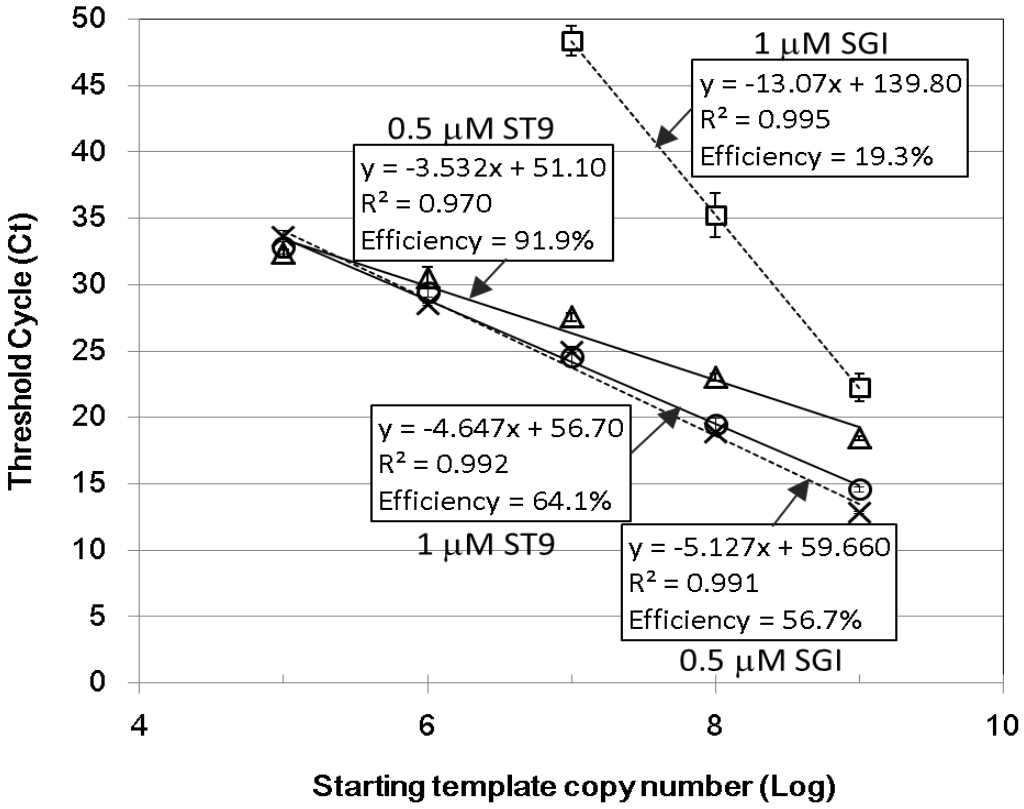

Fig. 2.3.6 RT fluoresence-based LAMP detection. (**a**) Change of relative fluorescence unit per time (baseline substracted): The initial *PVL* DNA template was 10^8 copies per reaction. Reactions were run at 65 ^{0}C for 50 min in the presence of ST9 or SGI at the concentration as indicated. (**b**) Comparison of the threshold cycle (Ct) values for two dyes at different concentrations. (n=3, mean ± SD). Linear trendlines were obtained to study the correlation coefficient. The R^2 values were 0.93 in both 10^8 and 10^5 copies of MRSA ST9 groups. (**c**) Standard curves of 1 μM and 0.5 μM ST9 or SGI were also generated. (n=4,mean ± SD). The LAMP efficiencies using 2 dyes were defined by the slopes of the standrad curves. For the Ct value, 1 cycle = 1 min.

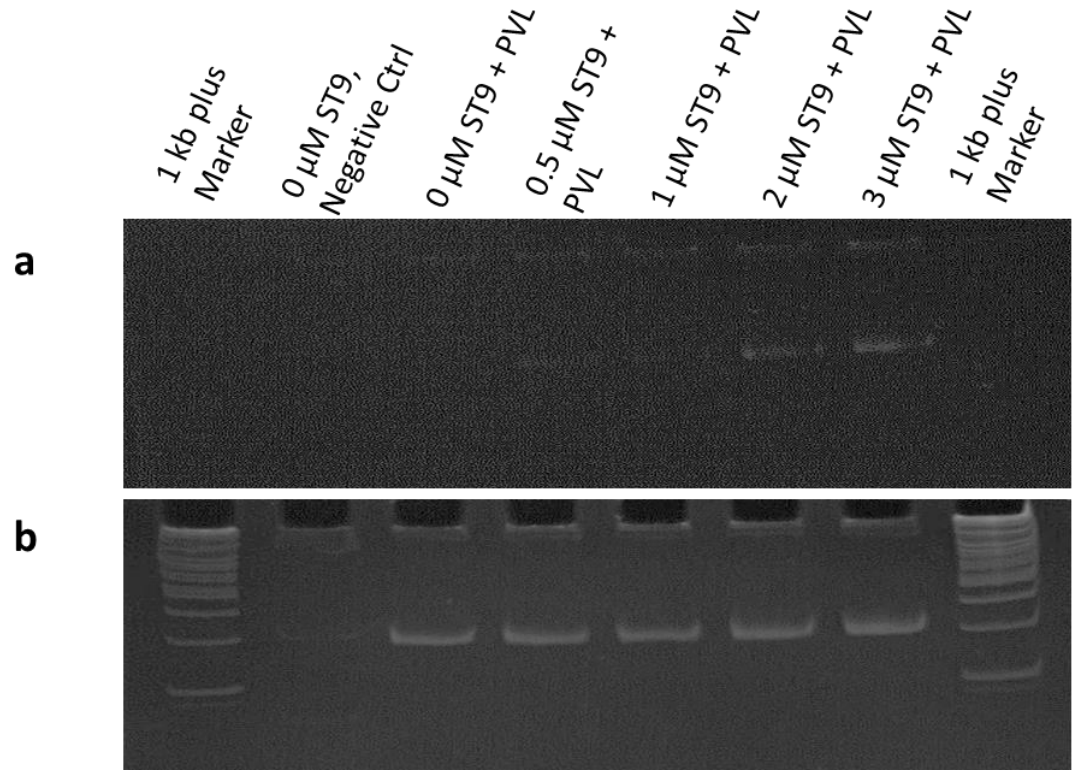

Fig. 2.3.7 12 % PA gel photos showing MRSA *PVL* gene PCR result with different concentration of ST9 dye. The DNA bands were captured before post-staining (a) or after post-staining GelRed^{TM} dye (**b**). The copies number of *PVL* DNA template was 1 x 10^{6} copies.

2.3.3Spectral- SPR method for detecting Lamplicons

In LAMP reaction, the biotin-FIP in the target DNA after amplification bound to the streptavidin immobilized on the gold surface to form the biotin-FIP-DNA stem-loop like Lamplicons. Different form PCR, the Lamplicons were of different sizes after LAMP reaction. It is expected that the longer the amplification time, the larger the amount of long Lamplicons. When bound to the streptavidin on the SPR gold surface, these larger Lamplicons would generate a bigger dip shift. In Figure 2.3.8, the RT-LAMP assay was done monitoring by SPR. The Lamplicons were immediately transferred from the 65 ^{0}C incubator and diluted with running buffer after different time intervals. To investigate the dip change of SPR-LAMP generated by the Lamplicons, 50 μL of running buffer were injected to the chamber before and after assay. According to the Figure 2.3.8, there was no dip change generated in the absence of *PVL* template although finishing 50 min LAMP reaction. On the contrary, the reaction mixture containing template gave a dip increase. It is indicated that the optical signal can be generated and distinguished by Lamplicons in SPR-LAMP assay.

As can be seen in Figure2.3.9, the change in the dip shift from the Lamplicons was: 30 min (LAMP reaction time) $\geqq$ 20 min > 0 min and negative control. The dip shift

from the 30 min reaction time was very close to that of the 20 min, suggesting that the streptavidin sites have been saturated with the Lamplicons after 20 min of reaction.

To confirm there were successful LAMP reaction in our experimental conditions, the Lamplicons used in the SPR detection were resolved by the agarose gel electrophoresis (1.5 % w/v) pre-stained with 1 X GelRed^{TM}. As can be seen in Figure 2.3.10, the Lamplicons after 30 min LAMP reaction at 65 ^{0}C showed a smear in lane 5. Obviously, the Lamplicons from the 20, 10 and 0 min Lamp reaction did not generate any GelRed^{TM} signals suggesting that the amount of these Lamplicons may not be high enough to be detected by the gel electrophoresis. Taken together, our SPR-LAMP reaction was able to generate the dip shift response and show the difference from the 0, 20 and 30 min Lamplicons. Our data therefore provide evidence to support the use of SPR-LAMP biosensor for MRSA detection, which provides a higher sensitivity than that of the conventional agarose gel electrophoresis.

(a)

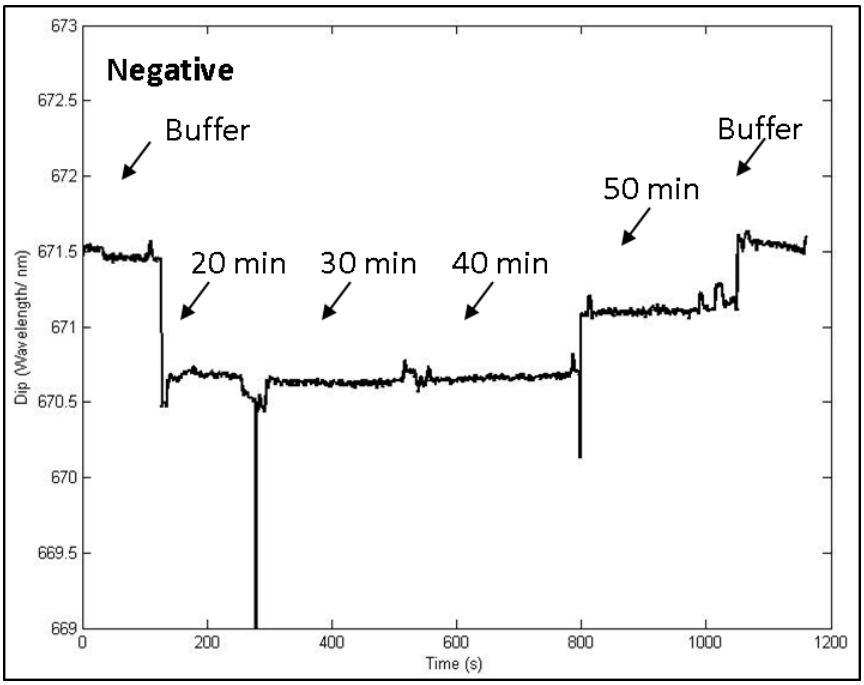
Negative
Buffer
Buffer
50 min
20 min
30 min
40 min
Dip (Wavelength/ nm)
Time (s)
673
672.5
672
671.5
671
670.5
670
669.5
669
0
200
400
600
800
1000
1200

(b)

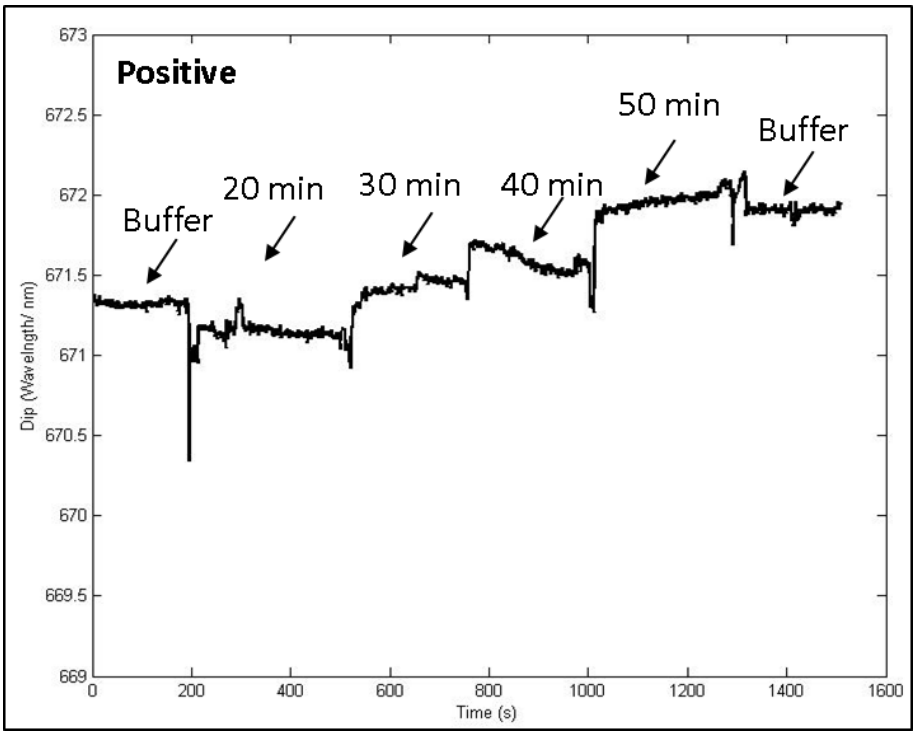
Positive
Buffer
20 min
30 min
40 min
50 min
Buffer
Dip (Wavelngth/ nm)
Time (s)
673
672.5
672
671.5
671
670.5
670
669.5
669
0
200
400
600
800
1000
1200
1400
1600

Fig. 2.3.8 RT-SPR-LAMP spectrum. LAMP reaction mixtures with (a) or without the presence of *PVL* template (b) were incubated at 65 ^{0}C. Reaction mixture was immediately diluted with the running buffer and injected into the SPR chamber after incubating for 20, 30, 40 and 50 min. 50 μL of running buffer was injected for rinsing the unbounded Lamplicons at the end of the assay.

(a)

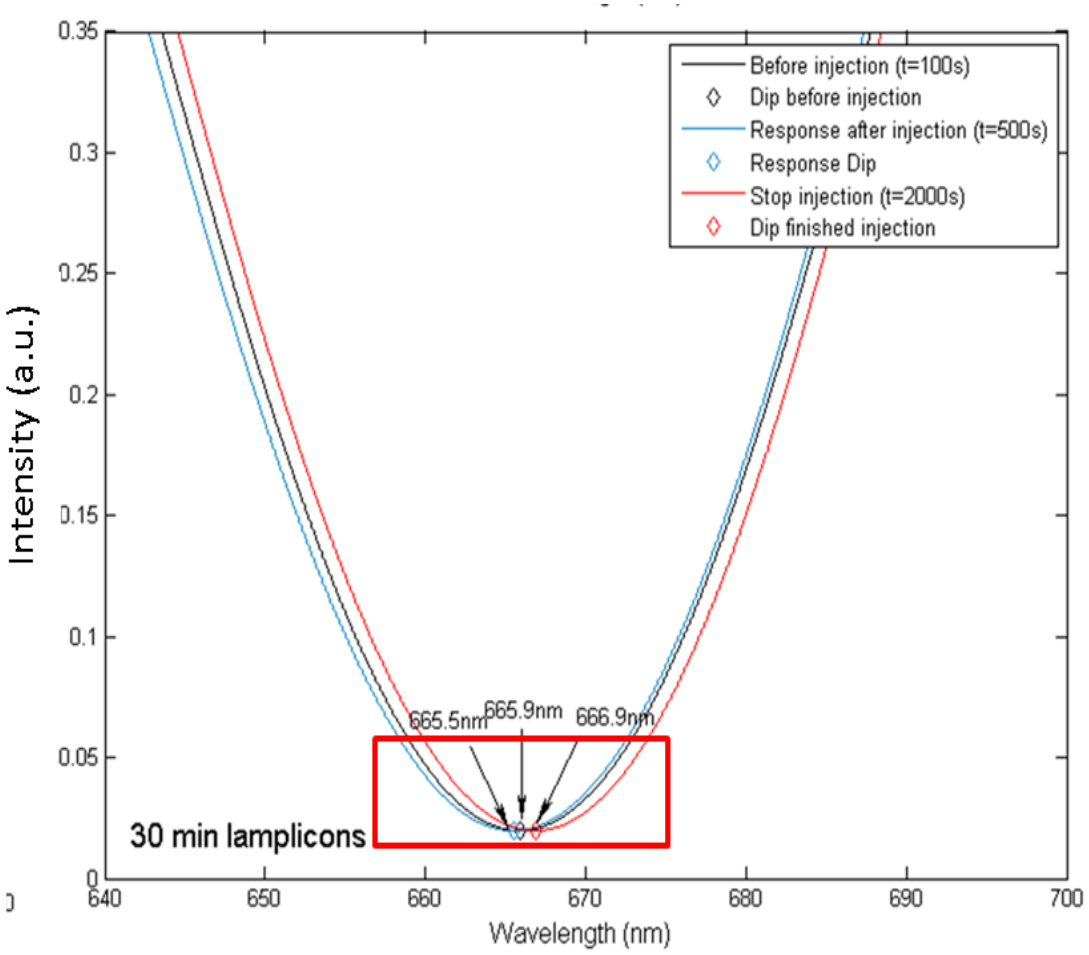

(b)

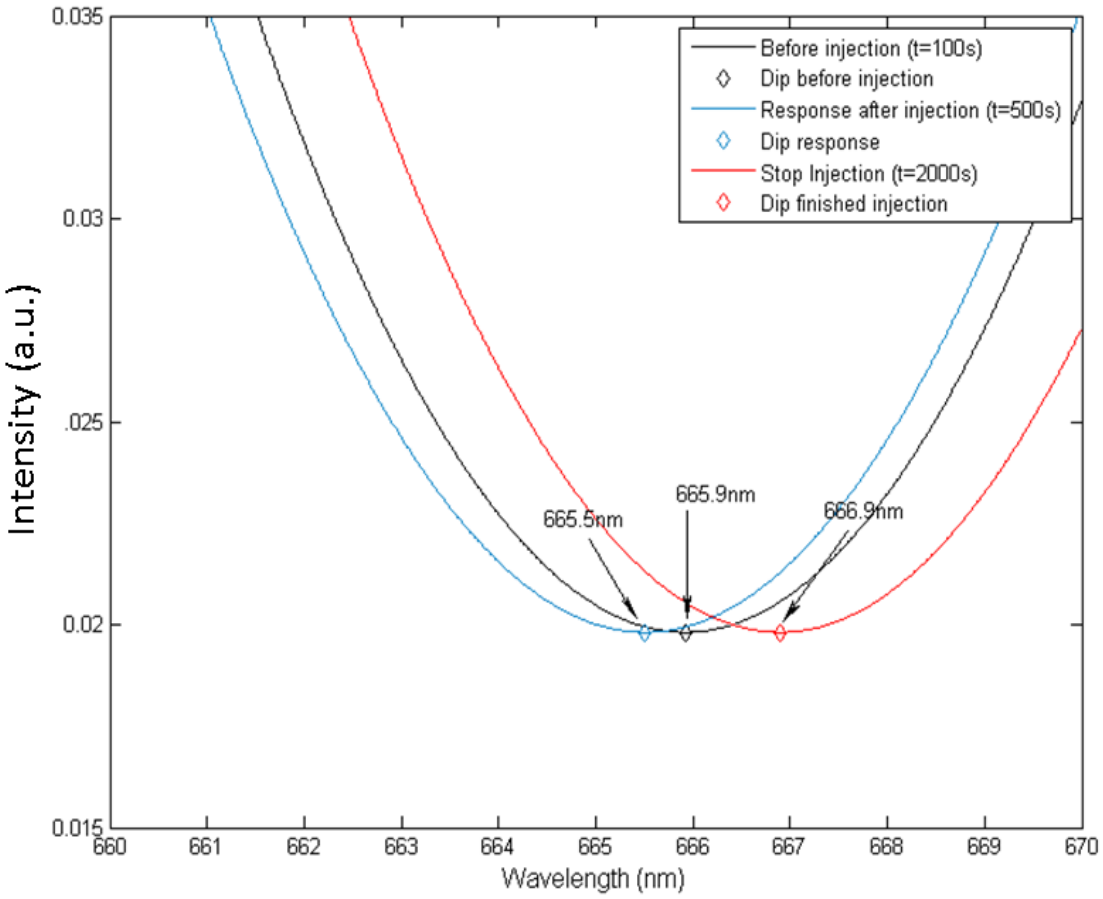
Before injection (t=100s)
Dip before injection
Response after injection (t=500s)
Dip response
Stop Injection (t=2000s)
Dip finished injection
665.5nm
665.9nm
666.9nm
Intensity (a.u.)
Wavelength (nm)
0.035
0.03
.025
0.02
0.015
660
661
662
663
664
665
666
667
668
669
670

(c)

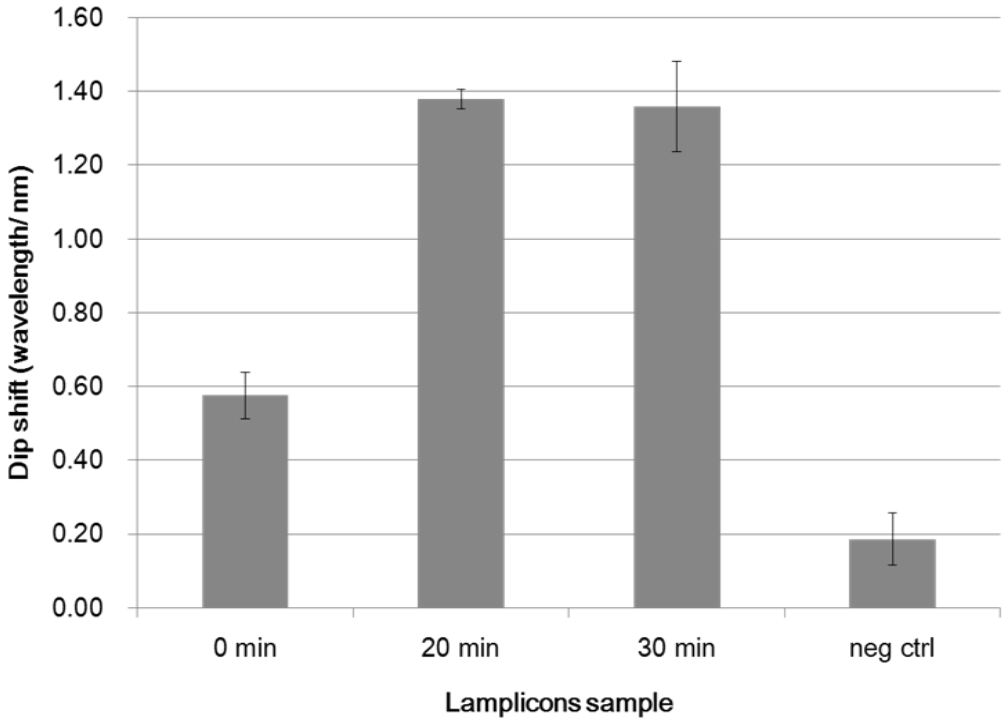

Fig. 2.3.9 SPR spectrum of MRSA *PVL* Lamplicons. (**a**) LAMP reaction using *PVL* template (10^8 copies), primers, Bst and dNTPs was performed at 65^0C for 0 (not shown), 20 (not shown) and 30 min. Lamplicons were then diluted and injected into the SPR gold chip chamber. The negative control was obtained by replacing the template with ddH_2O (30 min LAMP reaction). The black line indicated the baseline obtained before injecting samples. Blue line indicated the response after injecting samples. Red line indicated the spectrum finishing samples injection. The diamond showed the dip position in each spectrum curve. (**b**) The zoom in diagram (red box in (a)). Chart (**c**) showed the mean of the dip shift after finishing the samples injection (n=2).

	M	1	2	3	4	5
Incubation time	/	30 min	0 min	10 min	20 min	30 min
Template	/	ddH_2O	10^8 copies	10^8 copies	10^8 copies	10^8 copies

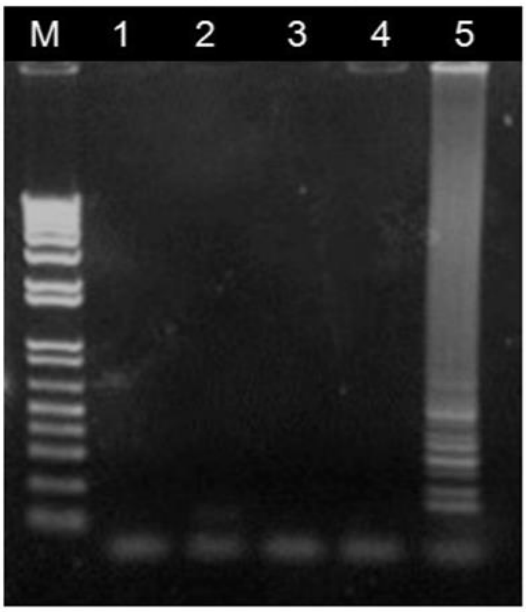

Fig. 2.3.10 1.5 % agarose gel electrophoresis of Lamplicons corresponding to SPR-LAMP detection.

2.4 Discussion

As mentioned in Section 2.1, isothermal DNA amplification is accurate, with the advantage in time saving due to the lacking in thermal cycles, when compared with the PCR. Hence, there is potential to apply the isothermal DNA amplification to develop the "point-of-care" diagnostic tool with enhanced efficiency for pathogen detection.

To develop a RT-LAMP assay, a fluorescent reporter is needed. SGI is a

commonly used fluorescent reporter in qPCR. We first tested the use of SGI for the RT-LAMP. SYBR Green was introduced in early 1990s as a fluorescent dye for probing nucleic acids [Yue et al., 1997]. SGI is ideal for probing double-stranded DNA (dsDNA) while SYBR Green II is highly selective for RNA and single stranded DNA. SGI carries two positive charges and binds to the dsDNA through two mechanisms, intercalation into the base-pairs and binding externally to the minor groove of dsDNA. Previous work showed that the latter emits stronger fluorescence after excitation and the unbound SGI exhibits very little fluorescence, 11-fold lower than that with the dsDNA binding [Zipper et al., 2004]. In fact, there are numbers of DNA binding dyes, including the SYBR, SYTO, YO-PRO, TOTO, and TO-PRO families etc., sharing different levels of binding affinities to nucleic acid. According to Gudnason et al., SYTO-82 and SYTO-13 did not show inhibitory effect on PCR, which may possible for multiplex reaction and increasing the qPCR efficiency.

During PCR, SGI remains stable during thermocycles. Also, SGI displays a wide dynamic linear range of up to 4 orders of magnitude. With these features, it is not surprising that SGI is widely used for the qPCR applications [Giglio et al., 2003]. ST9 is another commonly used dsDNA fluorescent probe which does not show preferential binding to GC rich sequences and PCR inhibition effect [Gudnason et al., 2007]. On the contrary, SGI shows preferential binding to GC rich sequences and

affecting the melting curve analysis [Gudnason et al., 2007]. However, in LAMP reactions, the primers binding regions are GC rich. Due to the above reasons, SGI perform strong binding affinity to the DNA strands in LAMP reaction, may affect the Bst DNA polymerase strand displacement activity. In PCR, Giglo et al. reported 2 μM of SGI could inhibit PCR reaction by about 22 %. The PCR reaction would be completely inhibited by SGI at the concentration of 20 μM, which also showed the dose dependent inhibitor effect on PCR reaction. It is suggested our finding of the side-effect of DNA molecular probes on LAMP reaction is sensible.

SPR has been reported for analyzing of DNA hybridization and the presence of DNA mutations [Su et al., 2008; Nelson et al., 2001; Carrascosa et al., 2009]. SPR worked as the surface absorbed the DNA probes, allowed the match and mismatch DNA sequences to hybridize, which had different binding affinities. In the previous reported study, scientists suggested the concentration of short DNA sequences (18 bp) at 10 nM could be easily detected. Actual data from the hybridization adsorption of DNA and RNA molecules result in a maximum 1 % change in the percent reflectivity [Nelson et al., 2001]. The change of reflectivity of DNA in SPR is quite small but sensible, due to the relatively small size and length of DNA is relatively smaller, to compared with the proteins or peptides.

One of the advantages using SPR as optical tool for DNA or RNA analysis is

that multiplex detection can be done by spotting different probes onto the gold chip surface, creating a DNA or RNA array [Brockman et al., 1999; Smith et al., 2001]. SPR imagine can be obtained by CCD capturing. In our study, Lamplicons after LAMP reaction can be distinguished from the one without target genes or without LAMP reaction, which had obvious Δ dip shift. As mentioned in the Chapter 1, Lamplicons are in stem-loop, with irregular length and size, which is able to increase the amount of target genes' fragments and the size of the DNA fragments. Hence, SPR-LAMP is potential for developing the multiplex DNA amplification and detection platform, which allows amplifying more than one target genes simultaneously for enlarging the signals. On the other hand, the LSPR effect of AuNPs in suspension for Lamplicons hybridization was not significant in our study. It may be due to some factors, such as the size of the AuNPs, and the concentration of salt or components in the LAMP reaction buffer. The AuNPs with the monolayer PNA or ssDNA fabrication, however, can work as the sensing beads, hybridized to matched sequences and give alternative signal enhancement in the gold chip surface [Hall et al., 2011].

References:

Aoi, Y., Hosogai, M. and Tsuneda, S. (2006). Real-time quantitative LAMP (loop-mediated isothermal amplification of DNA) as a simple method for monitoring ammonia-oxidizing bacteria. *J. Biotechnol.*, 125(4), 484-91.

Brockman, J. M., Frutos, A. G. and Corn, R. M. (1999). A multi-step chemical modification procedure to create DNA arrays on gold surfaces for the study of protein-DNA interactions with surface plasmon resonance Imaging. *J. Am. Chem. Soc.*, 121, 8044-51.

Carrascosa, L.G., Calle, A. and Lechuga, L.M. (2009). Label-free detection of DNA mutations by SPR: application to the early detection of inherited breast cancer. *Anal. Bioanal. Chem.*, 393(4), 1173-82.

Curtis, K.A., Rudolph, D.L. and Owen, S.M. (2008). Rapid detection of HIV-1 by reverse-transcription, loop-mediated isothermal amplification (RT-LAMP). *J. Virol. Methods.*, 151(2): 264-70.

Goodrich, T.T., Lee, H.J. and Corn, R.M. (2004). Enzymatically amplified surface plasmon resonance imaging method using RNase H and RNA microarrays for the ultrasensitive detection of nucleic acids. *Anal. Chem.*, 76(21), 6173-78.

Giglio, S.; Monis, P.T.; Saint, C.P. (2003). Demonstration of preferential binding of SYBR Green I to specific DNA fragments in real-time multiplex PCR. *Nucleic Acids Res., 31*, e136.

Gudnason, H., Dufva, M. et al. (2007). Comparison of multiple DNA dyes for real-time PCR: effects of dye concentration and sequence composition on DNA amplification and melting temperature. *Nucleic Acids Res.*, 35(19), e127.

Hall, W.P., Ngatia, S.N. and Van Duyne, R.P. (2011). LSPR Biosensor Signal Enhancement Using Nanoparticles-Antibody Conjugates. *J. Phys. Chem. C*

Nanomater. Interfaces., 115(5), 1410-14.

Katayama, Y., Ito, T. and Hiramatsu, K. (2001). Genetic Organization of the Chromosome Region Surrounding mecA in Clinical Staphylococcal Strains: Role of IS431-Mediated mecI Deletion in Expression of Resistance in mecA-Carrying, Low-Level Methicillin- Resistant Staphylococcus haemolyticus. *Antimicrob. Agents Chemothe.*, *45*, 1955-1963.

Kim, D.K., Kerman, K. et al. (2007). Label-free DNA biosensor based on localized surface plasmon resonance coupled with interferometry. *Anal. Chem.*, 79(5), 1855-64.

Li, H.H., Gyllensten, U.B. et al. (1988). Amplification and analysis of DNA sequences in single human sperm and diploid cells. *Nature*, 335, 414-417.

Mori, Y. (2001). Detection of Loop-Mediated Isothermal Amplification Reaction by Turbidity Derived from Magnesium Pyrophosphate Formation. *Biochem. Biophys. Res. Commun.*, *289*, 150-154.

Mori, Y., Kitao, M. et al. (2004). Real-time turbidimetry of LAMP reaction for quantifying template DNA. *J. Biochem. Biophys. Methods*, 59, 145-47.

Nelson, B.P., Grimsrud, T.E. et al. (2001). Surface plasmon resonance imaging measurements of DNA and RNA hybridization adsorption onto DNA microarrays. *Anal. Chem.*, 73(1), 1-7.

Notcovich, A.G., Zhuk, V. and Lipson, S.G. (2000). Surface plasmon resonance phase imaging. *Appl. Phys. Lett.*, 76, 1665-1667.

Notomi, T., Okayama, H. et al. (2000). Loop-mediated isothermal amplification of DNA. *Nucleic Acids Res.*, 28, 1-5.

Owczarzy, R., Moreira, B.G. et al. (2008). Predicting stability of DNA duplexes in solutions containing magnesium and monovalent cations. *Biochemistry*, 47,

5336-5353.

Pfaffl, M.W. (2001). A new mathematical model for relative quantification in real-time RT-PCR. *Nucleic Acids Res.*, 29, e45.

Saiki, R.K., Chang, C.A. et al. (1988). Diagnosis of sickle cell anemia and beta-thalassemia with enzymatically amplified DNA and nonradioactive allele-specific oligonucleotide probes. *N. Engl. J. Med.*, 319, 537-541.

Scarano, S., Mascini, M. et al. (2010). Surface plasmon resonance imaging for affinity-based biosensors. *Biosens. Bioelectron.*, 25, 957-66.

Smith, E.A., Wanat, M.J. et al. (2001). Formation, spectroscopic characterization and application of sulfhydryl-terminated alkanethiol monolayers for the chemical attachment of DNA onto gold surfaces. *Langmuir*, 17, 2502-07.

Su, X. and Kanjanawarut, R. (2009).Control of Metal Nanoparticles aggregation and dispersion by PNA and PNA-DNA complexes, and its application for colorimetric DNA detection. ACS Nano. 3(9): 2751-59.

Su, X., Teh, H.F. et al. (2008). Femromol SPR detection of DNA-PNA hybridization with the assistance of DNA-guided polyaniline deposition. *Biosens. Bioelectron.*, 23(11), 1715-20.

Tomita, N., Mori, Y. et al. (2008). Loop-mediated isothermal amplification (LAMP) of gene sequences and simple visual detection of products. Nat. Protoc., 3(5), 877-82.

Wang, R., Tombelli, S. et al. (2004). Immobilisation of DNA probes for development of SPR-based sensing. *Biosens. Bioelectron.*, 20(5), 967-74.

Yue, S.T., Singer, V.L. et al. (1997). Substituted Unsymmetrical Cyanine Dyes with Selected Permeability. US-patent 5658751.

Zipper, H., Brunner, H. et al. (2004). Investigations on DNA intercalation and surface

binding by SYBR Green I, its structure determination and methodological implications. *Nucleic Acids Res.*, 32, e103.

Chapter 3 Novel Tunable Resistive Pulse Sensing (TRPS) technique on MRSA DNA detection

3.1 Introduction

Nanoparticle is usually the particles with the size between 1 to 100 nm [Patel et al., 2008]. Rather than just focusing on physical and chemical studies, scientists pay more attention in biological and medical applications, including biosensors development in detecting proteins, DNA or pathogens [Salata 2004]. We herein focus on the use of gold nanoparticles (AuNPs) for biosensing. Due to the easy surface modification for DNA immobilization, optical effect and fluorescent-label free characters, AuNPs become widely used for nanoscale DNA analysis [Harriman and Leake 2011]. By thiolated DNA or biotin-avidin conjugation, DNA probes can be easily attached on the AuNPs. The specific sequence of target DNA can be hybridized with the AuNPs and form aggregations, which can be applied for SNP detection [Bao et al., 2005].

According to the pervious chapter, it is found that the traditional DNA binding dyes, SGI and ST9 shows different levels of inhibition to the LAMP reactions. It is suggested that the non-fluorescence detection may be suitable for real-time LAMP monitoring. To eliminate the usage of fluorochrome labeling, Tunable Resistive Pulse

Sensing (TRPS) was applied in the detection of Lamplicons, which are conjugated with the AuNPs. The principle of TRPS is based on a transient decrease of electrical current in the ionic current flow when a particle passes through a nanopore in the TRPS system. TRPS allows the particle-by-particle assessment of complex mixtures, which is similar to the working principle of flow cytometry. The advantage of using TRPS is that each of the AuNPs-Lamplicons assemblies can be analysis by its size and surface charge. Also, the concentration of the assemblies in the reaction mixture can be detected. By using the concept of TRPS, we can accurately quantify the Lamplicons and target gene in a fast and simple fashion.

In this chapter, our focus is on the use of AuNPs with TRPS in biosensor development, based on their size and optical properties. AuNPs have been widely used as probes and carriers for various biomedical applications (e.g. localized surface plasmon resonance) [Feldheim and Foss, Jr., 2001; Stewart et al., 2008]. For example, binding or hybridization events such as antibody-antigen interaction, DNA-DNA or DNA-PNA (peptide nucleic acid) can be determined on the basis of dispersion and aggregation of the AuNPs for the presence of disease markers [Sato et al., 2003; Pingarron et al., 2008; Kanjanawarut and Su, 2009; Upadhyayula 2012]. One of the DNA sequences modified AuNPs methods is polyvalent DNA gold nanoparticles,

co-discovered by Mirkin et al. and Paul Alivisatos [Mirkin et al., 1996]. With the interaction between gold and thiols (-SH), single-stranded DNA can form layer surrounding the AuNPs. Between the AuNPs, the phosphate backbone of DNA leads to the negative charge repulsion, which keeps the DNA strands out to the solution. The DNA strands can provide specific sequences targeting to the target genes [Mirkin et al., 1996]. Target DNAs can interact with the AuNPs and form aggregates, reporting colorimetric change in a highly sensitive and specific manner [Storhoff et al., 2000; Rho et al., 2009; Li et al., 2002].

Tunable Resistive Pulse Sensing (TRPS) is a non-optical AuNPs-DNA analytical method. The nanopore fabricated on an elastomeric membrane enables it to be tunable in size to suit and optimize analysis conditions thus improving the sensitivity, especially for assays where aggregates of different sizes are formed. Furthermore, the direct measure of particle counts and the rate of blockade events are directly proportional to particle concentration [Kozak et al., 2011; Henriquez et al., 2004; Roberts et al., 2012; Willmott et al., 2010].With the usage of TRPS, physical properties such as concentration, size, shape and surface charge of objects in suspension can be investigated rapidly and in a cost-effective manner [Kozak et al., 2011; Liu et al., 2010; Howorka and Siwy, 2009; Zhang et al., 2009]. These highlight

the potential of utilizing nanopore-based devices as a rapid sensing output platform.

In brief for the TRPS, two liquid compartments containing aqueous electrolytes are separated by a nanopore, and a constant voltage is applied between the liquid compartments. When the particle passes through the nanopore, it generates ionic resistance in the aperture. The transient increase in the resistance causes a transient decrease in the ionic current flowing through the nanopore. This change in the ionic resistance is known as ‘resistive pulse’ or ‘blockade event’ [Vogel et al., 2011]. The amplitude or the magnitude of the resistive pulse is a function of the volumetric size of the particle, while the width of the pulse (blockade duration) measures the time taken for the particle to pass through the pore, which is related to the shape and charge of the particle [Branton et al,, 2008; Kozak et al., 2011; Liu et al., 2010; Howorka and Siwy, 2009; Zhang et al., 2009]. It also allows particles to be counted during the passage of the particle through the pore. However, there is limitation in the size range of studying particles or structures in the fixed diameter nanopore TRPS system. Coulter counter, a widely accepted apparatus, due to the relatively large pore size, the particles with size less than 400 nm are undetectable [Roberts et al., 2012]. The pore size in Coulter counter limits the application in directly detection of biomolecules, such as protein, antigens and DNA.

Due to the above limitations, manufactures pay efforts to modify the size-specific synthetic pores. Nanopores with diameters between 2 to 500 nm can be fabricated by using different materials, including carbon nanotubes, silicon nitride or polymers etching by particle beams. In this study, we used a tunable nanopore instrument, qNano for the TRPS assay. It is a scanning ion occlusion spectroscopy (SIOS) device with a real-time stretchable polyurethane nanopore membrane. The pore is fabricated by mechanically puncturing a ~ 0.7 mm thick polyurethane membrane, with a conical shape elastic pore (Figure3.1.1a). The diameter of the pore can be controlled by stretching, in order to gate the threshold size for different biomolecules passing through [Roberts et al., 2010, 2012] (Figure3.1.1b).

(a)

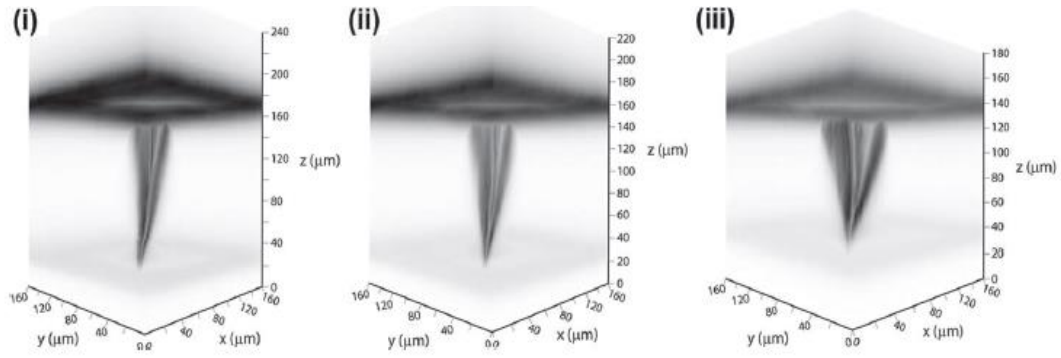

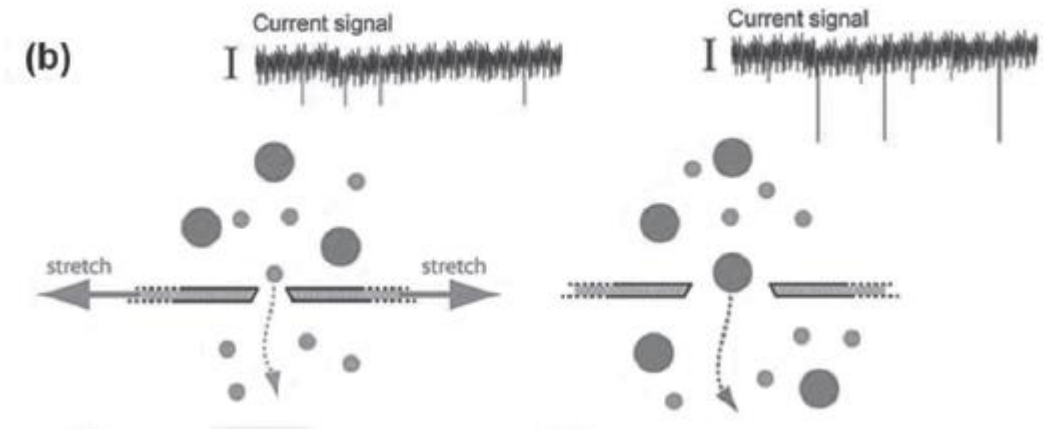

Fig. 3.1.1 (a) Confocal image of the conical pore with increasing macroscopic stretch (i) 0 mm, (ii) 5 mm and (iii) 10 mm. (b) Schematic diagram shows the principle of TRPS by stretching the membrane to gate the particles. [Robert et al., 2010]

The aim of the study in this chapter is to develop a novel detection method based on LAMP, TRSP and AuNPs. As a continuous study of Chapter 2, MRSA *PVL* gene was used as the study model.

The concept of quantitative TRPS is straightforward and has been well established ever since the 1950s with the patent of the Coulter Principle [Coulter 1953] and in the current resurgence of the development of pores for DNA-sequencing purposes [Branton et al., 2008]. To do the TRPS assay, a nanopore or micropore device is required. Compared with the other commonly used

nano-biotechnological sensing techniques, such as electron microscopy, flow cytometry, NP tracking analysis and dynamic light scattering, the nanopore TRPS system shares lower cost, simplicity in both design and implementation, and the capacity for true, label-free molecular detection [Roberts et al., 2012].

To demonstrate the use of this technique to detect disease marker, we described here the employment of AuNPs, TRPS technique and LAMP to detect the DNA of the *PVL* toxin gene of the MRSA [Johnsson et al., 2004]. As mentioned before, LAMP is a technique that amplifies DNA at one single temperature using the Bst DNA polymerase. The process of LAMP is available in the animation in the following web site (http://loopamp.eiken.co.jp/e/lamp/anim.html). When Lamplicons containing specific biotinylated primers are mixed with avidin-functionalized AuNP1s, AuNP1-Lamplicons are obtained via strong biotin-avidin interactions. As a part of diagnostic design, the assay sensitivity and specificity were further extended by utilizing a second AuNP (AuNP2) that was functionalized with thiolated B2 primers on its surface in order to hybridize with the loop region of the Lamplicons. After specific DNA-DNA hybridization, supra-AuNP1-Lamplicons-AuNP2 assemblies are formed [Basu et al., 2007; Alivisatos et al., 1996]. Figure 3.1.2 depicts the working principle of the LAMP-based AuNPs in combination with TRPS for the

detection of target DNAs. The setup of TRPS utilizing a nanopore sensor is illustrated in Figure 3.1.2c, and detailed experimental steps were reported in detail elsewhere [Roberts et al., 2012; Willmott et al., 2010; Low et al., 2011].

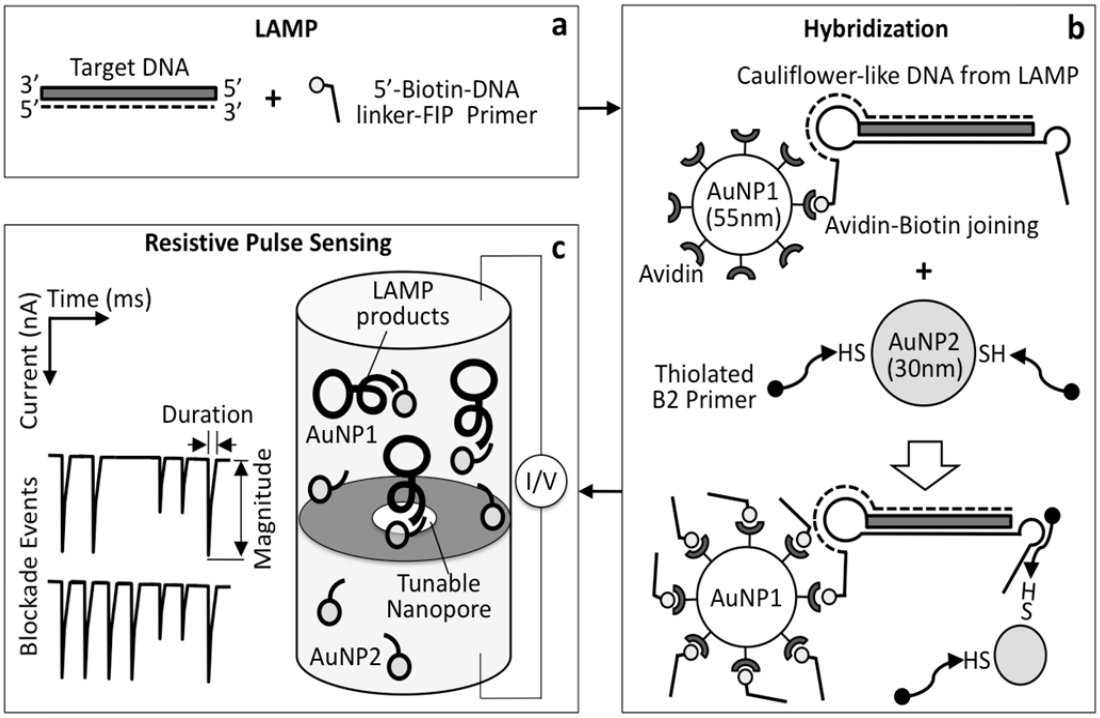

Fig. 3.1.2 Principle of the TRPS for detecting MRSA DNA with the combination of LAMP and AuNPs. (**a**) The target MRSA *PVL* gene is amplified by LAMP, with the use of 5'- Biotin linked FIP primer. (**b**) The Lamplicons are in cauliflower-like structure, conjugated with avidin functionalized AuNP1 (55 ± 2 nm). AuNP2 with thiolated B2 primer modified (30 ± 1.5 nm) is hybridized with the AuNP1-Lamplicons loop region to form assemblies. (**c**) The assemblies are subjected to TRPS system. The pulse magnitude and duration time are recorded.

3.2 Materials and Methods

3.2.1 Materials

3.2.1.1 Bacterial Cell Line

L. casei (ATCC 334) and *PVL*-positive *S. aureus* MW2 strain (ATCC BAA-1707) were purchased from American Type Culture Collection (ATCC).The genomic DNA (gDNA) of *S. aureus* Mu50 was obtained from ATCC (ATCC 700699).

3.2.1.2 Buffers and Reagents

All the buffers and reagents were prepared by dissolving chemicals into double distilled water (ddH_2O). The pH value was adjusted with HCl or NaOH.

Phosphate buffered saline (PBS) was composed of 136mMNaCl, 2.7 mM KCl, 1.5mM KH_2PO_4 and 8mM Na_2HPO_4. PBS is titrated to pH 7.4, and then sterilized by autoclave. PBS was stored at room temperature.

5X TBE Buffer was composed of 57 g Tris base, 27.5 g boric acid and 20 mL 0.5 M EDTA (pH 8.0), dissolved in 1 L of ddH_2O.

TRPS running buffer was composed of 10 mM sodium phosphate buffer containing 200 mM of NaCl.

12% Poly-acrylamide (PA) Gel was composed of 40% (v/v) acrylamide (30%) solution, 10% (v/v) 5X TBE buffer, 0.05% (w/v) ammonium per sulfate and 0.012 %

(v/v) TEMED. The buffer was freshly prepared for each experiment.

6X DNA loading dye was composed of 30% (v/v) glycerol, 0.25% (w/v) bromophenol blue and 0.25% (w/v) xylene cyanol FF. The dye was stored at 4 ^{0}C.

3.2.2 Methods

3.2.2.1 MRSA *PVL* DNA template preparation

Overlapping PCR was used to prepare *PVL* DNA template. Reaction was performed as described as Section 2.2.2.1.

3.2.2.2MRSA genomic DNA extraction

S. aureus MW2 and *L. casei* were cultured respectively in the nutrient broth and lactobacilli MRS broth at 37 ^{0}C overnight according to ATCC instructions. *E. coli* K12 was cultured at 37 ^{0}C in the LB broth overnight. The gDNA was extracted from 1 mL of overnight culture by Wizard® SV Genomic DNA Purification System (Promega).

The gDNA of *S. aureus* Mu50 was dissolved in nuclease-free water. The Mu50 gDNA was amplified with IllustraGenomiPhi V2 DNA Amplification Kit (GE Healthcare) and stored at -20 ^{0}C. The concentration of MW2 gDNA and Mu50 gDNA were measured by NanoDrop 2000 (Thermal Scientific), followed by dilution with nuclease-free water and stored at -20 ^{0}C for long-term storage.

3.2.2.3 PCR reaction

PCR reaction was performed similar as the overlapping PCR procedures as described in Section 2.2.2.2. The total volume of reaction mixture is 25 μL, with either F3 and B3 primers or Forward and Reverse primers for amplification.

Forward (5'→3'): GTCCAAATTTATTTGTTGGATATAAACCATATAGTCAA

Reverse (5'→3'): CATATCAATTATGTCCTTTCACTTTAATTTCATGA

3.2.2.4 LAMP reaction

LAMP reaction was done as described in Section 2.2.2.2.

3.2.2.5 Gel electrophoresis

PCR Amplicons and LAMP Lamplicons were detected by either Agarose gel (1.5% w/v) or 12% PA gel electrophoresis. Agarose gel electrophoresis was performed by loading 3 μL of Lamplicons or Amplicons into each well. The gel was then run for 20 min with constant voltage 120 V. The agarose gel was pre-stained with GelRed^{TM} nucleic acid gel stain (Biotium) for DNA visualization. For the 12 % PA gel electrophoresis, it was performed by loading 10 μL of Lamplicons or Amplicons into each well. The gel was run for 1 hr with constant voltage 120 V, followed by post-stained with GelRed^{TM} nucleic acid gel stain.

3.2.2.6 Synthesis of AuNPs

AuNPs were synthesized using standard sodium citrate reduction method as described [Turkevich et al., 1953; Kimling et al., 2006]. Typically, boiling MilliQ water (40 mL) was mixed with 2 mL of 10 mM $HAuCl_4 \cdot 3H_2O$ (> 49 % Au) and 1 mL of sodium citrate (1 %, w/v). The mixture was kept boiled, stirred well for 10 min and then cooled down to room temperature. To grow colloidal AuNP1s, a two-step hydroxylamine hydrochloride seeding process was performed according to Brown's protocol [Brown et al., 2000]. Briefly, 55 mL of AuNPs (as seeds) were mixed with 50 mL of distilled water, 1 mL of 10 mM $HAuCl_4 \cdot 3H_2O$ and 375 μL of 0.2 M $NH_2OH \cdot HCl$. The mixture was stirred at room temperature until no color change. The solution was then used as seeds for further colloid AuNP growing. The final product was AuNP1s.

The size and concentration of AuNP1s and AuNP2s were confirmed by TEM and UV-Visible spectrophotometry. From the TEM analysis, the size of the two AuNPs was confirmed to be 55 ± 2 nm (AuNP1) and 30 ± 1.5 nm (AuNP2), consistent with that reported elsewhere for the same standard preparation (Figure 3.2.2).

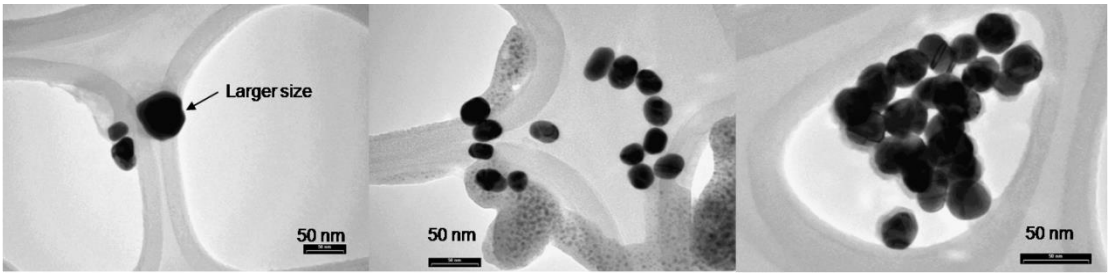

Fig. 3.2.2 TEM micrograph showing the exact sizes of AuNP1 and AuNP2.

3.2.2.7 AuNP1s functionalized with avidin

To conjugate DNA products with biotin-FIP probes on to the surface of AuNP1s after LAMP, AuNP1s were functionalized with avidin as described [Olofsson et al., 2003]. Avidin (0.05 mg) was added into NaCl solution (5 mM) with AuNP1s. The mixture was incubated at room temperature for 30 min. After removing excess avidin by centrifugation twice at 2,000 g at 4 ^{0}C for 60 min, AuNP1s were re-suspended in 250 μL of 5 mM NaCl and stored at 4 ^{0}C.

3.2.2.8 AuNP2s functionalized with thiol-DNA probe

The sequence of the LAMP probe B2-LB was complimentary to the target DNA with a 5'-ATAT-3' linker with C6 thiolation at the 5'-end (Sangon Biotech). The 5'-thiol-B2-LB probes were then diluted by 10 mM Tris-HCl (pH 7.4) with 0.1 μM DTT.

Functionalization of AuNP2s with 5'-thiol-B2-LB probe was performed as reported elsewhere [Zhao et al., 2009]. Briefly, the citrate-stabilized colloidal AuNP2s were incubated with dATP in a molar ratio of 1000 in a mixture of 50 mM NaCl and 10 mM sodium phosphate buffer (pH 7.4) at room temperature for 15 min. Subsequently, 2 nmoles of 5'-thiol-B2-LB probe was subsequently added into the AuNP2s mixture and the mixture was incubated at 60 ^{0}C for 3 hr. Excess dATP and thiol-DNA were removed by centrifugation (11,000 g, 15 min) twice. Finally, the functionalized AuNP2s were re-suspended in 50 mM NaCl and stored at 4 ^{0}C.

3.2.2.9 Tunable Resistive Pulse Sensing (TRPS) Assay

A commercially available tunable nanopore platform (qNano, IZON Science) was used for the TRPS assays. The setup and pore setting were calibrated with certified particle standards (Bangs Lab and IZON) with a sensing pore membrane (Part # NP200A, or # NP400A) that was adjusted to the desired setting (XY49 mm). The working principle of the nanopore platform, membrane structure and detailed experimental steps for TRPS were reported in detail elsewhere [Henriquez et al., 2004]. Briefly, electrolytes and samples were pipetted into the top and bottom fluidic electrochemical chambers. For assay measurements, AuNP1s with avidin (50 pM, 7

μL) were mixed with LAMP products (5 μL) and AuNP2s with the thiol-DNA probes (150 pM, 7 μL). The mixture was then adjusted to 50 μL by TRPS running buffer. Thirty-five microliter of AuNPs-LAMP mixtures were injected into the top electrochemical chamber. Each experiment was measured for at least 10 min and data were captured and analyzed with the V2.2 IZON software.

3.2.2.10 Scanning electron microscopy (SEM)

For scanning electron microscopy, the samples were characterized by SEM (FEI Quanta 400 FEG microscope). AuNPs-LAMP complexes were desalted with distilled water by centrifugation at 14,000 g for 20 min. Subsequently, 5 μL of the suspension was dried on a gold-coated silicon substrate (thickness 30 nm) at room temperature overnight.

3.2.2.11 Statistical calculation

Data were compared by one-way ANOVA. Results were expressed as mean ± SD (n=3), and *p*-values less than 0.05 were considered statistically significant.

3.3 Results

3.3.1 Demonstration of tunable pore in TRPS

In TRPS assay, a tunable pore can control the diameter of the nanopore by stretching and relaxing the arms of elastomeric nanopore membrane. By stretching the pore, nanopores will have the size similar to that of particles being detected. It is allowed to measure the larger size particles or maximized the resistive pulse for the smaller particles (Eldridge et. al). In Figure 3.3.1, when tuning the nanopore, by pulling the arms of nanopore membrane from 47.00 mm to 49.00 mm, the blockade duration produced by 207 nm standard particles was extended. At the same time, there was no change in the signal magnitude. For the larger size standard particles, which was in 355 nm, could gave a larger magnitude to compare with the 207 nm one (Figure3.3.1b, d).

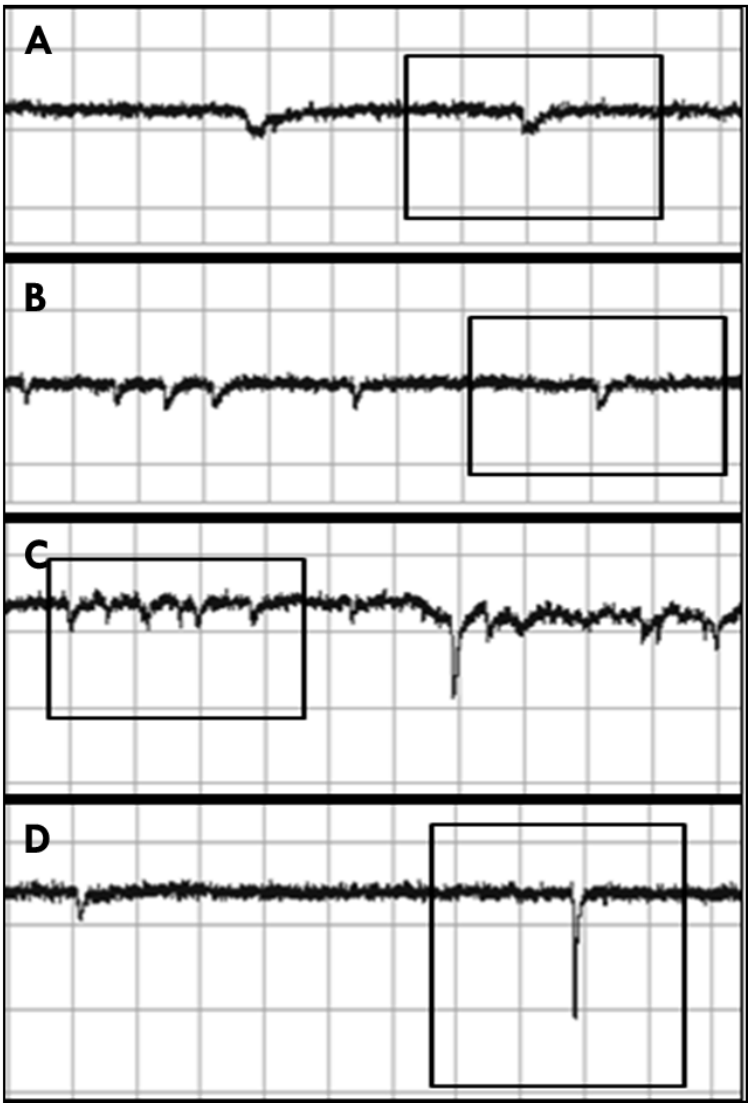

Fig. 3.3.1 Snapshot capturing raw data of standard particles passing through NP200 nanopore membrane in TRPS at the constant voltage supplied. The membrane was stretching to (**A**) 47.00 mm; (**B**) 48.00 mm; or (**C**) 49.00 mm respectively. The mean size of the standard particles was in 207 nm. (**D**) Signal produced from 355 nm particles when passed through NP200 membrane at length stretching to 48.00 mm.

3.3.2 Concentration estimation of the hybridization between Lamplicons and designed AuNPs system

To prove the existence of the hybridation of specific Lamplicons and designed AuNPs system, TRPS was chosen as the quantification method. The concentrations of the AuNPs in the presence of Lamplicons amplified from different initial copy numbers of *PVL* DNA templates were estimated within a constant time (30 min) (Figure3.3.2). The nanopore membrane in NP200 was chosen, which allowed the particles in size from 50 to 800 nm passing through the membrane. Due to the background noise and the nature aggregates, the larger aggregates with size > 175 nm was chosen for data enrichment. As shown in Figure 3.3.2, there were obvious elevations of the total assemblies concentration in the groups with the presence of Lamplicons (10^4 copies and 10^8 copies of initial *PVL* DNA templates), to compare with groups without Lamplicons and negative control (0 copy of initial *PVL* DNA template). At the same time, the concentration peaks of the assemblies' sizes were shift from right to left when increasing the initial *PVL* DNA templates. The result indicated it is more favorable for the assembly populations forming larger size with the involvement of Lamplicons. The size of the most abundant assemblies was in the following order: AuNPs with Lamplicons from 10^8 copies *PVL* DNA templates (about 300 nm) > 10^4 copies *PVL* DNA templates (250 – 300 nm) > 0 copy *PVL*

DNA template (Negative control) and AuNPs only (about 200 nm).

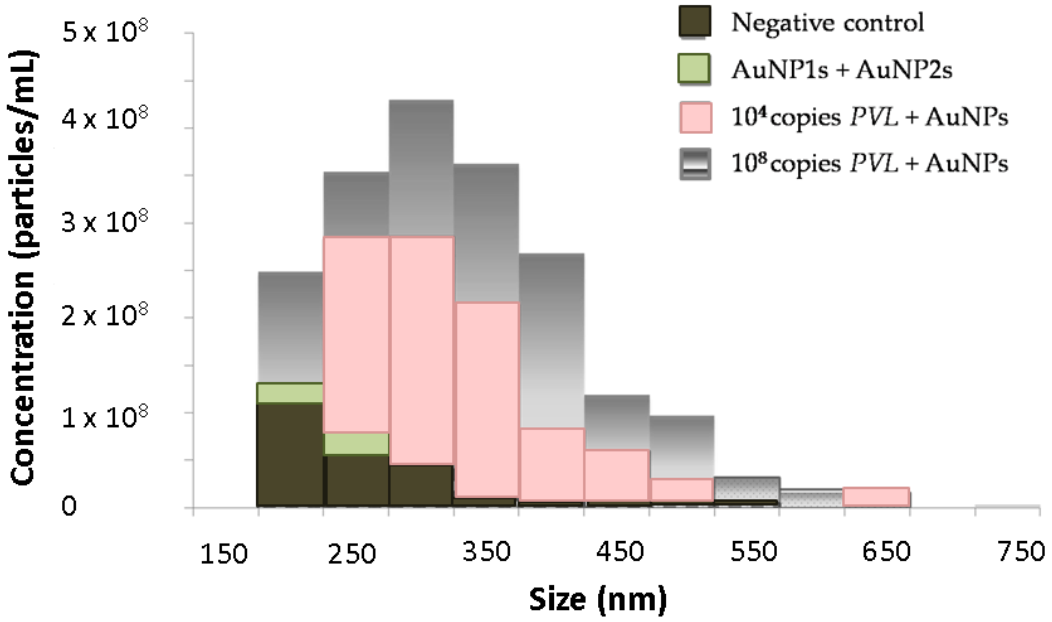

Fig. 3.3.2 TRPS assay to detect the concentration of the AuNPs assemblies by recording for 30 min. The nanopore membrane was chosen as NP200. The measuring threshold was chosen as 175 nm.

3.3.3 TRPS 2D dot plot analysis

With the above finding, the combination of LAMP, AuNPs system and TRPS can be utilized as a tool of DNA detection. It is interesting to study the relationship between the amounts of target DNA and AuNP-Lamplicons assemblies' size / shape, in order to establish a novel quantification method for DNA detection. Similar to the flow cytomteric (FCM) analysis, a 2D dot plotting can also be applied on TRPS analysis. As shown in the schematic diagram (Figure 3.3.3), each dot represents the individual blockade event duration time and its corresponding size can be shown in a 2D dot plot graph. Particles with irregular shape or increasing in surface charge have a longer duration time. The population of particles would be focus on the upper region (either upper-left (UL) or upper-right (UR) region). The X-axis represents the size of particles, which means the larger size of particles locate at the right hand size (RHS) of the graph. It was expected the after linking with Lamplicons, AuNP-Lamplicons would become clusters, which had size elevation and were less colloid in shape. The population would be shift from lower-left (LF) region to UR region.

The particle distribution of AuNP assemblies linked with Lamplicons among different amounts of *PVL* DNA templates were shown in Figure3.3.4. For each sample, particles were detected for 10 min in TRPS system. In the negative control

(Figure 3.3.4a), there was no *PVL* DNA template and Lamplicons, the population of assemblies was mainly located at the LF region. When the initial *PVL* DNA template increased from 10 to 10,000 copies (Figure3.3.4b-e), more and more Lamplicons were produced and conjugated with AuNPs. There was a significant increase of the number of AuNP-Lamplicons assemblies which differed in size and regularity. With the increase in target DNA, an increase in the number of larger sized assemblies was detected. The blockade peak duration of these larger sized assemblies had (on average) increased too. A change to the UR corner would indicate a possible lowering in charge density of ~10 to 20 times. By visual inspection of the number of peak durations, the larger sized assemblies at LR did increase in peak durations, i.e. 1.5 to 5 times higher than the peak durations of the smaller assemblies (of bottom left corner). This indicates a lowering in charge density of the larger assemblies, consistent with particles binding together to forming aggregates.

To compare the data between each group, the experiments were repeated three times, which were shown in Figure 3.3.5. It was observed that the initial *PVL* DNA target copy numbers affected the number of assemblies recorded in TRPS. In Figure 3.3.5a, the total number of blockade events and particles lager than 350 nm increased gradually when increased the copy number of DNA. The rate of formation of supra-assemblies appeared to have approximately double or triple when the DNA

copies were increased from 0 to 100 or 1000, respectively in terms of the number of assemblies in the two right quadrants of large supra-assemblies formed (Figure 3.3.5a, white bars). A close inspection of the data shows a noticeable gap in the total number of the supra-assemblies when the DNA copy number increased from 10 to 100 (Figure 3.3.5a, grey bars). These observations appear to indicate that as low as 10 to 100 copies of DNA is the limit of detection (LOD) under the current experimental setting (Figure 3.3.5a). The delta distribution histograms show the number of differently sized assemblies that were formed above the background after DNA hybridization (Figure 3.3.5b). A large amount of 200 to 550 nm assemblies was found in the supra-form that was abundantly present in all DNA hybridized samples. At a low DNA level of 10 copies, an appreciable amount of assemblies were formed that were around 200 nm. Also, an increase in DNA number copies from 10 to 10,000 increased the number of larger size assemblies present in the population (Figure 3.3.5b). An abundant proportion of particular sized assemblies might be due to a stable configuration of the AuNP1-Lamplicons-AuNP2.

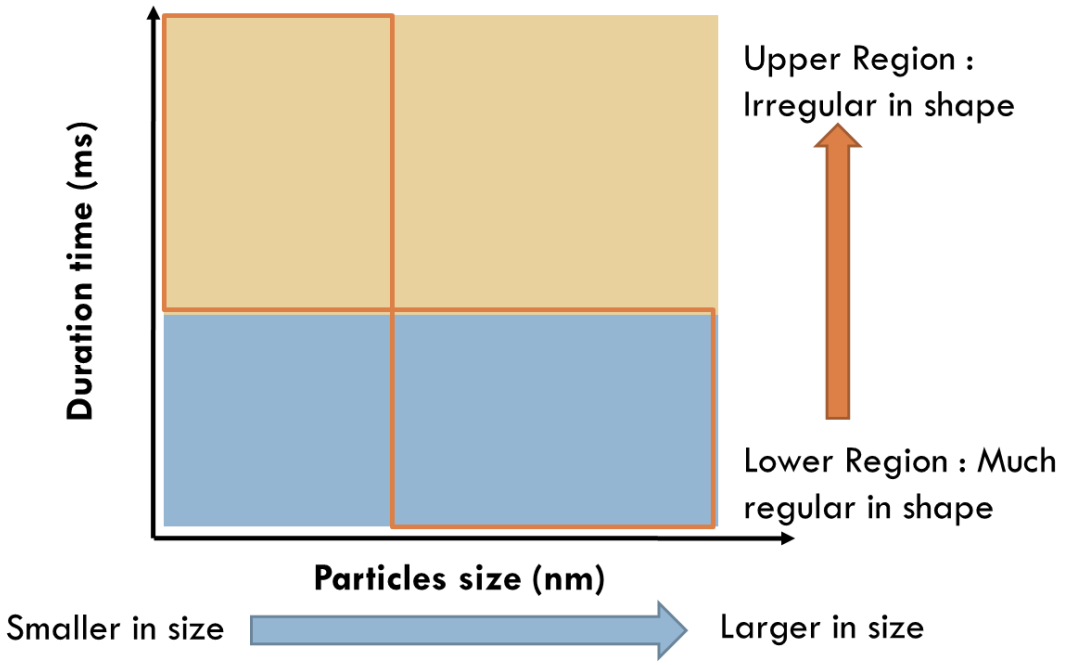

Fig. 3.3.3 Schematic diagram showing the TRPS 2D dot plot analysis. The dot plot can be divided into four quarters, upper-left (UL), upper-right (UR), lower-left (LF) and lower-right (LR). The upper region indicates the particles with relatively irregular shape. The UR and LR indicate the particles with larger size.

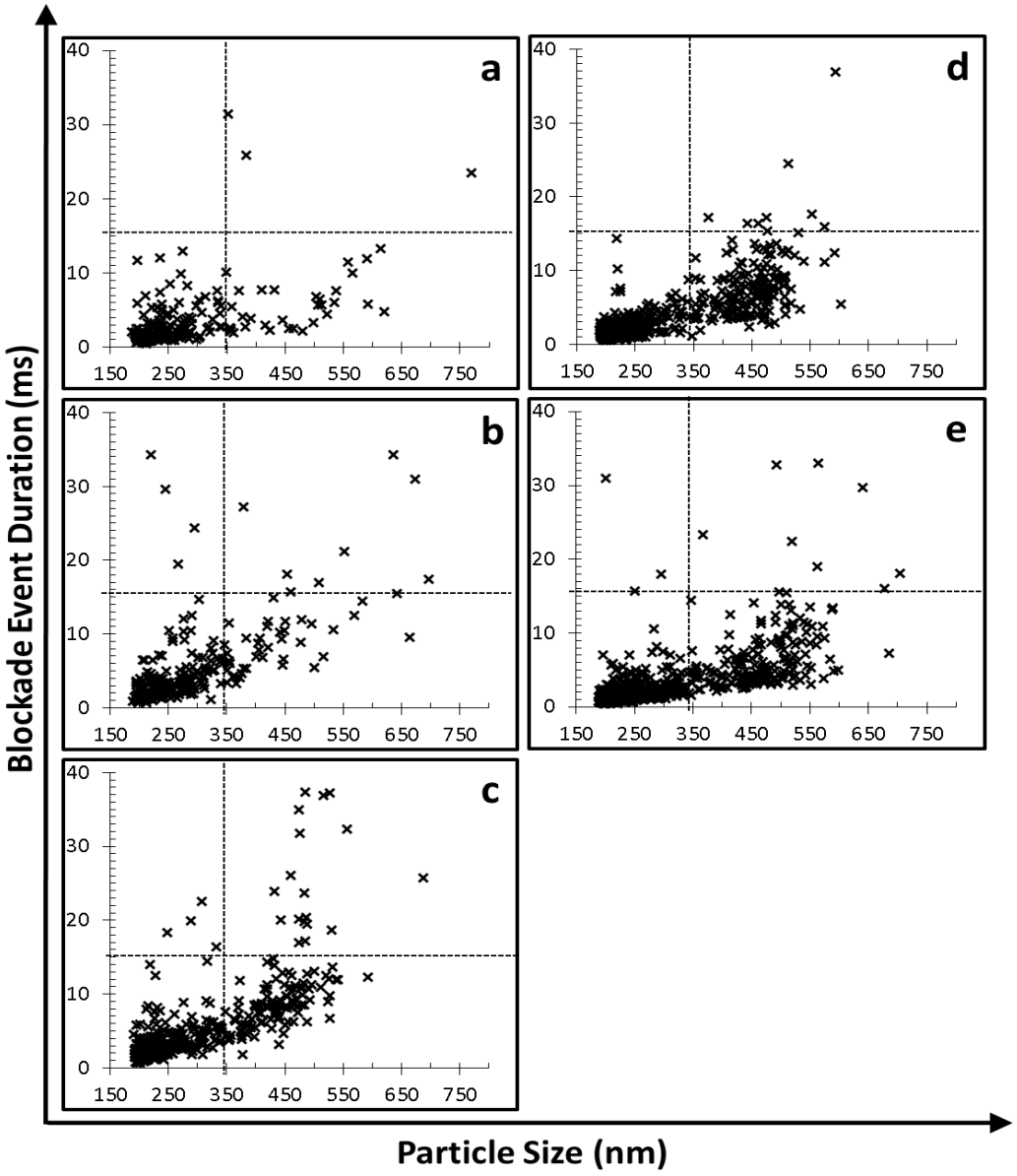

Fig. 3.3.4 2D Dot plots showing the distribution of size of assemblies and corresponding blockade duration time. Lamplicons were amplified from *PVL* DNA template in different copy numbers (**a**) 0; (**b**) 10; (**c**) 100; (**d**) 1000 and (**e**) 10 000 respectively, at 65 ^{0}C for 30 min. 5 μL of Lamplicons were then mixed with AuNP1 (50 pM, 7 μL) and AuNP2 (150 pM, 7 μL), followed by subjecting to TRPS to measure for 10 min.

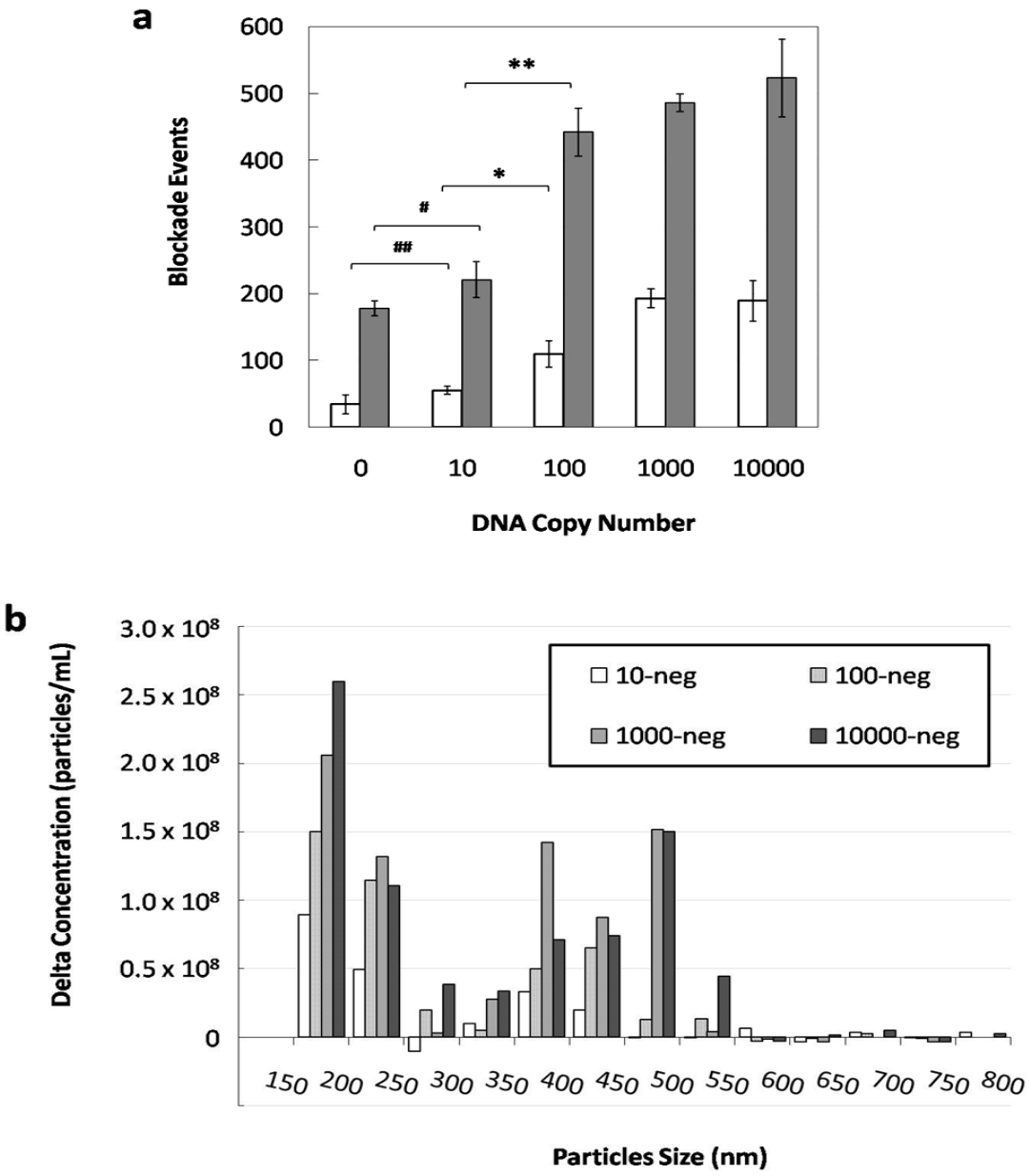

Fig. 3.3.5 TRPS data analysis. (**a**) The bar chat showed the total number of blockade events recorded in 10 min (grey bars) and the number of particles size larger than 350 nm (white bars), corresponding to the Fig. 3.3.4. (n = 3, mean ± SD) (* $p < 0.005$; ** $p < 0.001$; # $p < 0.01$; ## $p < 0.05$) (b) Delta (concentration against particle size) population histogram was calculated using IZON software. The

background concentration of negative control (ddH_2O as template) was subtracted from the supra-assemblies that were formed from the Lamplicons from different initial DNA templates (n = 1).

3.3.4 SEM imagining on AuNP-Lamplicons assemblies

According to the TRPS results, more larger cluster of AuNPs could be found with the involved of Lamplicons, to compare with the negative control. SEM imaging could give information of the characteristic of AuNP-Lamplicons supra-assemblies. The assemblies were desalted and resuspended into ddH_2O, followed by transferring onto a gold-coated silicon grid (Figure 3.3.6). In both 10^8 copies and 10^4 copies *PVL* DNA template involved groups (Figure 3.3.6a-b), large clusters of hundreds nanometers of AuNP1 and AuNP2 aggregate could be found. The aggregates were form as the network with the connection of AuNP1 linked with a serial of AuNP2s, whereas the small background aggregates (in about 150 nm) could be found in the absence of Lamplicons (Figure 3.3.6c-d). The clusters in the absence of Lamplicons were loosely bound. This indicated the specificity of the aggregation of AuNPs in the presence of specific Lamplicons, which was consistent to the TRPS results.

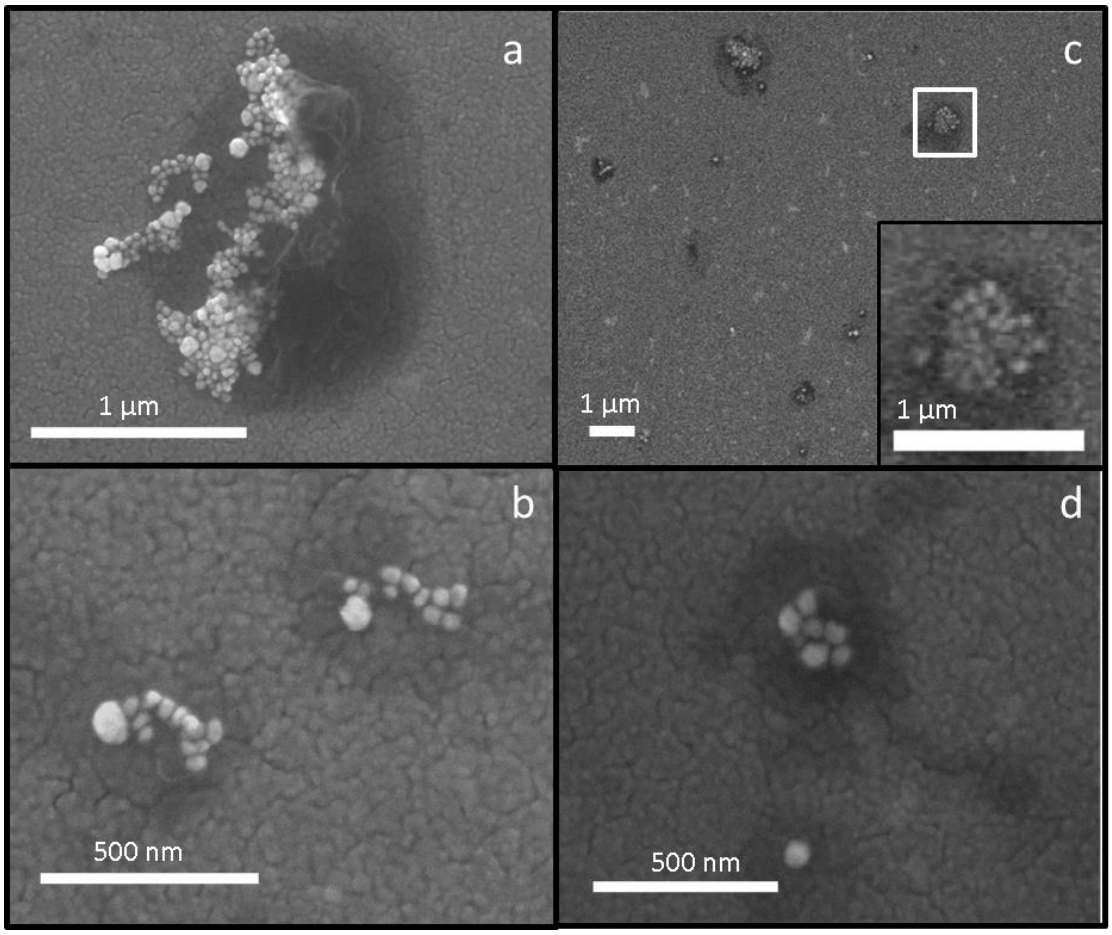

Fig. 3.3.6 SEM images showing the assemblies of AuNPs-LAMP in the presence of Lamplicons in different initial *PVL* DNA templates. (**a**) 10^8 copies; (**b**) 10^4 copies; (**c**) and (**d**) negative control (0 copy of template).

3.3.5 Detection and quantification of MRSA genomic DNA

The utility of the combined system of TRPS, LAMP and AuNPs on MRSA genomic DNA (gDNA) was tested. MRSA MW2 strain, MRSA Mu50 strain, *E. coli*K12 and *L. casei* were chosen as study models. To confirm the existence of *PVL* gene in the models, both PCR and LAMP were done to amplify the *PVL* gene, followed by 1.5 % agarose gel electrophoresis for detection. As shown in the gel electrophoresis diagram in Figure 3.3.7, both PCR and LAMP were able to amplify the *PVL* gene from the DNA template (lane 2, lane 8) and gDNA from the MRSA MW2 (lane 3, lane 9). The gel diagram also reveals that PCR (lane 2, lane 3) produced one single *PVL* DNA band (340 bp) while LAMP (lane 8, land 9) yielded a series of DNA fragments of different sizes. Also, both PCR and LAMP could not amplify the *PVL* from Mu50 (HA-MRSA) (lane 4, lane 10), and other non-MRSA bacteria such as *E. coli* (lane 5, lane 11) and *L. casei* (lane 6, lane 12). These results agreed with the finding that MW2 is a CA-MRSA containing the *PVL* gene while Mu50 strain is a HA-MRSA that does not carry any *PVL* gene [Gillet et al., 2002; Gordon et al., 2008]. The results also indicate that the primers are specific for the *PVL* gene amplification.

With this groundwork and confirmation, both MW2 and Mu50 were chosen as the positive and negative models for the LAMP-based AuNP TRPS assay. Snapshot

was captured to display the raw signal trace from the assay with the Lamplicons, if any, from the negative control, Mu50 and MW2 (Figure 3.3.8a-d). When the conjugated Lamplicon assemblies pass through the nanopore sensor, the number of clusters can be counted. Using the distinct size disparity of the peak signals of the conjugated groupings of the Lamplicon assemblies, it allows an additional way to assess for them. As can be seen, both the negative control (Figure 3.3.8a) and Mu50 (Figure 3.3.8b) did not produce large peak signals that were larger than a set threshold. However, after addition of Lamplicons from the MW2 produced an abundant amount of larger sized peak signals and the number of these events was also higher (Figure 3.3.8c) when compared to that before the addition of the Lamplicons and those raw signal traces in Figure3.3.8a-b. These results agreed with the information in Figure 3.3.7 that only MW2 could generate Lamplicons with the specific primers. Figure 3.3.8d shows the enlarged peak signals before and after the introduction of MW2 Lamplicons into the TRPS sensor. In this experiment, AuNP1s and AuNP2s were introduced into the fluid chamber at t = 0 and MW2 Lamplicons were mixed with the AuNPs at t = 60s. The raw signal traces show the baseline current, peak signal magnitude and blockade peak duration of assemblies recorded at specific time stamp points of when they passed through the TRPS sensor.

Before the addition of Lamplicons, native background AuNPs self-assembly (e.g.

350 nm) was observed (Figure 3.3.8d i and ii). In the presence of target Lamplicons, an increase in peak magnitudes and deeper peak signals were obtained for the supra-assemblies (Figure 3.3.8d, iii-vi). It was observed that both the peak magnitude and blockade peak duration of the assembly increased as time increased. Figure 3.3.9 shows a graphical representation of the summarized results of the assays with Lamplicons from the MW2 and Mu50 gDNA, and also the negative control without DNA. It is apparent that the percentage of the assembly with a threshold size > 400 or 450 nm in the total population events with the Lamplicons from the MW2 gDNA was significantly higher than that of Mu50 and the negative control. These results show that the LAMP-based AuNP TRPS system can differentiate the positive from the negative models, thus providing an approach to detect the presence/absence (yes/no) of the interactions.

MW2 gDNA (10, 100, 400, 1000, 4000 and 40000 copies) was employed for LAMP reactions followed by the TRPS assay with the AuNPs to construct a standard curve. As shown in Figure 3.3.10, a linear relationship was found between 10-40,000 copies of MW2 gDNA, showing a dynamic range of at least five log units, with a linear correlation with a $R^2 > 0.93$. Using the equation for LOD calculation [LOD = (3.3 x SD of the response)/Slope of standard curve] [Shrivastava and Gupta 2011], the LOD of the LAMP-based AuNPs TRPS system based on the top 4 data points

was found to be 530 copies (Top 5 points, LOD = 208, all the points, LOD = 172 copies) (Figure 3.3.10). The determined LOD value here was consistent and in agreement with the observations in Figure 3.3.5 that utilized DNA template.

For the sensitivity and specificity, 23 samples were tested, including 15 of MW2 gDNA contented samples and 8 of MW2 gDNA absence samples. All the samples were prepared by mixing various amounts of MW2 gDNA from same source into different buffers. As Table 3.3.1 shown, 12 out of 15 MW2 gDNA content samples were successfully giving positive result in TRPS with AuNP-Lamplicons system. Using the equation of sensitivity calculation [True Positive / (True Positive + False Negative) x 100%], the sensitivity of the designed LAMP-based AuNP TRPS system was 80%. In the MW2 gDNA absence group, 6 out of 8 could be successfully giving negative result, whereas the other two samples gave false positive result. Using the equation of specificity calculation [True Negative/ (True Negative + False Positive) x 100 %], the specificity of the system was 75 % (Table 3.3.1).

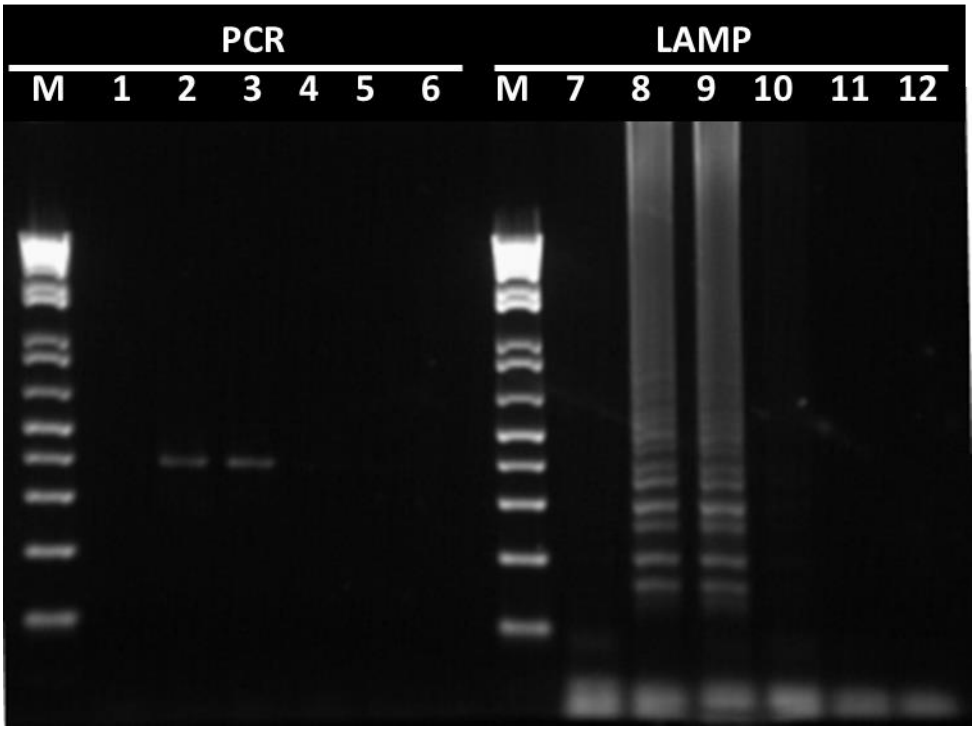

Fig. 3.3.7 1.5 % Agarose gel electrophoresis showing the PCR amplification (Lane 1-6) and LAMP amplification (Lane 7-12) of *PVL* gene. M: 1kb plus DNA ladder; Lane 1, 7: Negative control; Lane 2, 8: 10^8 copies of *PVL* DNA template; Lane 3, 9: MRSA MW2 gDNA; Lane 4, 10: MRSA Mu50 gDNA; Lane 5, 11: *E. coli* K12 gDNA; Lane 6, 12: *L. casei* gDNA. All of the gDNA were in 4 x 10^6 copies in 25 μL reaction mixture.

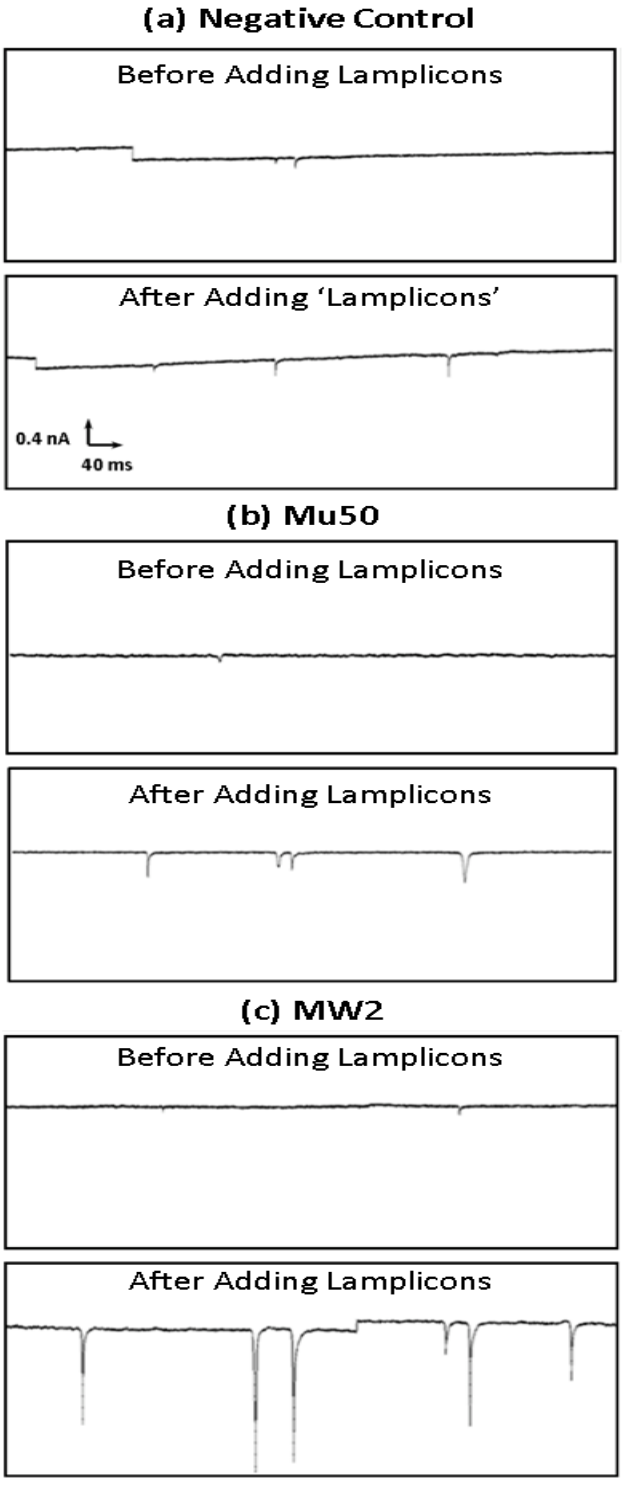
(a) Negative Control
Before Adding Lamplicons
After Adding 'Lamplicons'
0.4 nA
40 ms
(b) Mu50
Before Adding Lamplicons
After Adding Lamplicons
(c) MW2
Before Adding Lamplicons
After Adding Lamplicons

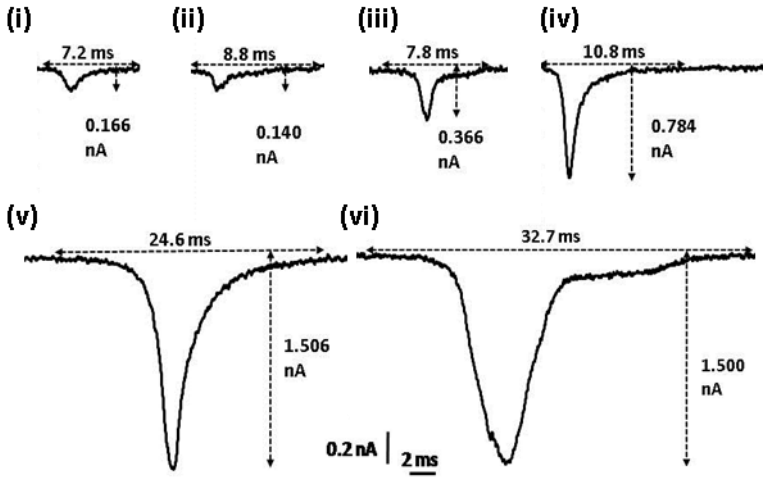

(d)

Fig. 3.3.8 Signal traces of gDNA detection from TRPS before and after the injection of Lamplicons. The Lamplicons were obtained from (**a**) Negative control (no DNA); (**b**) Mu50 gDNA or (c) MW2 gDNA respectively (Lamplicons added at t = 60 sec). (**d**) Typical individual peak signals of assemblies (i – ii) with only AuNP1 (50 pM, 10 μL) and AuNP2 (150 pM, 10 μL); (iii –vi) after injection of MW2 gDNA Lamplicons. The size of the assemblies were (i – ii) 350 nm (t = 12 and 20 sec); (iii) 450 nm (t = 240 sec); (iv) 750 nm (t = 274 sec); (v – vi) 1000 nm (t = 262 and 263 sec).

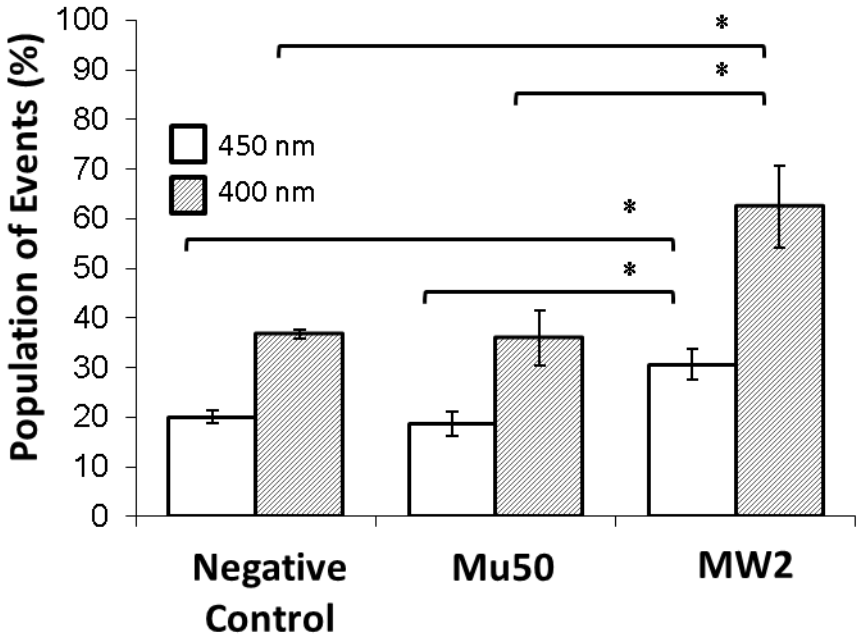

Fig. 3.3.9 Bar chats showed the percentage of total events for the AuNP-Lamplicons assemblies larger than 400 nm or 450 nm. Lamplicons were from Negative control (no DNA), Mu50 or MW2 gDNA respectively (n = 3, mean ± SD) (* $p < 0.01$).

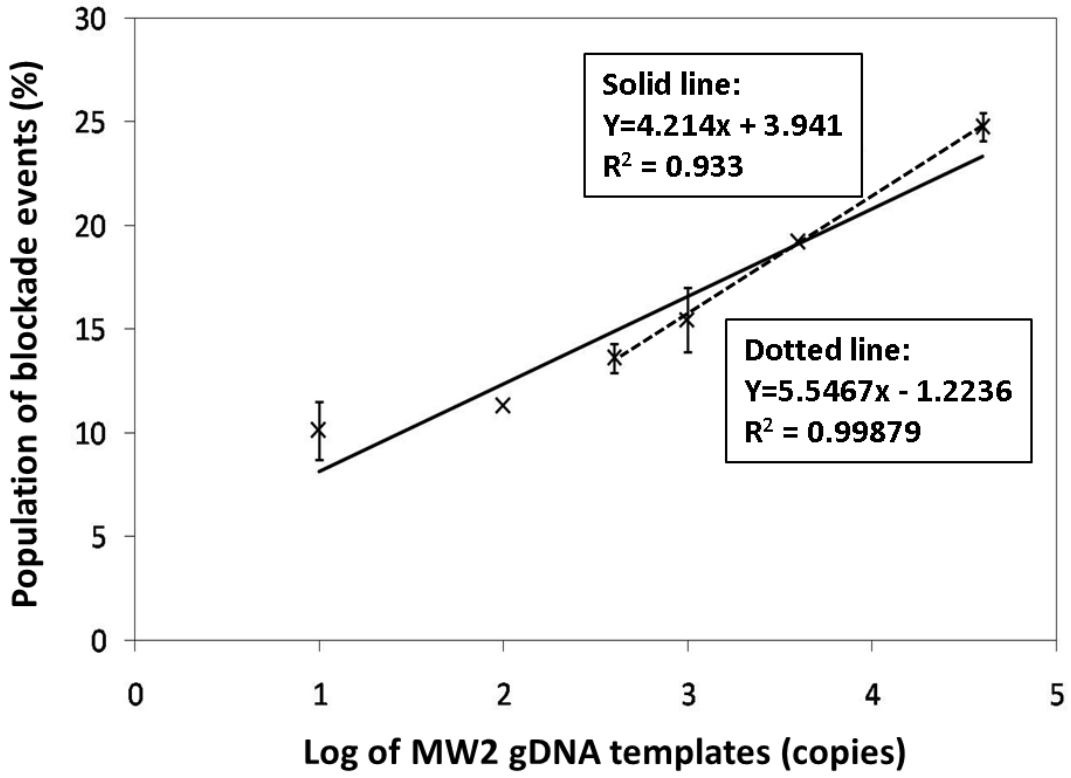

Fig. 3.3.10 Standard curve for detecting *PVL* gene from MW2 gDNA. The standard curve was obtained by calculating the percentage of population of blockade events (setting threshold as 350 nm) against the logarithm of MW2 gDNA copies.(n = 3, mean ± SD). Linear relationship was obtained by plotting both top four points and six points (R^2 = 0.999 or 0.933 respectively).

Table 3.3.1 Statistic analysis of LAMP-based AuNP TRPS system on testing MW2 gDNA presence and absence samples.

		N		N
Positive	True Positive	12	False Positive	2
Negative	False Negative	3	True Negative	6
Total		15		8

3.4 Discussion

The number of papers published in the topic related to DNA and AuNPs has a dramatic increased since 1996. In the previous studies, scientists studied a lot in the optical property and binding affinity between nucleotides and AuNPs. Either too tightly (e.g. > 10-13 nm) or too weakly (e.g. < 3 nm) DNA absorption, binding induced desorption has not been a popular signaling method. Also, if the AuNPs are too large in size, even a single nucleotide absorption might be strong enough, where DNA folding and hybridization may not include desorption or fluorescence signal change [Liu 2012]. On the other hand, to quantify the aggregation of AuNPs-DNA, there is only a few methods can be used. SEM or TEM can help us to observe the structure of AuNPs-DNA assemblies, also for calculating the number of assemblies in a specific area. However, it is not a good method for real-time monitoring the assemblies' formation [Roberts et al., 2012]. Due to the limitations mentioned above, there is room for developing novel technique for measuring the hybridization of target DNA and nanoparticles with non-optical assay.

In this study, it was demonstrated for the first time the use of the LAMP-based AuNP TRPS to detect the *PVL* gene of MRSA. This approach provides a straightforward and sensitive protocol for detection. Different from PCR, thermal cycles are not required in this assay to amplify the target DNAs. Instead, one single

temperature and four primers are used to isolate and amplify target DNAs by LAMP. Two gold nanoparticle samples (AuNP1 and AuNP2) are used to increase the assay sensitivity. The required amounts of sample and reagents for LAMP and TRPS are small, only 35 μL. Also, the combined TRPS approach and setup is affordable to most common laboratories. In this study, the LOD for detecting MRSA DNA template can be as low as 530 copies and the whole process is quantitative and can be completed within two hours. This approach has solved the problems for DNA quantification by using LAMP as well as the inhibition from dyes when the traditional fluorescence-based quantitative method is used in LAMP. As demonstrated, the size and number of AuNP assemblies are proportional to the amount of input target gene templates. By setting a standard curve, our approach can easily work as a quantitative LAMP machine without using molecular probes as reporters.

Also, that using TRPS to quantify the assemblies of AuNPs-DNA can avoid the limitation of signal generation due to the ssDNA absorption or size of AuNPs. For real application, this approach has a good selectivity for the *PVL* gene from the CA-MRSA (MW2) and the ‘signal-to-readout’ workflow is straightforward. Taken together, our results demonstrate that the combined LAMP-based AuNP TRPS is an effective tool to detect the *PVL* gene from the CA-MRSA. It can be used to report the

presence or absence (“yes/no” output) of other types of infectious microorganisms.

To conclude, here we demonstrate a novel detection method for quantifying the pathogen DNA after LAMP reaction, by quantifying the sizes and concentrations of the assemblies between target DNA Lamplicons and DNA probes functionalized AuNPs. TRPS is applied for non-optical investigation and real-time detection of the AuNPs-DNA assemblies. Due to the advantage of using a small amount of samples, the LAMP-based AuNP TRPS is a great nanoscale biosensing approach which can be developed on clinical usage.

References:

Alivisatos, A.P., Johnsson, K.P. et al. (1996). Organization of 'nanocrystal molecules' using DNA. *Nature*, 382(6592), 609-11.

Bada, T., Takeuchi, F. et al. (2002). Genome and virulence determinants of high virulence community-acquired MRSA. *Lancet*, 395, 1819-27.

Bao, Y.P., Huber, M. et al. (2005). SNP identification in unamplified human genomic DNA with gold nanoparticle probes. *Nucleic Acids Res.*, 33(2), e15.

Basu, S., Ghosh, S.K. et al. (2007). Biomolecule induced nanparticle aggregation : effect of particle size on interparticle coupling. *J. Colloid Interface. Sci.*, 313(2), 724-34.

Branton, D., Daemer, D.W. et al. (2008). The potential and challenges of nanopore sequencing. *Nat. Biotechnol.*, 26(10), 1146-53.

Brown, K.R., Lyon, L.A. et al. (2000). Hydroxylamine seeding of colloidal Au nanoparticles. 3. controlled formation of conductive Au film. *Chem. Mater.*, 12, 314-23.

Coulter, W.H. Means for counting particles suspended in a fluid. U.S. patent 2,656,508 (20 October 1953).

Ding, Y., Chen, Q. et al. (2009). Gold encapsulated chitosan-poly(acrylic acid) hybrid hollow nanospheres. *Macromol. Biosci*., 9(12), 1272-80.

Feldheim, D.L. and Foss, C.A., Jr. (2001). Metal Nanoparticles: Synthesis Characterization & Applications, first ed., CRC, Boca Raton, FL.

Francois, P., Harbarth, S. et al. (2008). Methicillin-Resistant *Staphylococcus aureus*, Geneva, Switzerland, 1993–2005. *Emerg. Infect. Dis.*, 14(2), 304-07.

Gillet, Y., Issartel, B. et al. (2002). Association between Staphylococcus aureus strains carrying gene for Panton-Valentine leukocidin and highly lethal

necrotising pneumonia in young immunocompetent patients. *Lancet*, 359, 753-9.

Gordon, R.J. and Lowy, F.D. et al. (2008). Pathogenesis of methicillin-resistant Staphylococcus aureus infection. *Clin. Infect. Dis.*, 46, 350-59.

Harriman, O.L. and Leake, M.C. (2011). Single molecule experimentation in biological physics: exploring the living component of soft condensed matter one molecule at a time. *J. Phys. Condens. Matter*, 23(50), 503101.

Henriquez, R.R., Ito, T. et al. (2004). The resurgence of coulter counting for analyzing nanoscale objects. *Analyst.*, 129, 478-82.

Howorka, S. and Siwy, Z. (2009). Nanopore analytics: sensing of single molecules. *Chem. Soc. Rev.*, 38(8), 2360-84.

Johnsson, D., Mölling, P. et al. (2004). Detection of Panton-Valentine leukocidin gene in Staphylococcus aureus by LightCycler PCR: clinical and epidemiological aspects. *Clin. Microbiol. Infect.*, 10(10), 884-89.

Kanjanawarut, R. and Su, X. (2009). Colorimetric detection of DNA using unmodified metallic nanoparticles and peptide nucleic acid probes. *Anal. Chem.*, 81(15), 6122-29.

Kimling, J., Maier, M. et al. (2006). Turkevich method for gold nanoparticle synthesis revisited. *J. Phys. Chem. B*, 110, 15700-07.

Kozak, D., Anderson, W. et al. (2011). Advances in resistive pulse sensors: devices bridging the void between molecular and microscopic detection. *Nano Today*, 6(5), 531-45.

Li, Z., Jin, R. et al. (2002). Multiple thiol-anchor capped DNA-gold nanoparticle conjugates. *Nucleic Acids Res.*, 30(7), 1558-62.

Liu, A.H., Zhao, Q.T. and Guan, X.Y. (2010). Stochastic nanopore sensors for the

detection of terrorist agents: current status and challenges. *Anal. Chim. Acta.*, 675(2), 106-15.

Liu, J.W. (2012). Adsorption of DNA onto gold nanoparticles and grapheme oxide: surface science and applications. *Phys. Chem. Chem. Phys.*, 14, 10485-96.

Low, M., Yu, S. et al. Investigative study of nucleic acid-gold nanoparticle interactions using laser-based techniques, electron microscopy, and resistive pulse sensing with a nanopore. *Aust. J. Chem.*, 64(9), 1229-34.

Mirkin, C.A., Letsinger, R.L. et al. (1996). A DNA-based method for rationally assembling nanoparticles into macroscopic materials. *Nature,* 382, 607-09.

Notomi, T., Okayama, H. et al. (2000). Loop-mediated isothermal amplification of DNA. *Nucleic Acids Res.*, 28, 1-5.

Olofsson, L., Rindzevicius, T. et al. (2003). Surface-based gold-nanoparticle sensor for specific and quantitative DNA hybridization detection. *Langmuir,* 19, 10414-419.

Patel, R.P., Patel, N.A. and Patel, D.J. (2008). Nanoparticles and its applications in field of pharmacy. *Phamaceutical Reviews*, 6(1), 1-9-2008.

Pingarr*ón,* J.M., Yáñez-Sedeño, P. and González-Cortés, A. (2008). Gold nanoparticle-based electrochemical biosensors. *Electrochim. Acta.,* 53 (19), 5848-66.

Rho, S.C., Kim, S.J. et al. (2009). Colorimetric detection of ssDNA in a solution. *Curr. Appl. Phys.*, 9, 534-37.

Roberts, G.S., Kozak, D. et al. (2010). Tunable Nano/Micropores for Particle Detection and Discrimination : Scanning Ion Occlusion Spectroscopy. *Small*, 6(23), 2635-38.

Roberts, G.S., S. Yu, S. et al. (2012). Tunable pores for measuring concentrations of

synthetic and biological nanoparticle dispersions. *Biosens. Bioelectron.*, 31(1), 17-25.

Salata, O.V. (2004). Applications of nanoparticles in biology and medicine. *J. Nanobiotechnology*, 2(1), 3.

Sato, K., Hosokawa, K. and Maeda, M. (2003). Rapid aggregation of gold nanoparticles induced by non-cross-linking DNA hybridization. *J. Am. Chem. Soc.*, 125, 8102–03.

Shrivastava, A. and Gupta, V.B. (2011). Methods for the determination of limit of detection and limit of quantitation of the analytical methods. *Chron. Young Sci.*, 2(1), 21-25.

Sowerby, S.J., Broom, M.F. and Petersen, G.B. (2007). Dynamically resizable nanometer-scale apertures for molecular sensing. *Sens. Actuators B: Chem.*, 123, 325-30.

Stewart, M.E., Anderton, C.R. et al. (2008). Nanostructured plasmonic sensors. *Chem. Rev.*, 108, 494-521.

Storhoff, J.J., Lazarides, A.A. et al. (2000). What controls the optical properties of DNA-linked gold nanoparticle assemblies?. *J. Am. Chem. Soc.*, 122(19), 4640-50.

Tomita, N., Mori, Y. et al. (2008). Loop-mediated isothermal amplification (LAMP) of gene sequences and simple visual detection of products. *Nat. Protoc.*, 3(5), 877-82.

Turkevich, J., Stevenson, P.C. and Hillier, J. (1953). The formation of colloidal gold. *J. Phys. Chem.*, 57, 670-73.

Upadhyayula,V.K.K. (2012). Functionalized gold nanoparticle supported sensory mechanisms applied in detection of chemical and biological threat agents: A

review. *Anal. Chim. Acta.*, 715, 1-18.

Vandenesch, F., Naimi, T. et al. (2003). Community-acquired methicillin-resistant Staphylococcus aureus carrying Panton-Valentine leukocidin genes: worldwide emergence. *Emerg. Infect. Dis.*, 9(8), 978-84.

Vogel, R., Willmott, G. et al. (2011). Quantitative Sizing of Nano/Microparticles with a Tunable Elastomeric Pore Sensor. *Anal.Chem.*, 83(9), 3499-506.

Willmott, G.R., Vogel, R. et al. (2010). Use of tunable nanopore blockade rates to investigate colloidal dispersions. *J. Phys. Condens. Matter*, 22, 454116.

Zhang, H.P., Chon, C.H. et al. (2009). Methods for counting particles in microfluidic applications. *Microfluid. Nanocluid*., 7, 739-49.

Zhao, W., Lin, L. and Hsing, I.M. (2009). Rapid synthesis of DNA-functionalized gold aanoparticles in salt solution using mononucleotide-mediated conjugation. *Bioconjugate Chem.*, 20, 1218-22.

Chapter 4 Application of DNA functionalized Nanoflowers particles (NFs) for human cells transfection

4.1 Introduction

Biocompatible NPs have been utilized as carriers on non-viral eukaryotic cells transfection for basic and therapeutic application. The NPs used as DNA-carriers are commonly composed of cationic lipids or polymers, with relatively large in size with positive charges that enhance their clearance from circulation [Corsi et al., 2003]. In 2001, Mao et al. reported the novel non-viral transfection method by using Chitosan-DNA NPsin HEK293 cells [Mao et al., 2001]. The chitosan-DNA NPs can protect plasmid DNA from nuclease degradation, but with two to ten times lower transfection efficiency when compared with the Lipofectamin^{TM}-DNA transfection. AuNPs have high affinity to DNA. The modified AuNPs, mixed monolayer protected gold clusters (MMPCs) have been reported as the carrier of plasmid DNA for the transfection in mammalian cells [Sandhu et al., 2002]. In 2007, McBain et al. reported the polyethyleneimine (PEI) molecules functionalized iron oxide NPs for DNA delivery and transfection [McBain et al., 2007]. Iron oxide NPs with PEI functionalized is not only capturing DNA, but also can be driven by magnetic field.

Chapter 4

As the increasing interest in utilizing of NPs and nanotechnology, the safety of nanomaterials in clinical usage becomes highly concerned. In this decade, there are reports on nanomaterials toxicity: the surfactant which can stabilize the NPs, such as CTAB on AuNPs is highly toxic to human erythrocytes and basophile [Lau et al., 2011; Cheung et al., 2012]

In this study, we used human basophil (suspension cells) and human embryonic kidney cells (adherent cells) to demonstrate the use of the flower-like NPs, nanoflowers (NFs) conjugated with DNA for transfection. Due to their unique structure, NFs share higher surface area to volume ratio that compare with other kinds of NPs. NFs can be applied for nucleic acid delivery by making use of the unique features for targeted drug/gene delivery and therapeutic purposes. We aim to show the feasibility of plasmid-functionalized NFs as a non-cytotoxic tool for targeted gene delivery for biomedical purposes. By using the green fluorescent protein (GFP) or red fluorescent protein (RFP) genes containing plasmid, the fluorescent signals released from the treated cells were measured as a reflection of the efficiency of transfection. Also, the toxicity of NFs used in this system was investigated.

4.2 Materials and Methods

4.2.1 Materials

4.2.1.1 Cell lines

Human Basophil KU812 cells were provided from Prof. C. K. Wong's lab (Department of Chemical Pathology, CUHK).

Human embryonic kidney cells HEK293 cells (293T cells) were obtained from American Type Culture Collection, USA.

4.2.1.2 Buffers and reagents

Buffers and reagents were prepared by dissolving chemicals to distilled water, followed by pH calibration with NaOH or HCl, unless otherwise specific.

2 X AlarmaBlue working solution was freshly prepared with 2 mL of AlamarBlue® reagent, mixed gently with 8 mL of fresh RPMI or DMEM medium.

HEPES buffer (without BSA) was composed with 140 mM NaCl, 5 mM KCl, 10 mM HEPES, 2.5 mM $CaCl_2$ and 10 mM Glucose. The pH value was adjusted to 7.4. The HEPES buffer was sterile by filtration.

Phosphate buffered saline (PBS) was prepared by using 2.7 mM KCl, 1.5 mMKH_2PO_4, 136 mM NaCl and 8 mM Na_2HPO_4. The pH value was adjusted to 7.4. PBS was sterile by autoclave and then stored at room temperature.

4.2.2 Methods

4.2.2.1 Cell culture and preparation

KU812 cells and 293T cells were cultured according to the ATCC instructions. Briefly, KU812 cells were cultured at a cell density of 1 x 10^5 cells/mL in RPMI 1640 culture medium (Gibco, USA) supplemented with 10 % fetal bovine serum (Gibco, USA) and 1 % penicillin/streptomycin (Gibco, USA) at 37 ^{0}C and 5 % CO_2, and passaged twice a week.

293T cells were cultured in DMED culture medium (Gibco, USA) supplemented with 10 % fetal bovine serum (Gibco, USA) and 1% penicillin/streptomycin (Gibco, USA) at 37 ^{0}C and 5 % CO_2, and passaged twice a week.

4.2.2.2 Alamar blue assay

Human basophils (1x10^6 cells/mL) were treated with different NFs concentration for either 48 hr at 37 ^{0}C, 5 % CO_2. After treatment, the cells were stained with AlamarBlue® reagent (Invitrogen, USA) according to the protocol suggested by the company. Briefly, 100 μL of cells were seeded into 96-well plate with additional of same volume of 2 X AlarmaBlue working solution, and then incubated for 3 hr at 37 ^{0}C, 5 % CO_2. Absorbance at 570 nm and 600 nm was measured with a microplate reader (Tecan Infinite M200) for cell viability. Positive

control was achieved by adding 1 μM staurosporine (STS) to cells to induce apoptosis.

4.2.2.3 Preparation of linearized plasmids

Circular plasmids pEGFP-N1 and pDsRed1-C1 were double-digested by restriction enzymes BamHI and EcoRI. Briefly, 10 μg of circular plasmids were added into 500 μL of reaction mixture, followed by incubation at 37 ^{0}C for 2 hr. The linearized plasmids were stored at 4 ^{0}C.

4.2.2.4 Preparation of plasmids functionalized NFs

The NFs were prepared in house in the Department of Chemistry, CUHK, and they were characterized in our previous study [Xuan et al., 2011]. Then they were separately conjugated to the surface of the NFs by 1-Ethyl-3-(3-dimethylaminopropyl) carbodiimide (EDC) conjugation according to the instruction manual by Thermo Scientific. In brief, for a 300 μL reaction, 25 mg of EDC was dissolved in 100 μL of linearized plasmid (2 μg), which was then quickly mixed with 100 μM of NFs in 0.1 M imidazole. Immediately mixing by vortex, an additional 200 μl of 0.1 M imidazole was added into the mixture. Subsequently, the reaction mixture was incubated at 37 ^{0}C for 2 hr. The conjugated NFs were gathered

by centrifugation at 12,000 rpm for 10 min, followed by resuspending in HEPES buffer (without BSA).

4.2.2.5 Tunable nanopore-based resistive pulse sensing

TRPS assay were done as described in Section 3.2.2.9. Briefly, the NP2000 were chosen as the nanopore membrane for the assay. 40 μL of NPs sample was injected to the flow cells for size and concentration measurement. The size of NFs was calibrated with the standard polymer particles (mean size 960 nm).

4.2.2.6 PCR assay

PCR was done as decried in Section 2.2.2.1. Briefly, the supernatant, NFs, no EDC NF-Plasmid and NF-Plasmid were 5 fold diluted with ddH_2O before mixing with the reaction mixture, followed by PCR process.

4.2.2.7 Flow cytometry

After the treatments, human basophils (1 x 10^6cells/mL) were washed by PBS and subject to flow cytometeric analysis (FACSCanto, BD Biosciences) for measuring the green and red fluorescence from the control and transfected cells. Results were processed and analyzed using WinMDI software. Mean fluorescence

intensity (MFI) and peak value were calculated from the histograms.

4.2.2.8 Statistical analysis

The differences between the results of experimental and control treatments were analyzed for statistical significance by Student's t-test. Each experiment was repeated for three times, each with three determinations. The trend of response from different batches of cells was similar if not identical. All data points in the bar chart are mean ± SD (standard deviation) from three different sets of experiments executed at different dates.

4.3 Results

4.3.1 Size analysis of plasmids functionalized NFs

In Figure 4.3.1, size of the NFs (NF), Plasmid conjugated NF without EDC as linker (no EDC NF-Plasmid) and also the plasmid conjugated with NF (NF-Plasmid) were estimated by the TRPS assay. As mentioned before, the TRPS system has been widely used for analyzing particles size by recording particles one-by-one. In this study, a nanopore membrane NP2000 was chosen for size analysis. As shown in Figure 4.3.2a, the NF is a flower like structure which contains a large surface area for DNA conjugation, it is expected that the NF would have a size enhancement after

plasmid functionalization. Both mean size (the average size of the population) and mode size (the size appeared most in the population) were recorded. According to the bar charts in Figure 4.3.1a, NF-Plasmid had a significant enhancement in terms of mean size when compared with that of the NF alone or the NF with NF-Plasmid groups in the absence EDC. The mean size of the NF and also the NF without EDC NF-Plasmid were found to be 950 and 1000 nm (in sphere size) respectively, whereas that of the NF-Plasmid was around 3,000 nm (Figure 4.3.1b). Although the mode size of the NF-Plasmid was around 1800 nm, far smaller than the mean size, it was still significantly larger than the mode size of the NF and the NF with NF-Plasmid groups but without the addition of EDC for conjugation. The huge difference between the mean and mode size of the NF-Plasmid may be due to the different amount of plasmids randomly conjugated onto the NFs.

To confirm the size enhancement of NFs before and after plasmids functionalization, TEM assay and Energy Dispersive X-Ray Analysis (EDx) were done (Done by Mr. Lee S.F., from the Department of Chemistry, CUHK). From the TEM images, the size of NFs was in approximately 200 nm in diameter, which is far smaller than the one measured by the TRPS (Figure 4.3.2). It was clear to see the flower-like shape structure, with a core in the middle. The DNA can conjugate onto

the NFs, which is the branch extended from the core. The branch is constructed with γ-AlOOH as nanosheet, providing high surface areas for functionalization. The NF-EDC which is lacking in plasmid, remind the original shape with ~ 200 nm in diameter (Figure 4.3.2a). After conjugation with plasmids, the NFs became agglomerate with several cores inside the cluster. The size of NF-Plasmid was obviously enlarged, with more than 500 nm in diameter. A large network of flower-like shape NFs was found in TEM imaging after conjugation with plasmids and EDC, as seen in the Figure 4.3.2b. The Edx showed the existence of the elements for composing the NFs, including Fe, O, Si and Al. A connection between NFs was also found in the one without EDC NF-Plasmid, but with the smaller size of network to compare with the NF-Plasmid (Figure 4.3.2c). Both TEM and TRPS confirmed that NFs had size enlargement after conjugating with plasmids.

PCR was done to amplify the plasmids among different samples, in order to confirmed the successfully functionalization of plasmids. Also, after conjugation process, the supernatants were also collected by centrifugation for PCR. In Figure 4.3.3, no amplicon was found in the negative control and bare NF group. For the linearized plasmids, NF-Plasmid, and the supernatant of no EDC NF-Plasmid, there were significant amount of DNA band with 629 bp in size (Lane 3, 4 and 7, expected

size of amplicons: 629 bp). In the no EDC NF-Plasmid and the supernatant of NF-Plasmid, there was lack of amplicons (Lane 5, 6). The result confirmed that the linearized plasmids could be successfully conjugated onto the NFs with the EDC linkage, but not in the one without EDC. Hence, the supernatant of NF-Plasmid was lacking in plasmids, whereas the plasmids still remained in the supernatant of no EDC NF-Plasmid.

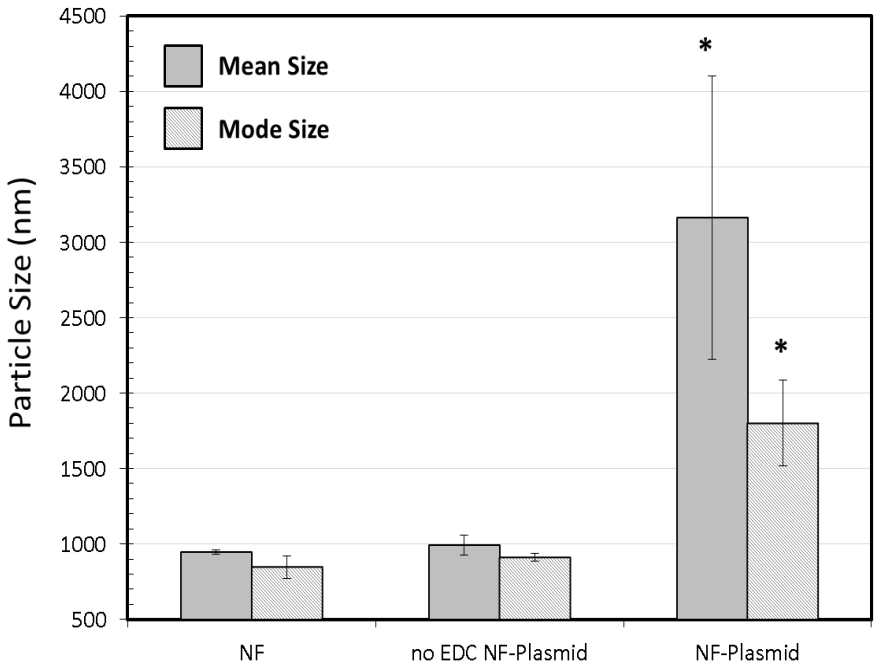

Fig. 4.3.1 TRPS assay for investigating the size of NF, NF with no EDC conjugated plasmid, and plasmid conjugated NF. The mean and mode size were measured with qNano machine and showed as bar charts. NP2000 nanopore membrane was chosen for the TRPS assay (n=3, mean ± SD) (* $p < 0.05$).

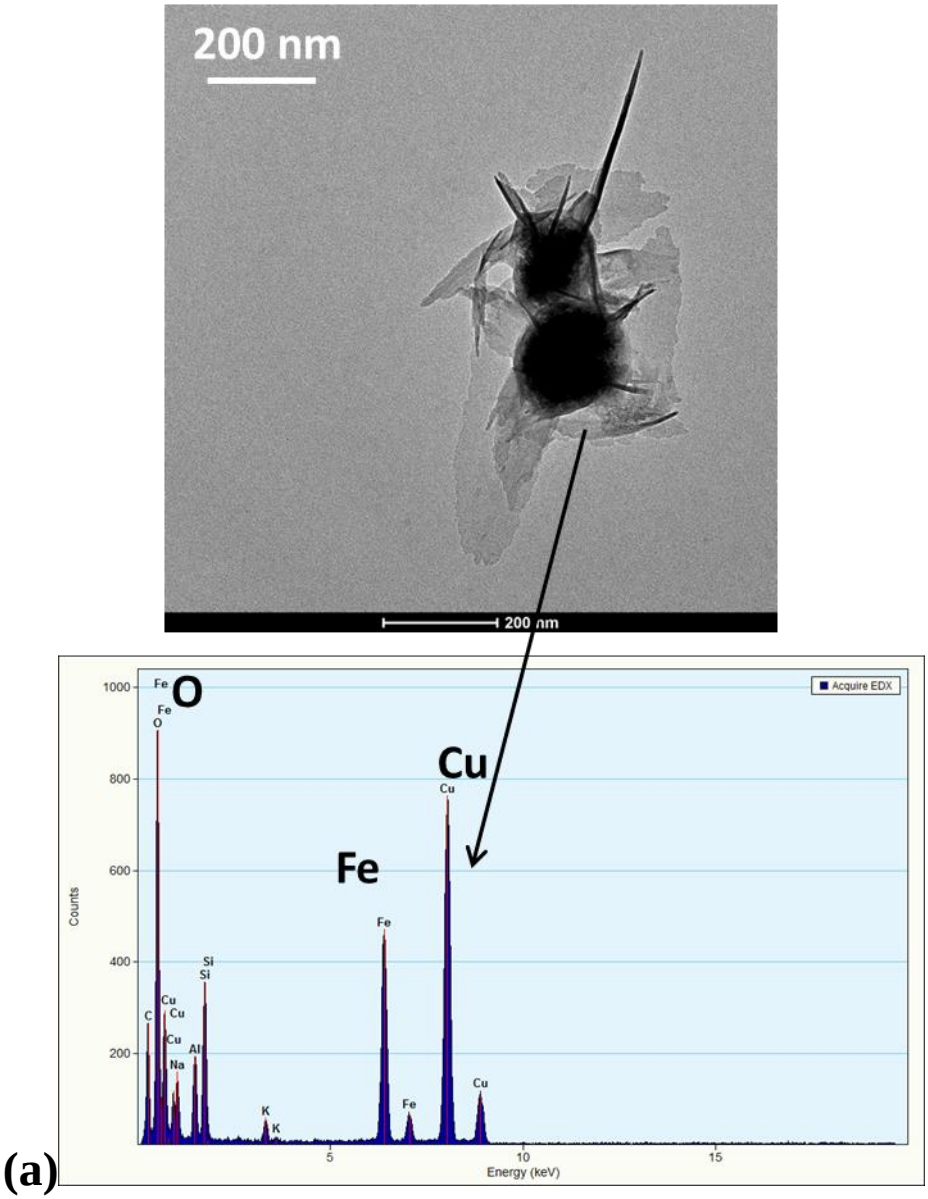
200 nm
200 nm
Acquire EDX
Counts
Energy (keV)
1000
800
600
400
200
5
10
15
O
Cu
Fe
Fe
O
Cu
Cu
Cu
Cu
C
Na
Al
Si
Si
K
K
Fe
Fe
Cu
Cu

(a)

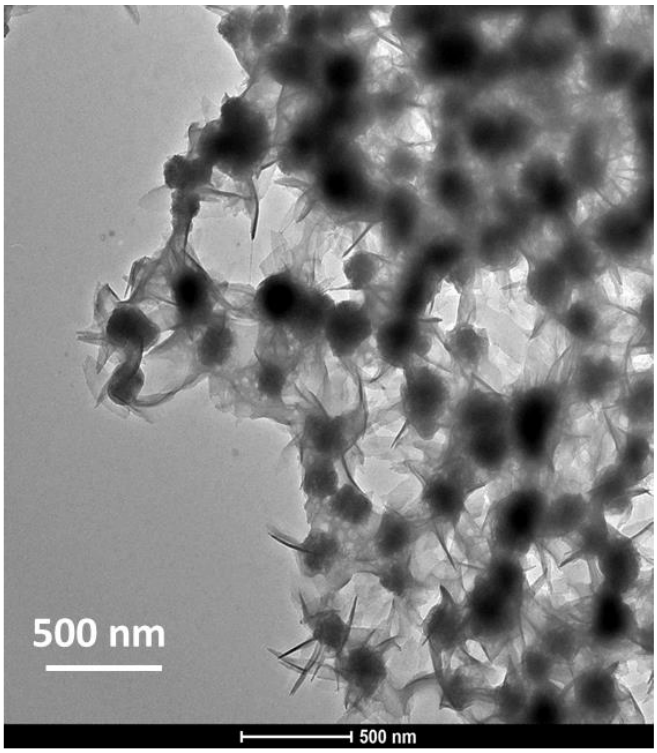
500 nm
500 nm

(b)

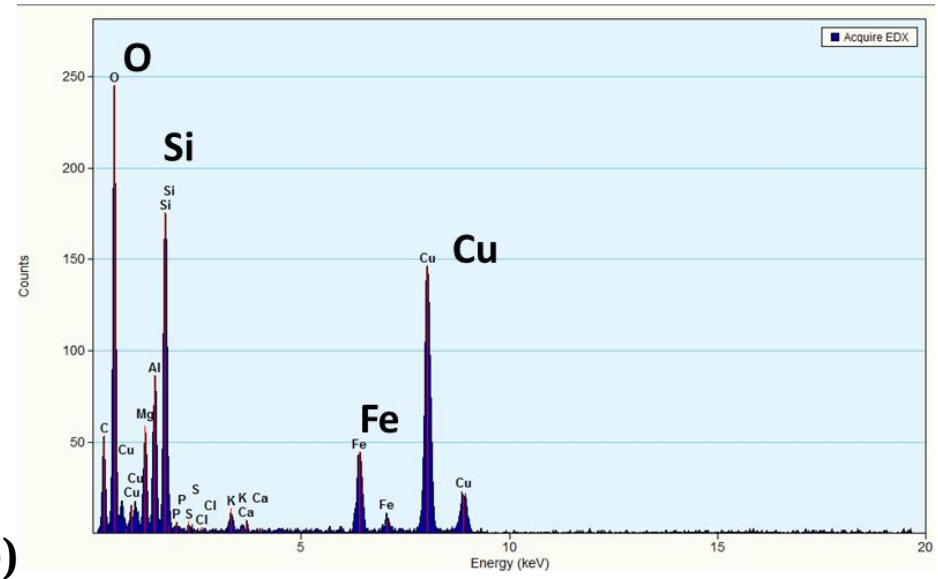
Acquire EDX
O
Si
Cu
Fe
Counts
Energy (keV)
250
200
150
100
50
5
10
15
20

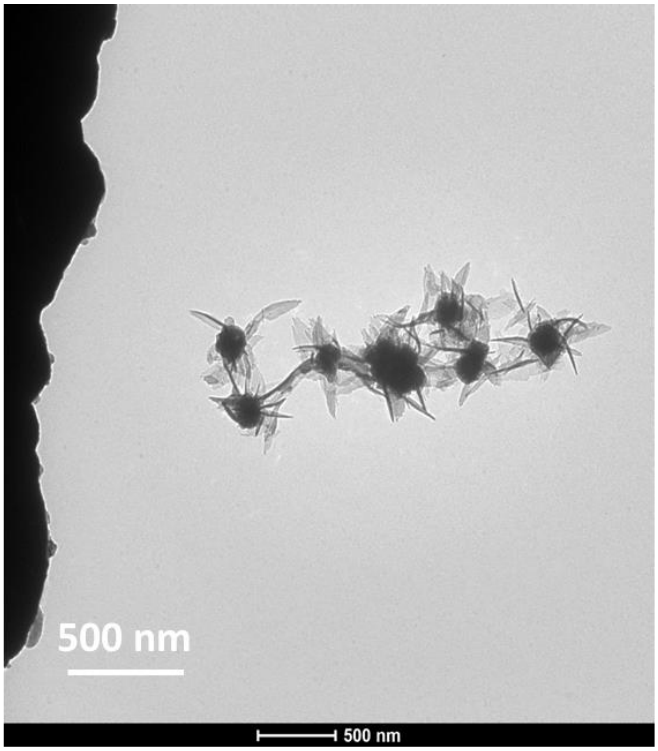

(c)

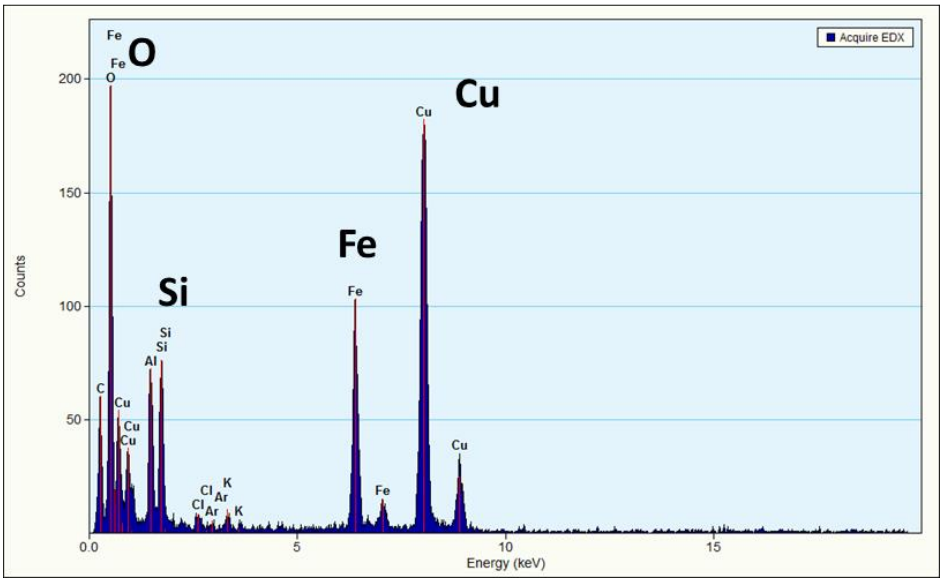

Fig. 4.3.2 TEM images and EDx of NFs. NFs were conjugated with (**a**) EDC only, (**b**) with both EDC and Plasmids, or (**c**) with Plasmids but no EDC. EDx results showed the existence of NFs, which had high peaks on Fe, Si, O and Cu, and significant amount of Al.

Lane	1	2	3	4	5	6	7	M
NFs	/	v	/	v	v	v	v	/
pEGFP-N1	/	/	v	v	v	v	v	/
EDC	/	/	/	v	/	v	/	/
SUP	/	/	/	/	/	v	v	/

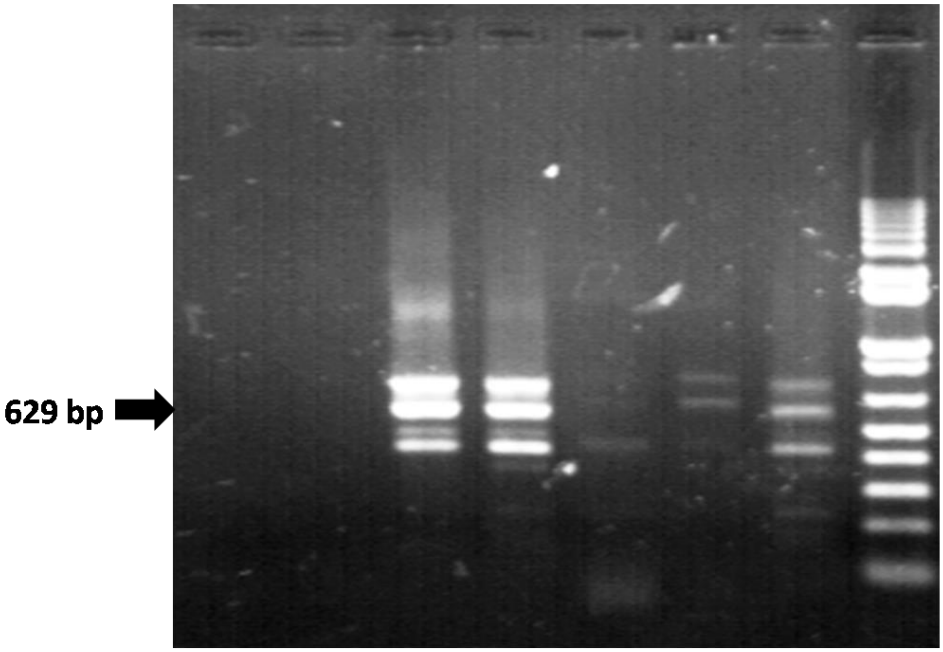

Fig. 4.3.3 1.5 % agarose gel electrophoresis image showing PCR assay of NFs and plasmids functionalized NFs. Lane 1: negative control (ddH_2O); 2: NFs only; 3: plasmid only (pEGFP-N1); 4: NF-Plasmid; 5: no EDC NF-Plasmid; 6: Supernatant of NF-Plasmid; 7: Supernatant of no EDC NF-Plasmid; M: 1 kb plus DNA ladder. (SUP: Supernatant)

4.3.2 NFs and functionalized NFs toxicity to suspension and adhesion cells

Toxic effect from NPs is a common problem. It is therefore important to understand the level of cytotoxicity of NFs in human cells before using them for transfection. In this connection, Alamar blue assay was performed to estimate the cytotoxicity of the NFs. As shown in Figure 4.3.4, the NFs used in this study demonstrated no or very little cytotoxicity to the human basophils (KU812 cells) when compared to that of negative control as well as the positive apoptogenic control (1 μM staurosporine (STS)). The cell viability maintained approximately 100 % under the challenge of NFs from 3 nM to 300 μM, in both short-term (4 hr) and long-term (24 hr) treatment. Therefore, these results indicate that the NFs were biocompatible and useful for further application with the basophils KU812 cells.

Besides the human basophils (suspension cells), another cell line, human embryonic kidney cells (293T cells, adhesion cells) was chosen as a model for studying the transfection effect of plasmids carried by the NFs. The working concentration of NF-Plasmid for cells transfection in our study was 0.1 nM. In order to further understand the cytotoxicity level of the NFs in KU812 cells and 293T cell, the concentrations of the plasmids functionalized NFs chosen were in 0.1 nM and 0.05 nM for alamar blue assay and the incubation time was extended to 48 hr.

According to the results in Figure 4.3.5, both bare NFs and no EDC NF-Plasmids groups demonstrated no or very little cytotoxicity in both the KU812 cells (Figure 4.3.5a) and 293T cells (Figure 4.3.5b). On the contrary, cells treated with the NF-Plasmid, EDC contained NFs groups, had decreasing viability when compared to that with the non-EDC contained NFs treated groups. The viability index of KU812 cells and 293T cells treated with 0.1 nM NF-Plasmid were found between 70 to 80 %. When decreasing the NF-Plasmid concentration to 0.05 nM, the cell viability in both cell lines increased.

NF-Plasmid was composed of NFs, linearized plasmids and EDC. EDC worked as a linker to connect linearized plasmids and NFs in order to have successfully functionalization. To investigate whether the cytotoxicity was due to the EDC, mixtures containing NFs and EDC (NF-EDC) were added into cells. According to Figure 4.3.5a, no matter under NF-Plasmid or NF-EDC treatments, KU812 cells had similar rate of viability. It was suggested that the cytotoxicity effect was, at least in part, due to the EDC linker. Not surprisingly, similar effects were found after treating 293T cells with EDC contained NFs for 48 hr. The viability rates of 293T cells treated with NF-EDC were slightly elevated when compared with that of the NF-Plasmid treatment groups (Figure 4.3.5b). These results thus indicate that the

EDC used to connect the NFs and linearized plasmids is slightly cytotoxicity to human cells. Taken together, it seems likely that the 293T cells had a higher EDC tolerance than that of the KU812 cells.

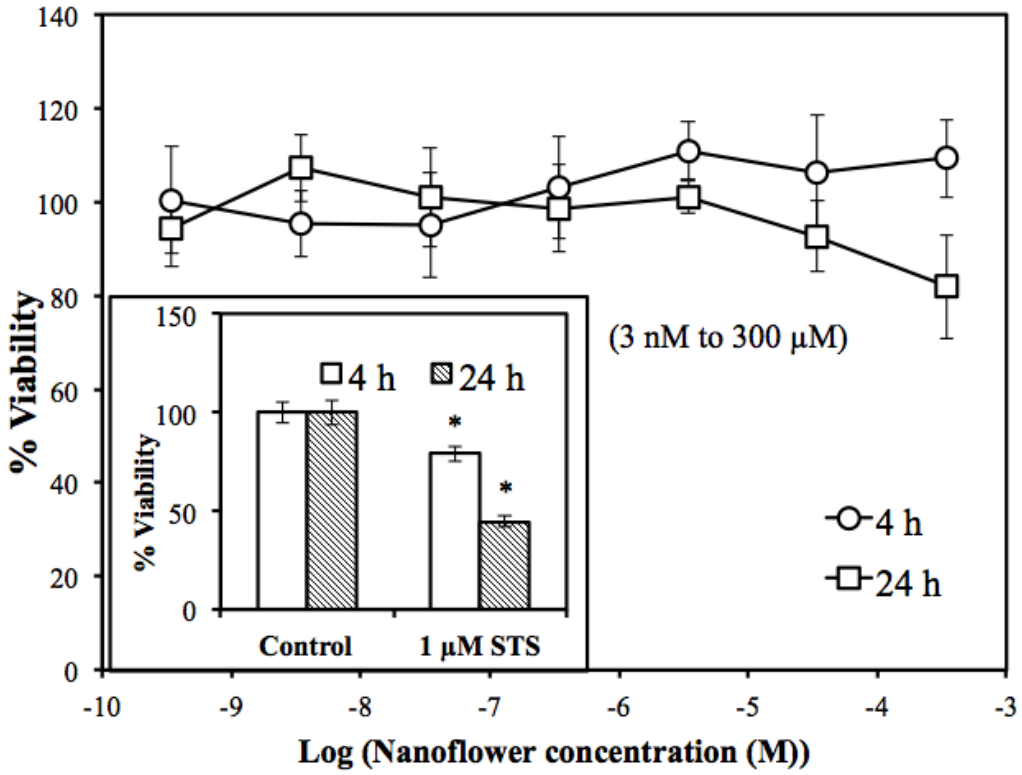

Fig 4.3.4 Alamar blue assay for determining the NFs toxicity to KU812 cells. KU812 cells (1 x 10^6 / mL) were treated under different concentrations of NFs, in a range between 3 nM to 300 µM for either 4 or 24 hr. The positive control was done by treating 1 µM of STS. Results were mean ± SD (n = 3), * $p < 0.01$ compared to control.

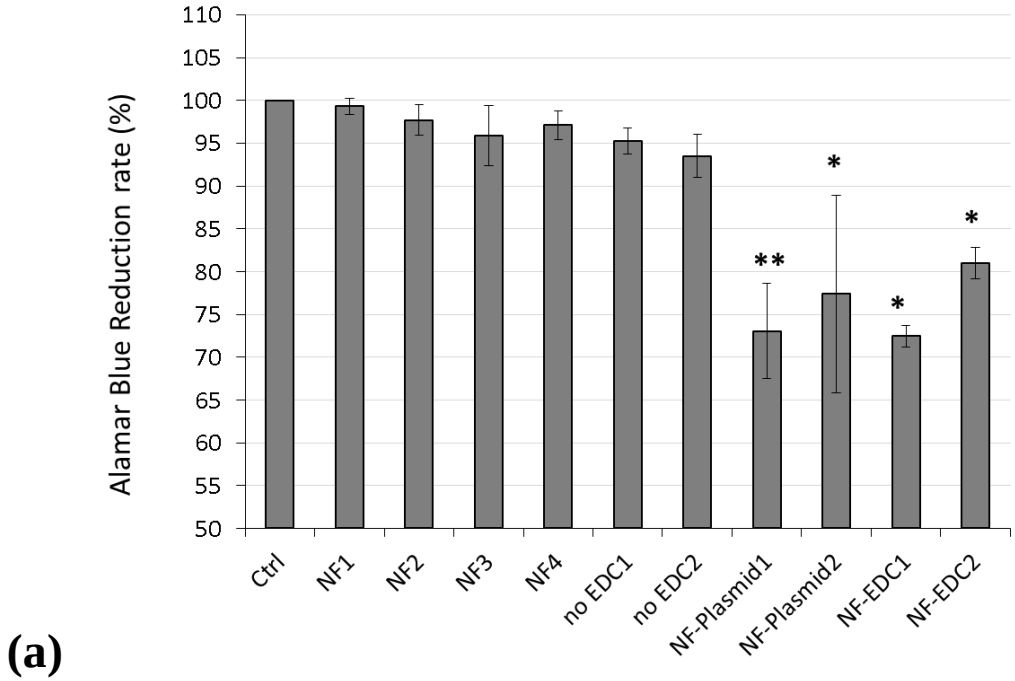

(a)

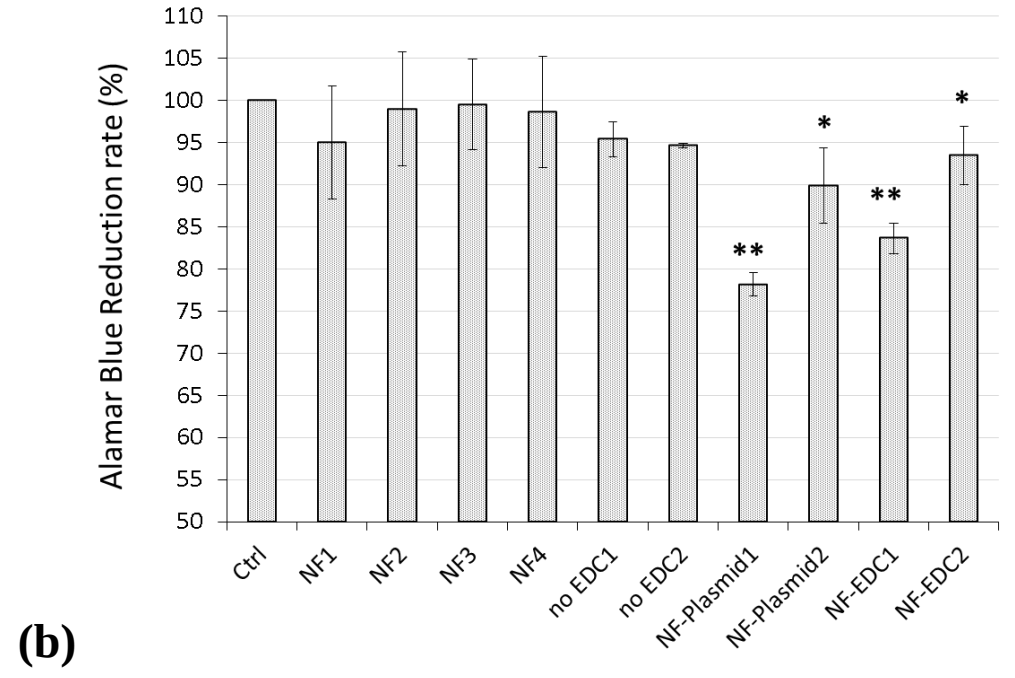

(b)

Fig. 4.3.5 Alamar blue assay on the cell viability of (a) KU812 cells and (b) 293T cells under a treatment with NFs, no EDC NF-Plasmid, NF-Plasmid and NF-EDC for 48 hr. Ctrl: control group, without any NFs; NF1: 0.4 nM NFs; NF2: 0.2 nM NFs; NF3: 0.1 nM NFs; NF4: 0.05 nM NFs; no EDC1: 0.1 nM no EDC

NF-Plasmid; no EDC2: 0.05 nM no EDC NF-Plasmid; NF-Plasmid1: 0.1 nM NF-Plasmid; NF-Plasmid2: 0.05 nM NF-Plasmid; NF-EDC1: 0.1 nM NFs with EDC; NF-EDC2: 0.05 nM NFs with EDC. The working concentration for transfection was 0.1 nM NF-Plasmid. Results are n = 3, mean ± SD, * $p < 0.05$, ** $p < 0.01$.

4.3.3 Florescent proteins expression in KU812 cells and 293T cells after the transfection with the GFP plasmid conjugated with NF

Next, the transfection efficiency of NF-Plasmid in both suspension (KU812 cells) and adhesion cells (293T cells) were studied. In this study, two plasmids, pEGFP-N1 and pDsRed1-C1 containing the GFP and RFP genes respectively, were chosen for transfection. KU812 cells were incubated with either the culture medium alone, or the medium containing NF, plasmid, no EDC NF-Plasmid, or NF-Plasmid for 24 or 48 hr, followed by flow cytometric analysis to investigate the green (Ex 488 nm, Em 530 ± 30nm) or red (Ex 488 nm, Em695 ± 40nm) signals for the GFP and RFP respectively.

In Figure 4.3.6a-b, histograms showed the fluorescence signal in KU812 cells under different treatments. To compare with the control group, cells did not show any obvious peak shift after either 24 or 48 hr of treatment with the bare NFs, plasmid or no EDC NF-Plasmid. For the NF-Plasmid treated groups, there were slightly increased in either the RFP or GFP expression after 24 hr treatment, compared with the other treatment groups. The populations with RFP and GFP expression in the selected region (M1) were 14.16 % (KU812, RFP) and 29.77 % (KU812, GFP) respectively after transfection for 24 hr (Figure 4.3.6a-b), which have elevated 0.96-

and 1.3-fold increase when compared with the control groups. These results suggest that the plasmids alone in the medium could not be carried into cells and successfully expressed if the cells were only incubated with the linearized plasmids or NFs without plasmids conjugation in the absence of EDC linking. In Figure 4.3.6c-d, the bar charts showed the event populations with both the RFP and GFP expression 48 hr after transfection. The cell populations with either RFP or GFP expressions in the NF-Plasmid treated groups were significantly larger than the other treatment groups (Figure 4.3.6c-d). At 48 hr post-transfection, approximately half of the cell populations were positive in fluorescent proteins expression. In comparison, the RFP-positive and GFP-positive cell populations were approximately 6.8- and 4.5-fold larger than the control groups, respectively. Although an increasing population size with fluorescence was detectable 24 hr after transfection, some of the cells needed a longer time to produce fluorescent proteins. NF-Plasmid, no matter conjugated with linearized pEGFP-N1 or pDsRed1-C1, could carry the plasmids into the KU812 cells, and expressed fluorescent proteins successfully after incubation for 48 hr.

Experiments were repeated by using the adherent 293T cell line. In 293T cells, loss of cell adhesion was found in the NF-Plasmid treatment groups. Hence, the cells

suspensions were also collected for fluorescence signal measurement. Similar to the KU812 cells, the histograms showed no peak shift in 293T cells treated with plasmids or no EDC NF-Plasmid, when compared with that of the control groups (Figure 4.3.7a). However, there was a slightly increase in the cells populations with fluorescence under the NFs treatment. Because of the lacking of plasmids, it was suggested that the fluorescence signals may due to the NFs.

For the NF-Plasmid treated 293T cells, after transfection, part of the cells lacking in the ability of adhesion. Hence, cells could be derived into adhesion and suspension fractions. According to the histograms shown in Figure 4.3.7a, only 22.31 % and 17.21 % of cells in the adhesion fractions were RFP and GFP positive respectively, close to the NF alone treated groups. It indicates that the fluorescence signals detected from the adhesion fraction might not be due to the production of fluorescent proteins. On the contrary, cells found in suspension fractions were obviously highly RFP or GFP expressed. There were nearly 80 % of cells expressing fluorescence signals (Figure 4.3.7a-c). According to the above results, NFs worked as carriers to bring the plasmids into the 293T cells. And the expression of GFP or RFP blocked the surface adhesion behavior. Also, the transfection efficiency using NFs as a tool was higher in 293T cells than KU812 cells in our study.

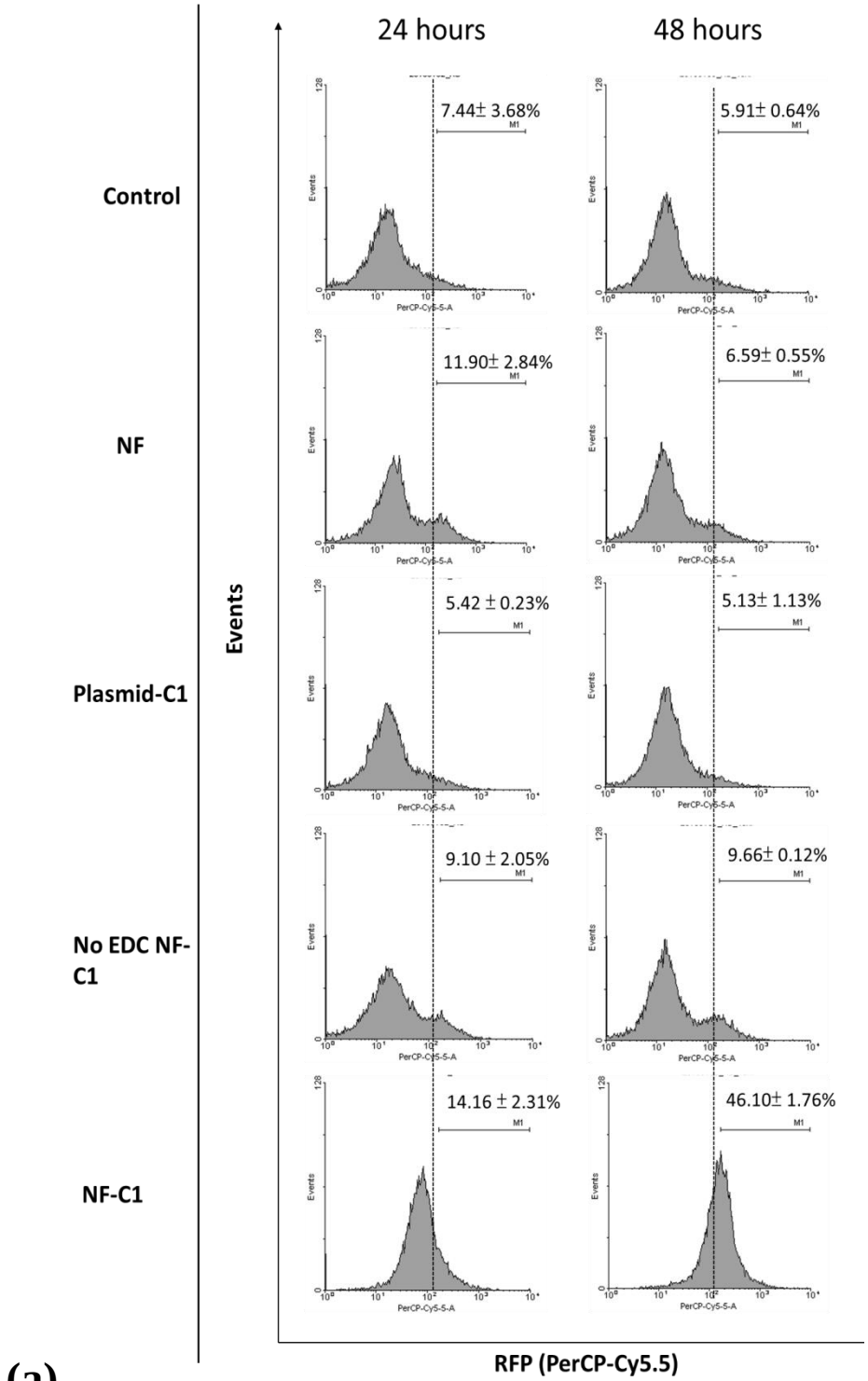
24 hours
48 hours
Control
NF
Plasmid-C1
No EDC NF-C1
NF-C1
7.44± 3.68%
5.91± 0.64%
11.90± 2.84%
6.59± 0.55%
5.42 ± 0.23%
5.13± 1.13%
9.10 ± 2.05%
9.66± 0.12%
14.16 ± 2.31%
46.10± 1.76%
M1
Events
PerCP-Cy5-5-A
RFP (PerCP-Cy5.5)

(a)

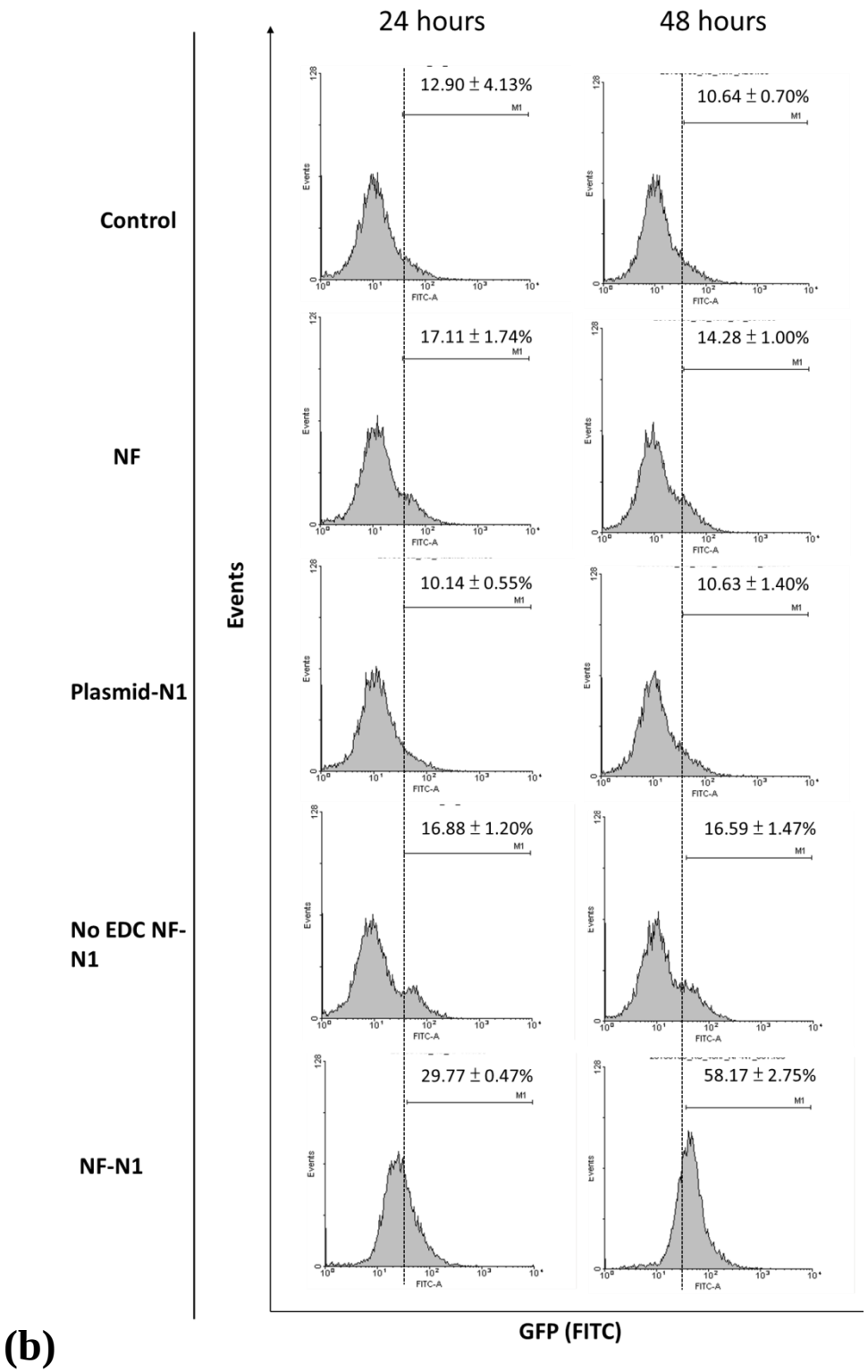
24 hours
48 hours
Control
NF
Plasmid-N1
No EDC NF-N1
NF-N1
12.90 ± 4.13%
10.64 ± 0.70%
17.11 ± 1.74%
14.28 ± 1.00%
10.14 ± 0.55%
10.63 ± 1.40%
16.88 ± 1.20%
16.59 ± 1.47%
29.77 ± 0.47%
58.17 ± 2.75%
M1
Events
FITC-A
GFP (FITC)

(b)

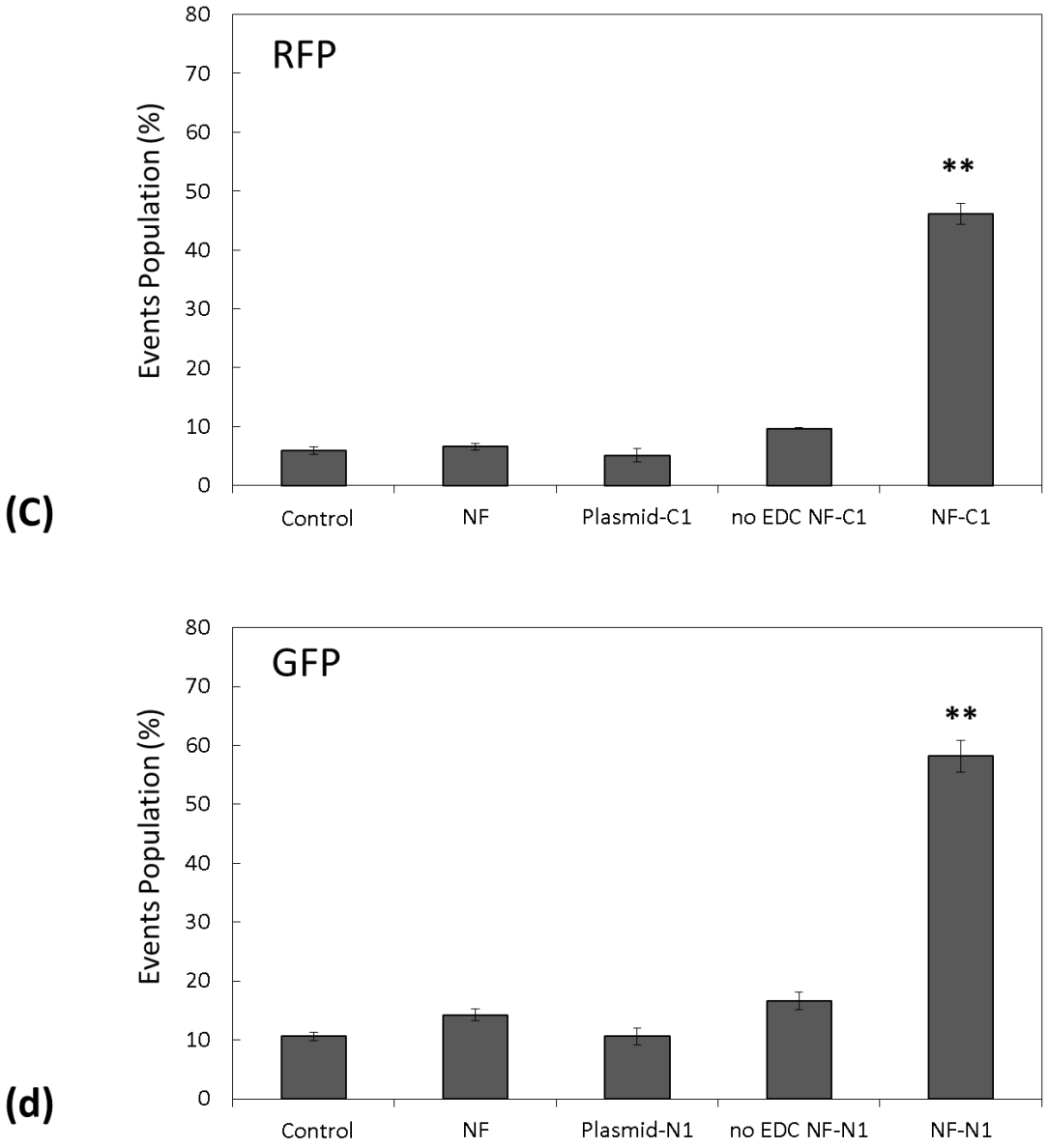

Fig. 4.3.6 Fluorescence signal of (a) RFP or (b) GFP in KU812 cells detected by flow cytometry after transfecting with pDsRed1-C1 or pEGFP-N1 functionalized NFs for 24 hr and 48 hr. Corresponding bar charts showed the events population of cells with (**c**) RFP or (**d**) GFP expression, transfected for 48 hours (n =3, mean±SD)(** $p < 0.01$).

(a)

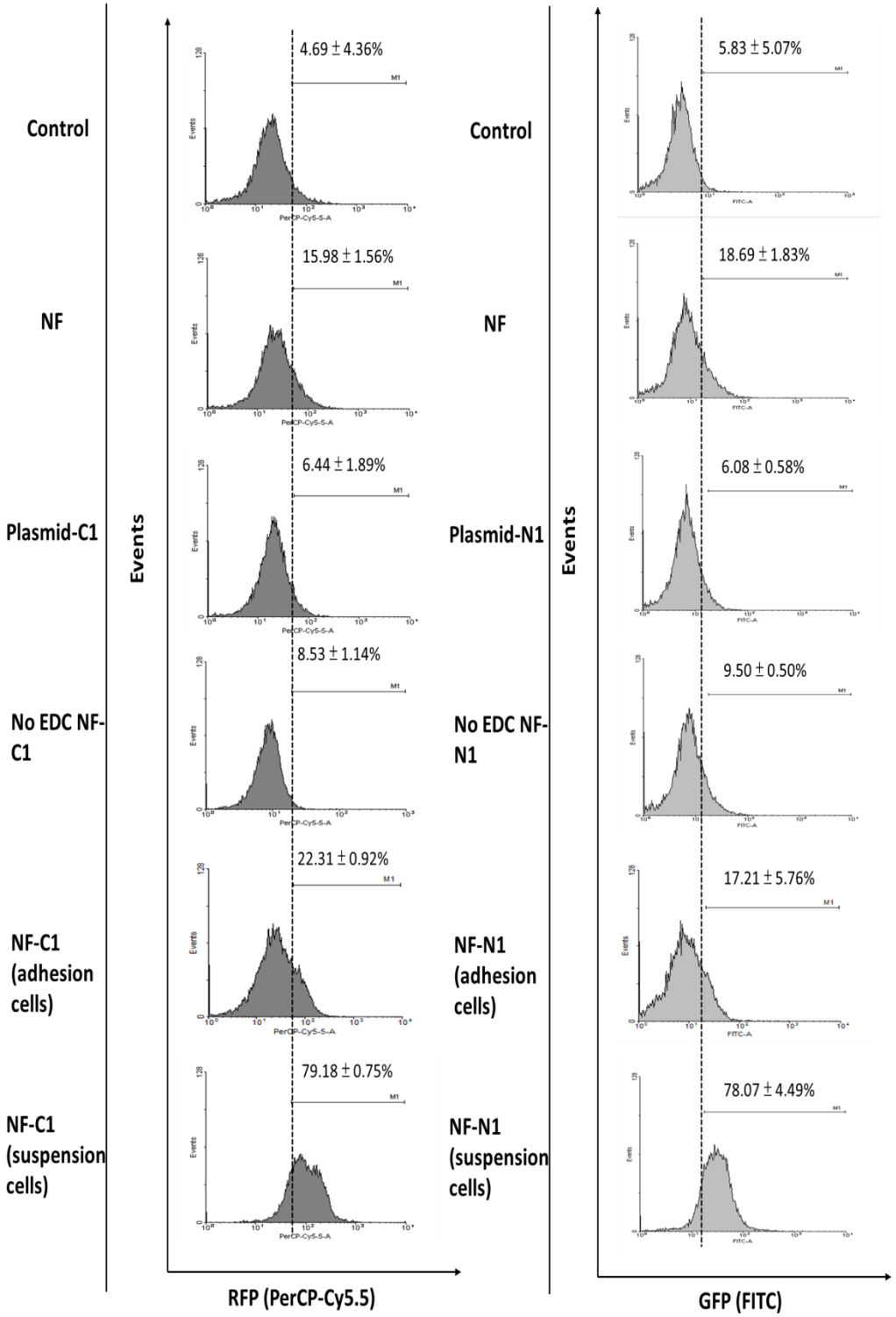
Control
NF
Plasmid-C1
No EDC NF-C1
NF-C1 (adhesion cells)
NF-C1 (suspension cells)
4.69 ± 4.36%
15.98 ± 1.56%
6.44 ± 1.89%
8.53 ± 1.14%
22.31 ± 0.92%
79.18 ± 0.75%
Events
RFP (PerCP-Cy5.5)
Control
NF
Plasmid-N1
No EDC NF-N1
NF-N1 (adhesion cells)
NF-N1 (suspension cells)
5.83 ± 5.07%
18.69 ± 1.83%
6.08 ± 0.58%
9.50 ± 0.50%
17.21 ± 5.76%
78.07 ± 4.49%
Events
GFP (FITC)

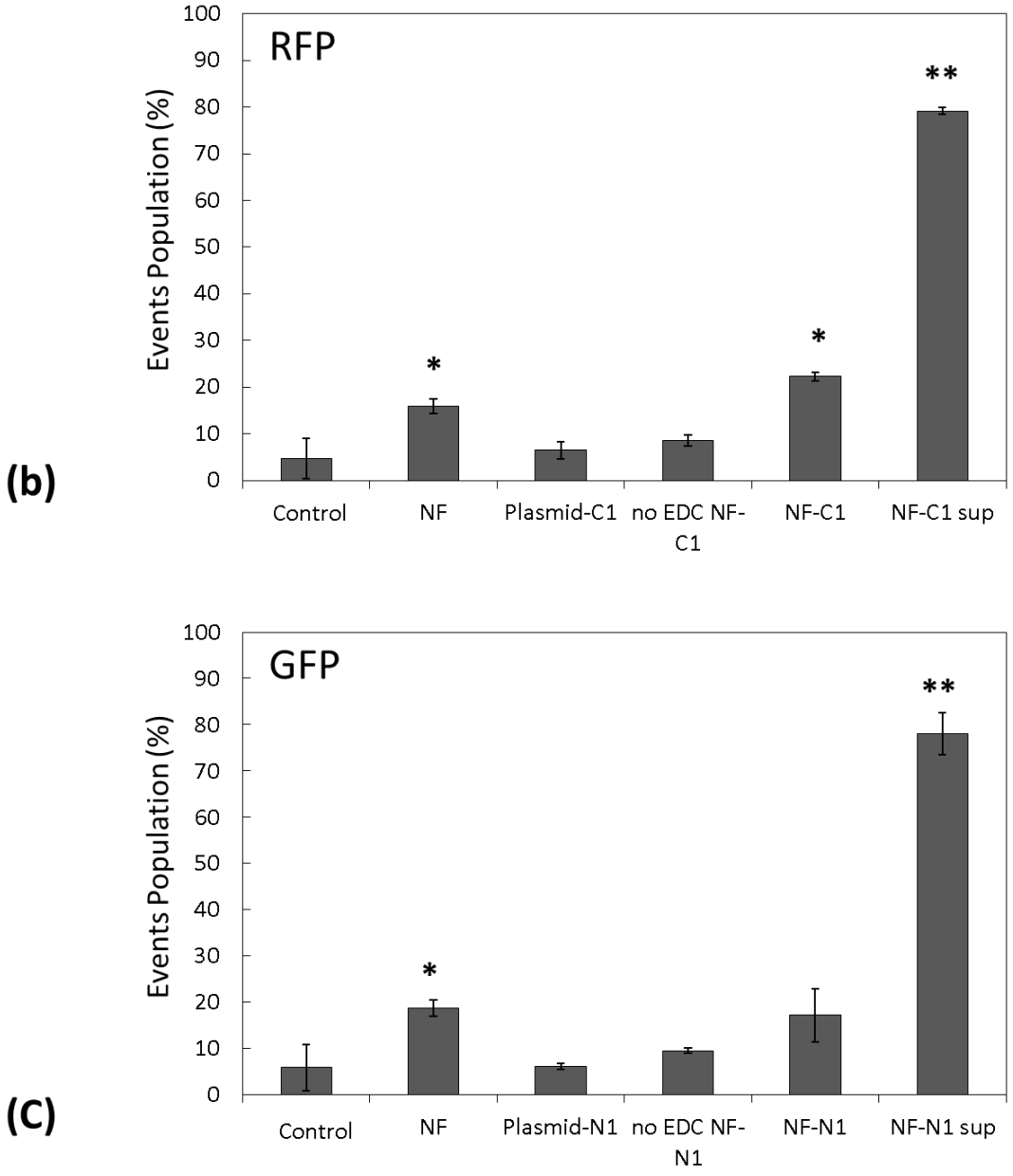

Fig. 4.3.7 Histograms showed the fluorescent signal (a) RFP or GFP in 293T cells detected by flow cytometry after transfecting with pDsRed1-C1 or pEGFP-N1 functionalized NFs for 24 hr and 48 hr. Corresponding bar charts showed the events population of cells with (**b**) RFP or (**c**) GFP expression, transfected for 48 hours (n =3, mean±SD)(* $p< 0.05$, ** $p< 0.01$).

4.3.4 FSC and SSC investigation after transfections

By the flow cytometry, changes in SSC and FSC were seen under the treatment with the NF-Plasmid. In view of this interesting observation, we tried to analyze the SSC against the FSC in a 2D dot plots, in order to find out the relationships between NF-Plasmid transfection and cells size and cellular complexity. To have a clear picture, a FSC dependent gate was set. As shown in Figure 4.3.8, a trapezoid area was chosen as the FSC gate, which was the region of the major cell population. In the groups treated with the medium containing NFs alone, a small population with high SSC and low FSC was appeared (arrow, Figure 4.3.8b, d-e), which was absent in either the control or plasmid treated group (Figure 4.3.8a, c). . To distinguish whether the small population was due to NFs particles or the aggregation of NFs, NFs were mixed with culture medium for flow cytometry assay. It was found that no event can be recorded. Hence, it was believed that the small population was caused by the aggregation of NFs. The percentages in the arrow shown areas were approximately 6 % and 10 % of total population in the NFs treated and NF-Plasmid treated groups respectively. Hence, this small population was excluded for analysis. Figure 4.3.9 showed the relative FSC histograms and bar charts among different groups. To compare with the control group, cells did not showed any FSC change at 48 hours post-transfection with bare NFs, plasmid or no EDC NF-Plasmid (Figure

4.3.9a) suggesting the cell size did not change. However, for the NF-Plasmid treated groups, an obvious decrease in FSC could be seen (Figure 4.3.9a, overlapping histogram). For comparison, the mean values of FSC among different groups were elevated after the same gating. The FSC mean value remained the same in the control, NFs, Plasmid and no EDC NF-Plasmid groups, whereas there was a significant decrease in the FSC mean value in the NF-Plasmid treated group after gating, suggesting that the cell size decreased after the NF-Plasmid transfection and GFP/RFP expression.

At the same time, there was no significant change in the mean value of SSC in the NF-Plasmid treated group, with reference to other groups (Figure 4.3.10a-b). The SSC mean values of all groups remained same. In summary, approximately half of the KU812 cells could express fluorescent proteins after treating with the NF-Plasmid, with a decrease in cell size and unchanged internal complexity.

Due to the above finding, we raised a question whether the decreased of FSC value was caused by the transfection of NF-Plasmid and expression of fluorescent proteins. In order to find out the answer, the RFP dependent gating was set as shown in Figure 4.3.11. The upper region was positive in RFP expression, which was

defined as R1 (red color labeled), whereas the lower region (R2) without the RFP expression (green color labeled). The RFP gating was combined with FSC gating for SSC against FSC 2D plots analysis (Figure 4.3.12a-e). In these 2D plots, it was clear to see that RFP was expressed in the selected cell population. In Figure 4.3.12a-d, for the control group, cells treated with NFs, Plasmid, and no EDC NF-Plasmid, the majority of cells were RFP negative in RFP (label in green). However, in Figure 4.3.12e for the NF-Plasmid treated cells, the majority of cells were RFP positive. The arrow showed population was absent in the NF-Plasmid treated group, which was negative in the RFP expression among the other groups. To compare the FSC mean values between R1 and R2, the mean values of FSC were plotted as bar chart in Figure 4.3.12f. Besides the NF-Plasmid treated group, the FSC mean value in each group in R1 was obviously lower than the one in R2, which indicated the cells with RFP positive would have a smaller cell size. At the same time, the population in the NF-Plasmid treated group shifted to the right hand side in the 2D plot, with a decrease in the FSC mean value (Figure 4.3.12e-f). Of note, the FSC mean value of R1 region in the NF-Plasmid treated group was same as the one in the R1 regions in other groups. However, the FSC mean value in the NF-Plasmid treated group R2 region was as low as the one in same group R1 region. These results indicate that RFP expression would be one of the reasons leading to cells size reduction. After the

transfection of NF-Plasmid, even lacking in expressing fluorescent proteins, the cells size of overall population was decreased for unknown reason. However, as the populations in R1 region among other groups without successfully transfection were only around 10 to 14 %, the majority of populations were located in the R2 region, which had a larger cell size when compared with that of the successfully transfected one. Hence, the overall FSC could also help us to define whether cells were successfully transfected with the NF-Plasmid or not.

Additionally, in R1 region, there were significantly enhanced of SSC mean values in the NF and no EDC NF-Plasmid treated groups with reference to the control. It is suggested that the cells had increased the granularity as a result of endocytosis of the NFs. On the other hand, no change was found in the SCC mean value in the R2 region among all groups. However, a reduction in the SSC mean value was found in the R1 region of the NF-Plasmid treated group suggesting a decrease in cell complexity (Figure 4.3.12g). These results indicate that cells with successful transfection had characteristics in both cell size and granularity decrease.

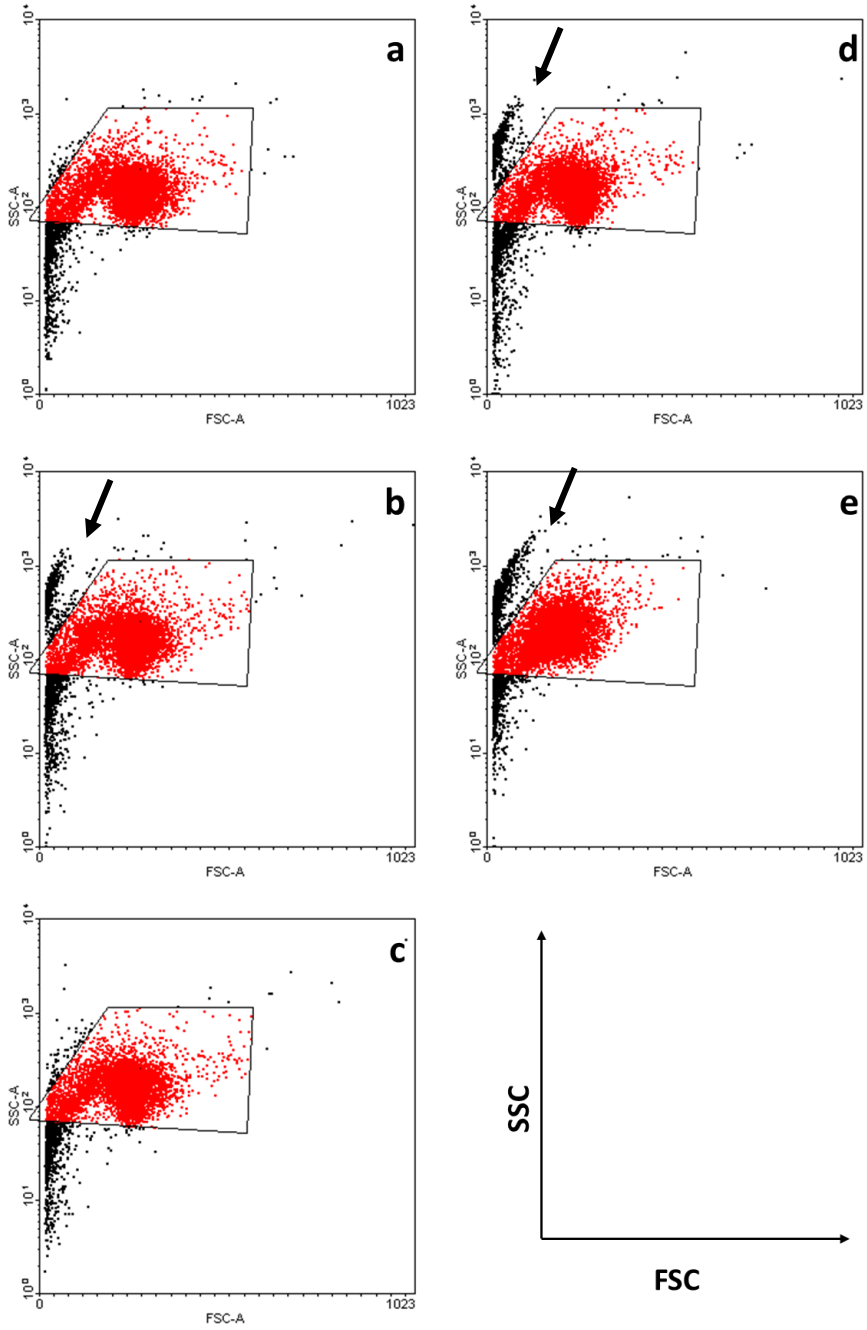

Fig. 4.3.8 2D plots (SSC against FSC) of KU812 cells 48 hr after transfection. Cells were incubated with 0.1 nM of (**a**) no NFs (medium only, Control); (**b**) NFs; (**c**) Plasmid-C1; (**d**) no EDC NF-C1; (**e**) NF-C1 for 48 hours at 37 ^{0}C, followed by flow cytometry assay. Gating according to the FSC was set (Trapezoid area) for analysis.

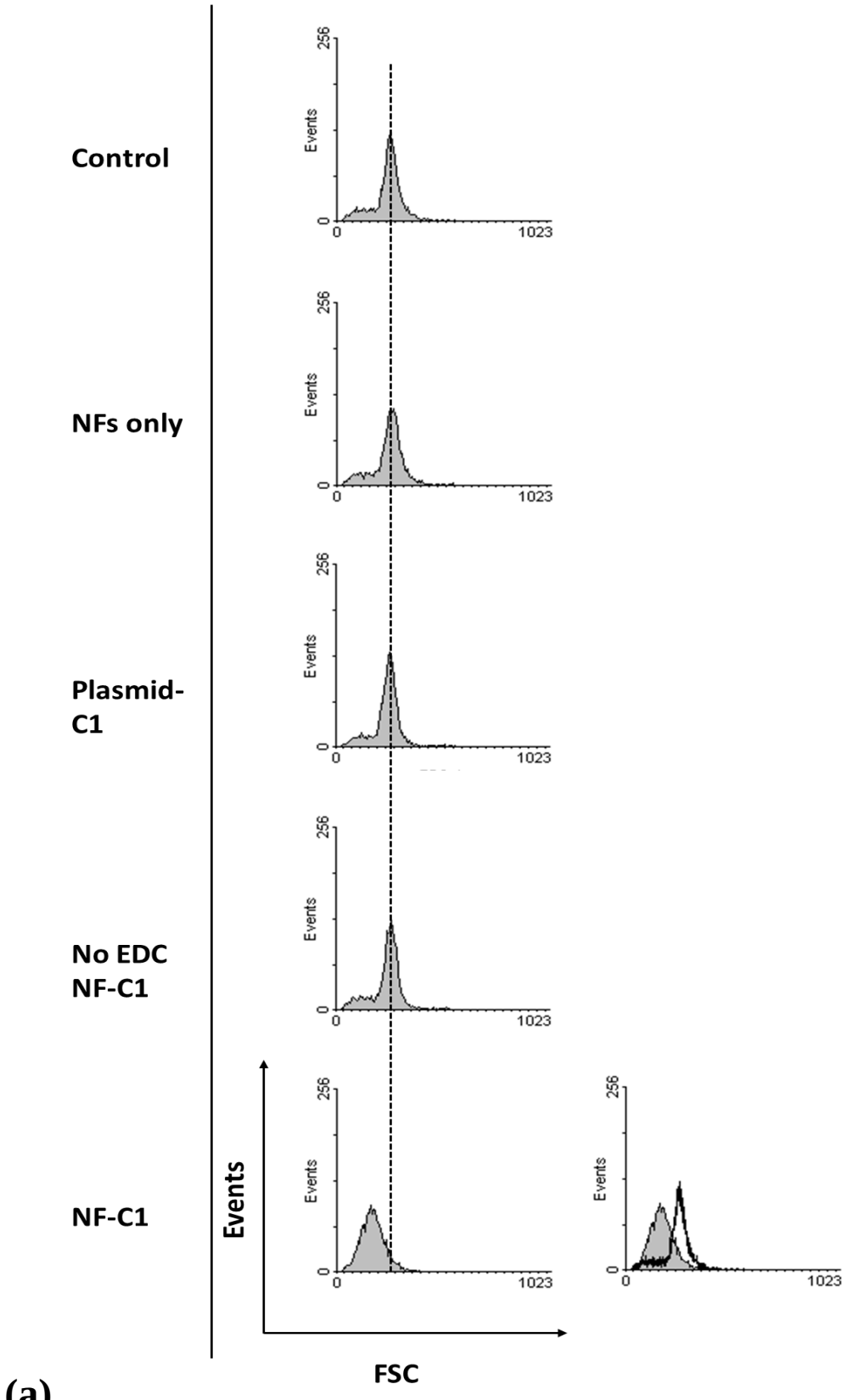
Control
NFs only
Plasmid-C1
No EDC NF-C1
NF-C1
Events
FSC
256
0
1023

(a)

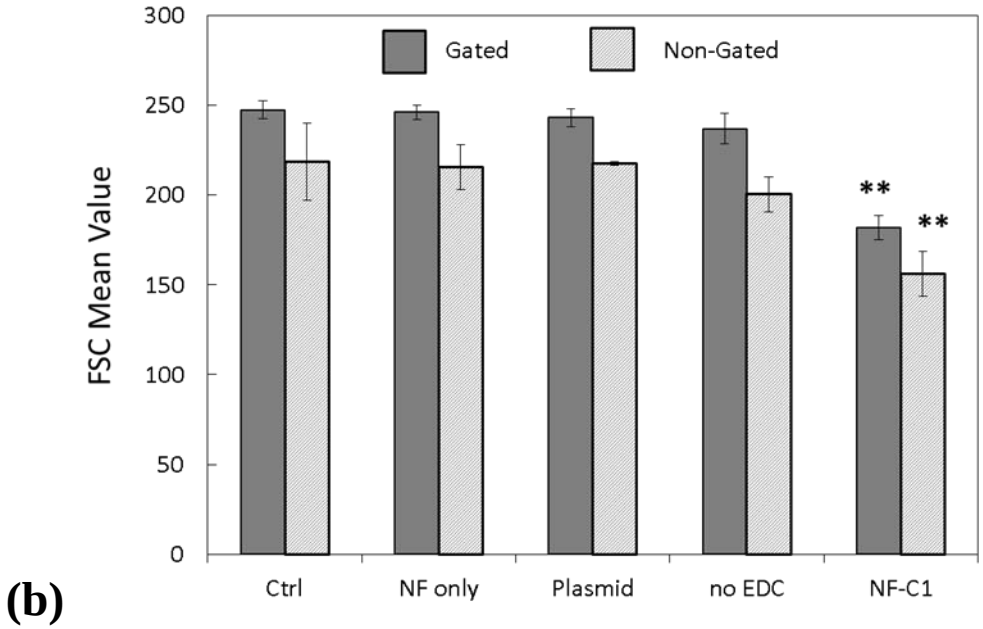

(b)

Fig. 4.3.9 Analysis (with FSC gating) of FSC of KU812 cells 48 hr after treatments. The gating was showed as Fig. 4.3.8. The histograms were showed in (**a**). The FSC histograms of control group (black liner region) and NF-C1 treated group (shaded region) were overlapped. In (**b**), the mean value of FSC from different groups were compared (n = 3, mean ± SD)(** $p < 0.01$).

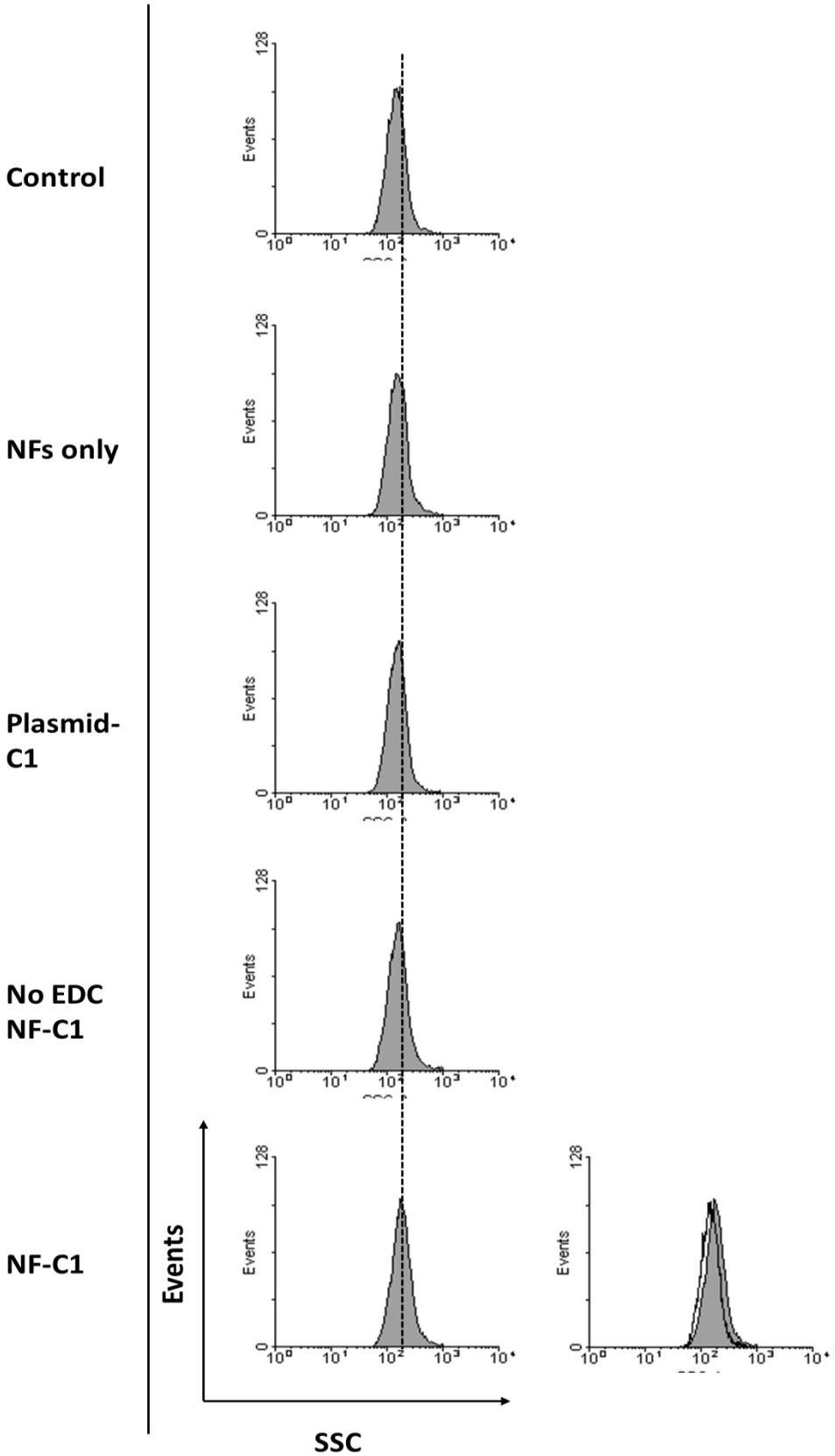
Control
NFs only
Plasmid-C1
No EDC NF-C1
NF-C1
Events
SSC
128
0
Events
10^0 10^1 10^2 10^3 10^4

(a)

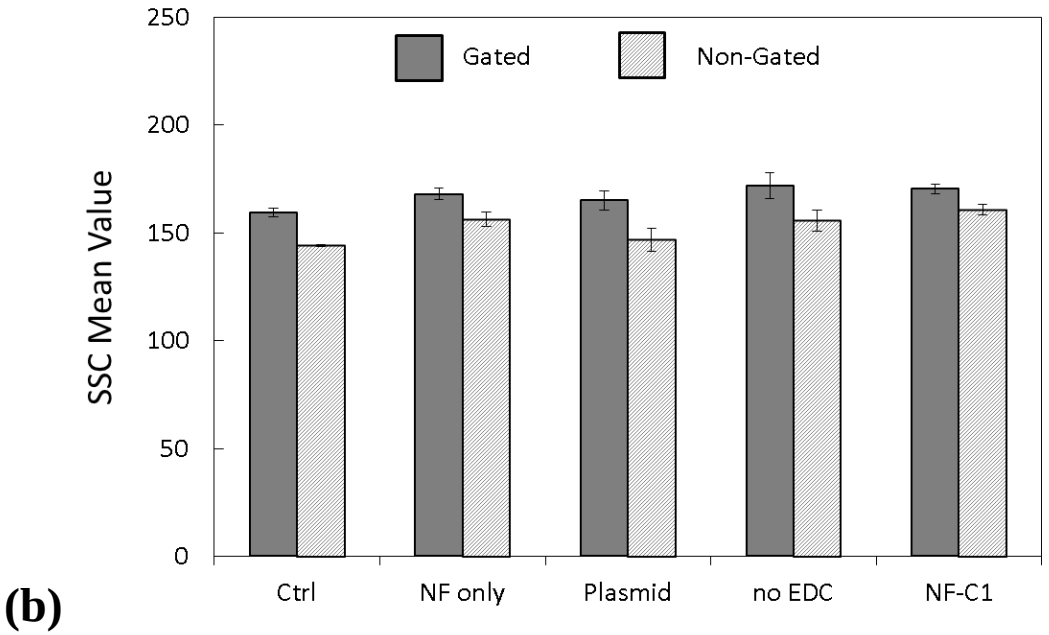

(b)

Fig. 4.3.10 Analysis (with FSC gating) of SSC of KU812 cells 48 hr after treatments. The gating was showed as Fig. 4.3.8. The histograms were showed in (**a**). The SSC histograms of control group (black liner region) were overlaid with NF-C1 treated group (shaded region). In (**b**), the mean values of SSC from different groups were compared (n = 3, mean ± SD).

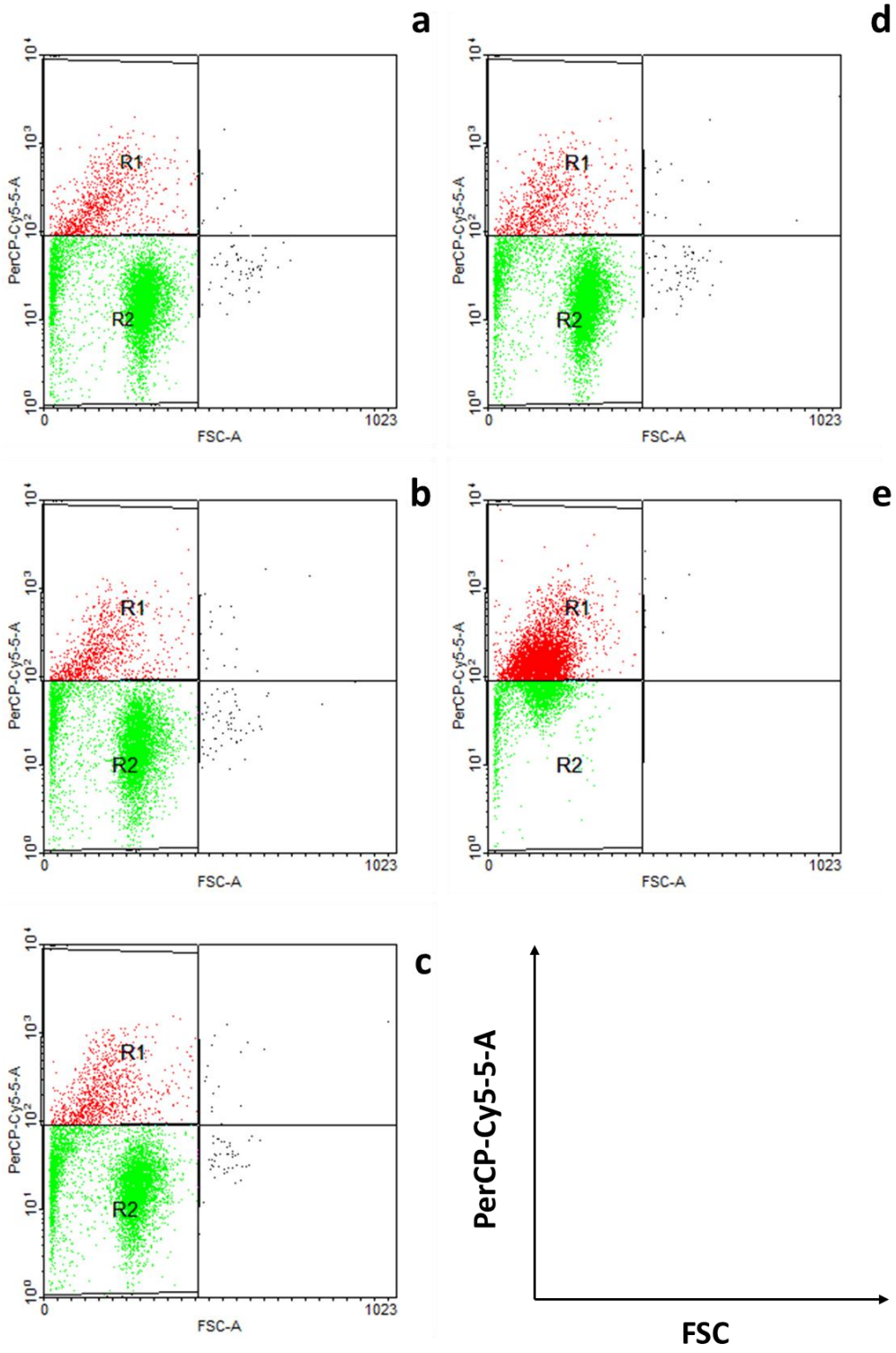

Fig. 4.3.11 RFP signal against FSC 2D plots of KU812 cells 48 hr after transfection. Cells were incubated with 0.1 nM of (**a**) no NFs (Control); (**b**) NFs; (**c**)

Plasmid-C1; (**d**) no EDC NF-C1; (**e**) NF-C1 for 48 hours at 37 ^{0}C, followed by flow cytometry assay. RFP signal dependent gating was set as shown in Region 1 (R1, positive in RFP expression) and Region 2 (R2, negative in RFP expression).

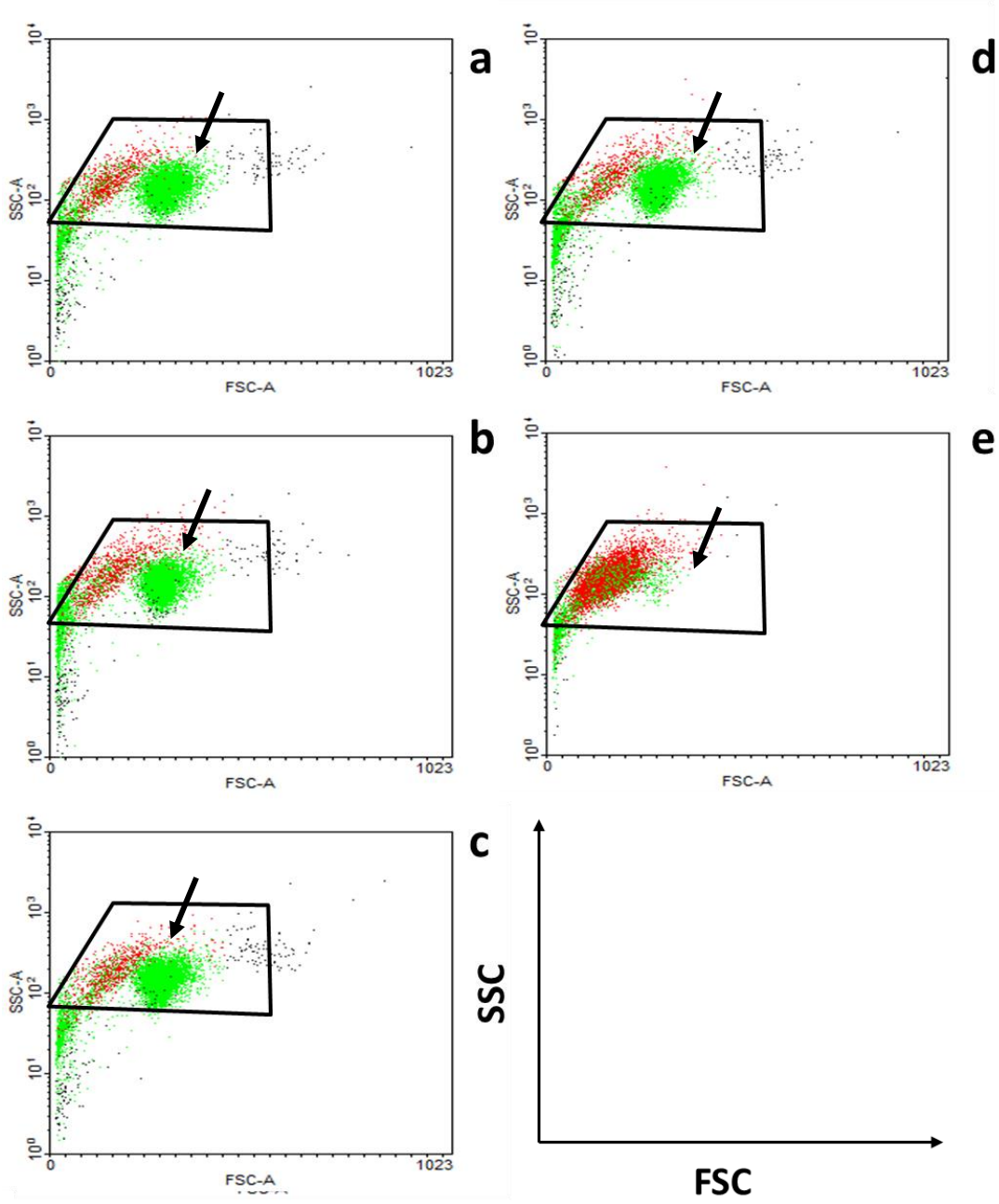

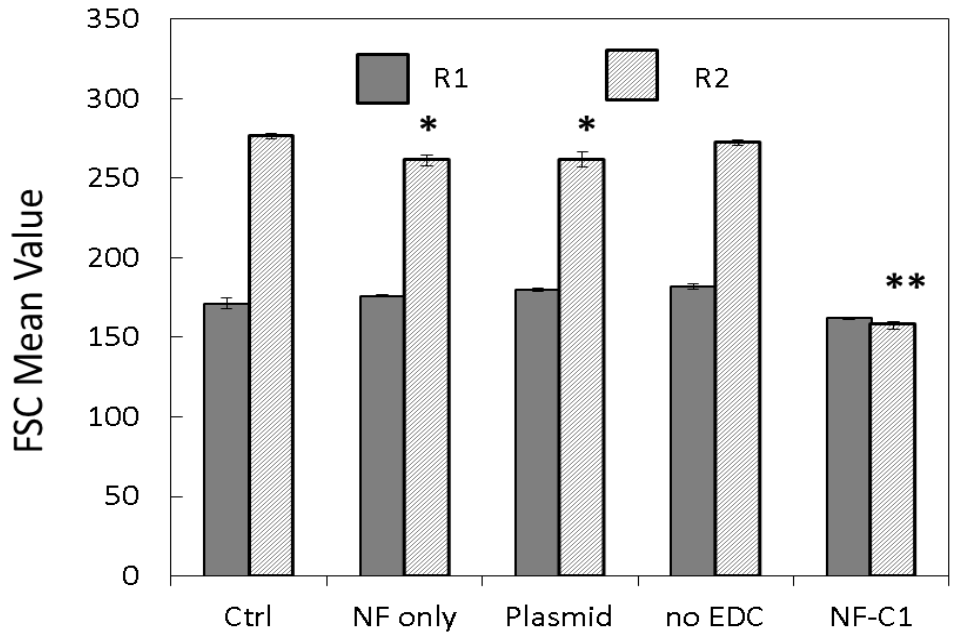
f
FSC Mean Value
350
300
250
200
150
100
50
0
R1
R2
*
*
**
Ctrl
NF only
Plasmid
no EDC
NF-C1

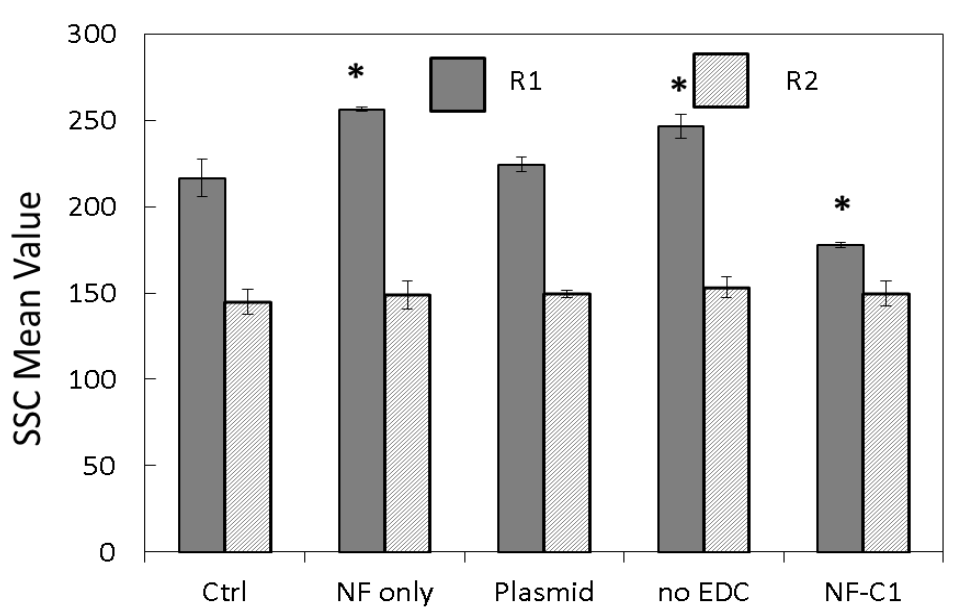
g
SSC Mean Value
300
250
200
150
100
50
0
R1
R2
*
*
*
Ctrl
NF only
Plasmid
no EDC
NF-C1

Fig. 4.3.12 Combined FSC gating as RFP signal gating for analyzing KU812 cells flow cytometry assay after undergoing 48 hr transfection. Cells were incubated with 0.1 nM of (**a**) no NFs (Control); (**b**) NFs; (**c**) Plasmid-C1; (**d**) no EDC NF-C1; (**e**) NF-C1 for 48 hours at 37 ^{0}C, followed by flow cytometry assay. The RFP signal dependent gating and FSC gating were shown as Fig. 4.3.11 and Fig. 4.3.8 respectively. The corresponding (**f**) FSC mean values and (**g**) SSC mean values were shown as bar charts. (n = 3, mean ± SD) (* $p < 0.05$, ** $p < 0.01$)

4.4. Discussion

NPs can be used as carriers to transfer DNA into cells. One of the purposes of gene transfer is for gene therapy. As mentioned in Section 4.1, the free linearized plasmids can hardly be and functionalized after entering mammalian cells. According to the result of fluorescence signal measurement, it matched with this statement that treating free linearized plasmid could hardly induce the expression of fluorescent proteins in both suspension and adherent cells. Only the NFs carrying plasmids with EDC linkage could successfully induce the expression of fluorescent proteins in cells. Cells can uptake the NPs or NFs by phagocytosis or reacting with sub-cellular structures [Simko et al., 2011; Xia et al., 2006]. The uptake process can be passive, without specific membrane receptors or by adhesive interaction. However, whether the cells retain the NPs, or trigger any chemical reactions, depend on the size and composition of the particles.

The study in this chapter confirmed that the NFs used in our project did not show cytotoxicity to human basophil and embryonic kidney cells. The NF-Plasmid would lead to the decrease in cell viability. Our results indicate that the slight cytotoxic effect was caused by the crosslink agent, EDC although not too many papers report the cytotoxicity of EDC in mammalian cells in literature [Moshnikova

et al., 2006]. EDC is a well-known crosslinking agent which has been commonly used together with NHS, in nanomaterial modification or scaffold synthesis and it is believed EDC is a suitable crosslinker in the NFs modification. Another agent which can be used for plasmids functionalization is polyethylenimine (PEI). NPs functionalized with PEI and plasmids demonstrated low cytotoxicity in human glioblastoma cells [Leung 2013].

Besides the cytotoxicity, the transfection efficiency has been a concern. The transfection efficiency of human cells using other methods such as Lipofectamin® or viral infection can be affected by the cell lines. In our study, it was found that the transformation efficiency of NF-Plasmid in 293T cells was relatively higher than the KU812 cells. Overall, the cell viability remained more than 70 % in both KU812 cells and 293T cells 48 hr after treating the cells with 0.1 nM of NF-Plasmid. In addition, the expression rate of fluorescent proteins was more than 50 %, which had satisfied transfection efficiency. The study confirmed that NFs is a good nanomaterial for gene transfer.

In our project, we report the relationship between the NF-Plasmid transfection and cell morphology for the first time. It was confirmed that KU812 cells had a

reduction in cell size and granularity after transfection, together with the expression of the fluorescent proteins. By this finding, it provides another dimension for cell screening and sorting after NF-Plasmid transfection.

References:

Cheung, K.L., Chen, Q.L. et al. (2012). CTAB-coated gold nanorods elicit allergic response through degranulation and cell death in human basophils.*Nanoscale*, 4(15), 4447-49.

Corsi, K., Chellat, F. et al. (2003). Mesenchymal stem cells, MG63 and HEK293 transfection using chitosan-DNA nanoparticles.*Biomaterials,* 24(7), 1255-64.

Lau, I.P., Chen, H. et al. (2011). *In vitro* effect of CTAB- and PEG-coated gold nanorods on the induction of eryptosis/erythroptosis in human erythrocytes.*Nanotoxicology*, 6, 847-56.

Leung, K.C., Chak, C.P. et al. (2013). Enhanced cellular uptake and gene delivery of glioblastoma with deferoxamine-coated nanoparticle/plasmid DNA/branched polyethylenimine composites. *Chem. Commun.*, 49, 549-51.

Mao, H.Q., Roy, K. et al. (2001).Chitosan-DNA nanoparticles as gene delivery vehicles.*J. Control. Release.*, 70(3), 399-421.

McBain, S.C., Yiu, H.H.P. et al. (2007).Polyethyleneimine functionalized iron oxide nanoparticles as agents for DNA delivery and transfection. *J. Mater. Chem.*, 17, 2561-65.

Moshnikova, A.B., Afanasyev, V.N. et al. (2006). Cytotoxic activity of 1-ethyl-3-(3-dimethylaminopropyl)-carbodiimide is underlain by DNA interchain cross-linking. *Cell. Mol. Life Sci.*, 63, 229-34.

Sandhu, K.K., McIntosh, C.M. et al. (2002). Gold nanoparticle-mediated transfection of mammalian cells.*Bioconjug Chem.*, 13(1), 3-6.

Simko, M., Fiedeler, U. et al. (2011).The impact of nanoparticles on cellular functions. Nano trust dossiers.7. 1-4.

Xia, T., Kovochich, M. et al. (2006).Comparison of the abilities of ambient and

manufactured nanoparticles to induce cellular toxicity according to an oxidative stress paradigm.NanoLetter.6(8).1794-807.

Xuan, S., Wang, F. et al. (2011).Hierarchicalcore/shell Fe3O4@SiO2@γ-AlOOH@Au micro/nanoflowers for protein immobilization.*Chem. Commun. (Camb.)*, 47(9), 2514-16.

Chapter 5 Use of TRPS to study the drug effect of Polyphyllin D (PD) and silver nanoparticles (AgNPs)) on the induction of eryptosis in human erythrocytes (RBCs)

5.1 Introduction

In this chapter, we tried to further demonstrate the usage of TRPS for cell-based assays with human erythrocytes (RBCs). TRPS has recently been used widely in the nanotechnology field to qualify and quantify non-optically the aggregation dynamics of NPs without labeling [Vogel et al., 2011; Willmott and Parry, 2011; Roberts et al., 2010; Low et al., 2011]. Now, more and more groups start to use TRPS as the technique for viral and bacterial study.

Mature human red blood cells (RBCs) are the most abundant and specialized cell type in our body. Apart from transporting oxygen and carbon dioxide, RBCs also play an important role in the onset of many complications such as heart disease and strokes [Bornéet et al., 2011]. For instance, RBCs release ATP into the blood, which stimulates the release of nitric oxide from endothelial cells leading to vasodilation and inhibition of platelet aggregation [Ellsworth et al., 2009]. Exposure of cells to some toxic molecules elicits a cell death process in RBCs called

eryptosis/erythroptosis although human RBCs are devoid of cell nucleus and mitochondria for the induction of apoptosis [Lang et al., 2012a, b]. Cell shrinkage is one of the early hallmarks for eryptosis/erythroptosis [Lang et al., 2012a, b]. In view of the fact that the average size of human erythrocytes, generally about 8 µm in diameter and 1 µm in thickness [Khairy et al., 2008], falls in the detection range of the TRPS system, we tried to use the TRPS for the first time to study the toxic side effects of Polyphyllin D (PD), a potential anti-cancer drug which kills drug-resistant liver cancer cells [Ong et al., 2008], in terms of change in cell size and externalization of phosphatidyl-serine (PS), another feature of eryptosis/erythroptosis in RBCs. One of the common side effects of using anti-cancer drugs in patients is the development of anemia. We therefore asked whether we could employ the TRPS to monitor the change in size and blockade duration in the human erythrocytes to study the toxic side effects of PD.

Additionally, as reported in Chapter 4, NFs or other nanomaterials can be used for different applications in the biomedical field. One of the examples is using nanosilver particles (AgNPs) as materials of scaffold for wound healing and anti-bacterial agent. Hence, in the second part of this chapter, AgNPs were chosen as the model nanomaterials to study the cytotoxicity of AgNPs, if any, in the human

RBCs using TRPS. AgNPs are defined as a cluster of silver atoms with at least one dimension in 1-100 nm. AgNPs can be synthesized by different production methods with different stabilizers, surfactants and shapes. In this study, AgNPs were produced in house by reducing $[Ag(NH_3)_2]^+$under UV light in the presence of poly(vinyl pyrrolidone) (PVP) as stabilizer [Chaloupka et al., 2010].

Traditionally, Annexin V is a molecular probe which binds with the PS on the apoptotic cells or eryptotic RBCs. Annexin V can be modified with fluorochrome conjugation for signal reporting, which convinces the flow cytometry and confocal microscopy assay. Here we try to combine the TRPS and Annexin V-tagged NPs, to study the effect of PD or AgNPs in RBCs, to report the concept to employ TRPS for cell-based toxicity studies.

5.2 Materials and Methods

5.2.1 Materials

Polyphyllin D (PD) was obtained from Shanghai Fine Chemical. PD was dissolved in DMSO at 50 mM as stock storing at -20 ^{0}C in dark.

Annexin-V-RFP was synthesized in house and purified by nickel affinity

column, store at -20 ^{0}C in dark.

BcMag^{TM} His-Ni Magnetic beads (mean size 1 µm diameter) were obtained from Bioclone Inc. (CA, USA).

AgNPs (28 nm edge length silver nanoparticles) were supplied by Dr. H.F. Lu, Department of Electronic Engineering, CUHK. AgNPs were produced by reducing $[Ag(NH_3)_2]^+$under UV light in the presence of PVP as stabilizer. The size of AgNPs was characterized by its extinction spectrum (Figure 5.2.1a). The size of AgNP was estimated to be 29.0 ± 3.6nm, which is characterized by 490nm extinction peak. AgNPs were in a decahedronal shape and SEM image is shown in Figure. 5.2.1 b.

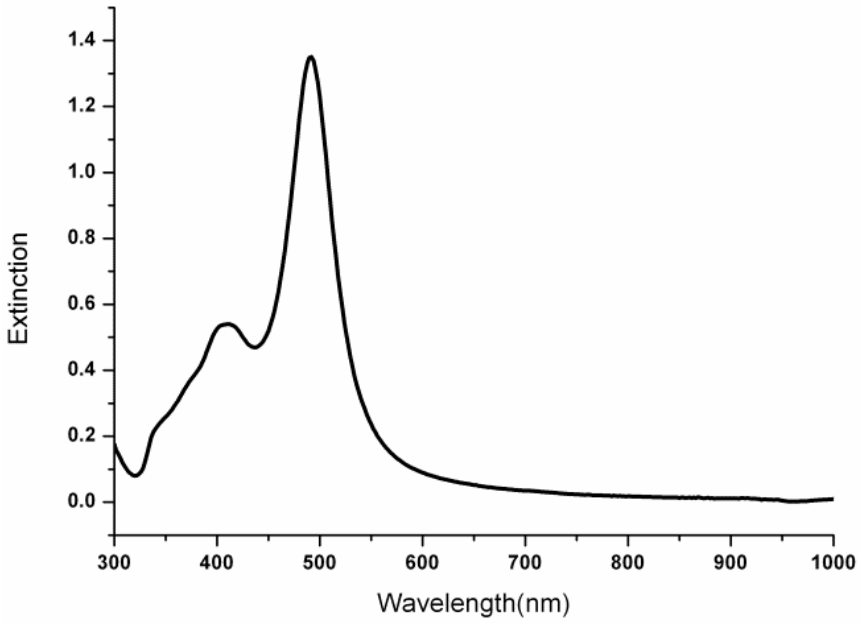

(a)

(b)

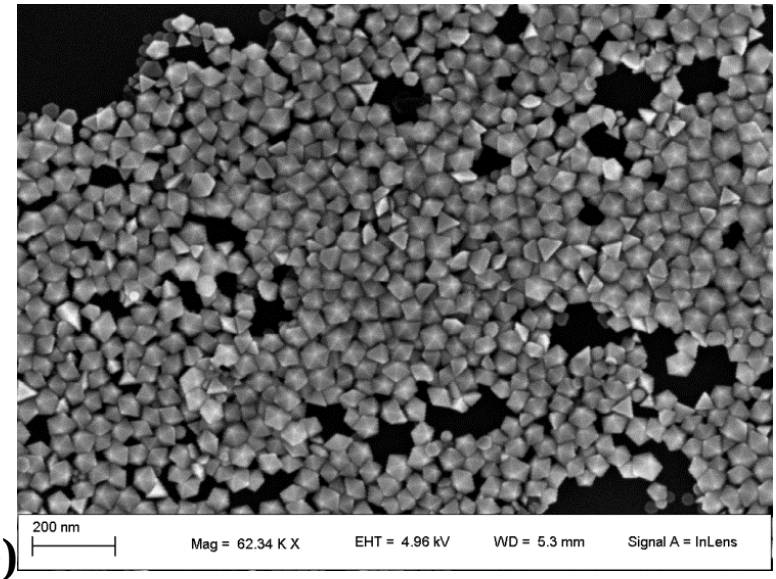

Fig. 5.2.1 The UV-vis extinction spectrum and SEM image of AgNPs used in this study. (**a**) Silver nanodecahedrons with 490nm extinction peak were estimated to be 29.0 ± 3.6nm in edge length. (**b**) The shape and size of AgNPs were captured by SEM.

A commercially available size-tunable nano/micropore platform (qNano, IZON Science) was employed for the TRPS assay.

5.2.2 Methods

5.2.2.1 Human Erythrocytes Preparation and Culture

This study was approved by the Clinical Research Ethics Committee of the Chinese University of Hong Kong (Protocol number: CRE-2012.025), the Hong Kong Special Administrative Region, China. Two to three droplets of fresh human

RBCs were obtained from healthy donors following informed consent by puncturing fingertips with a sterile lancet with depth setting. Heparinized RBCs were washed three times with isotonic PBS (136.9 mM NaCl, 2.7 mM KCl, 10 mM Na_2HPO_4, and 1.5 mM KH_2PO_4, pH7.4) for experiments.

RBCs (1.5 x 10^7/mL) were resuspended with HEPES buffer (140 mM NaCl, 5 mM KCl, 10 mM HEPES, 2.5 mM $CaCl_2$, 10 mM Glucose and 0.1% (w/v) BSA, pH 7.4) in 12-well plates. Simultaneously, PD was added into RBCs in final concentration as 0.31, 0.63, 1.25, 2.50 and 5.0 μM respectively. The RBCs were incubated at 37 ^{0}C for 24 hr. For the ionomycin treatment group, 2 μM (final concentration) was added into RBCs, followed by 37 ^{0}C incubation for 24 hr.

In AgNPs treatment groups, AgNPs were added into each of the well in 12-well plates. Before applying AgNPs to cells, AgNPs were first centrifuged in 12,000 rpm for 10 min. The supernatant was then removed and the AgNPs pellet was resuspended with HEPES buffer into suitable concentration. The final concentrations of AgNPs were in a range from 2 x 10^{10} particles/mL to 3.1 x 10^8 particles/mL, in 2-fold dilutions. RBCs were incubated at 37 ^{0}C for 24 hr.

For the antioxidant containing group, RBCs were co-treated with AgNPs and 1 mM of N-acetylcysteine (NAC). The control group was done by adding HEPES buffer instead of AgNPs solution.

Independent experiments were repeated. Results shown in this paper represent typical responses from at least 3 independent trials.

5.2.2.2 Hemolysis assay

Human erythrocytes (1.5 x 10^7/mL) were incubated in HEPES buffer with PD at 37 ^{0}C for 3 hr. After treatment, 100 μL of supernatant from each treatment group was transferred to 96-well plates. The absorbance of supernatant was determined against blank (HEPES buffer) at 415 nm with a fluorescent plate reader (Tecan) for the leakage of hemoglobin (Hb). Total cell lysis was achieved by incubating cells with Triton X-100 (final concentration: 0.1 % (v/v)).

For studying the hemolytic effect of AgNPs, same procedures were done as AgNPs replaced PD, for incubating at 37 ^{0}C for 24 hr. NAC (1 mM) was added into cells as the anti-oxidant.

5.2.2.3 Confocal laser scanning microscopy

After treatments, erythrocytes (1.5 x 10^5/mL) were washed by HEPES buffer by centrifugation at 2000 rpm for 5 min, followed by staining with Annexin V-RFP (5μL in 1000 μL of cells suspension) for 15 min at room temperature in dark. Cells were then observed by confocal microscopy after washing. For the Annexin V-magnetic beads staining groups, 1.25 μL of Annexin V conjugated beads (preparation procedure was described in section 5.2.2.4) were added in 1000 μL of cells

suspension, followed by observation by confocal microscopy after 15 min of incubation, without washing. Cells were imaged using a confocal laser scanning microscope (FluoView FV1000, Olympus) equipped with a laser (543 nm) for excitation. Red Fluorescence Protein (RFP) signal was acquiredat583 nm, and images were processed by FluoView application software FV10-ASW 3.0 (Olympus).

5.2.2.4 Conjugation of Annexin V-RFP onto Magnetic beads

BcMag^{TM} His-Ni Magnetic beads (100 µL) were transferred into a 1.5 mL eppendorf tube. The supernatant was removed completely by placing a magnetic separator, followed by washing with 4 volumes of 1 X binding/washing buffer (0.5 M NaCl, 100 mM HEPES, 10 mM imidazole, pH 8.0) twice. The beads were resuspended with one volume of 1 X binding/washing buffer. 100 µg of Annexin V-RFP (contained His-tag) was added into the beads. Beads and protein mixture were mixed well by inverting several times and incubated for 20 min at room temperature with continuous rotation. After incubation, beads were washed with 8 volumes of 1 X binding/washing buffer for three times. The conjugated beads were resuspended with one volume of 1 X binding/washing buffer and store in dark at 4 ^{0}C.

5.2.2.5 Tunable RPS analysis

The working principle, structure and design and detailed experimental procedures of the TRPS using qNano (IZON Science) were reported elsewhere [Ito et al., 2004; Ito et al., 2004 and Henriquez et al., 2004], similar to the procedure as described in Chapter 3 (Section 3.2.2.9). Briefly, the setup and pore setting were optimized using a tunable nano/micropore NP4905 (IZON Science) and certified particle standards (NIST (National Institute of Standards and Technology)-traceable certified polymer beads, mean size = 4422 nm) (Bangs Lab). Pore stretch was maintained at 48.50 mm with a constant voltage of 0.1 V. For the size measurement of human erythrocytes, 35 µL of cell suspension (in HEPES buffer with 0.1% w/v BSA) was added to upper liquid compartment and a constant air pressure of 1 mmH_2O was applied to maintain steady flow of electrolytes or aggregates. Working procedures followed supplier's instructions. Each measurement was recorded for 1,500 blockade events. Results were processed and analyzed by software application (V2.2.56) from IZON Science (Figure 5.2.2).

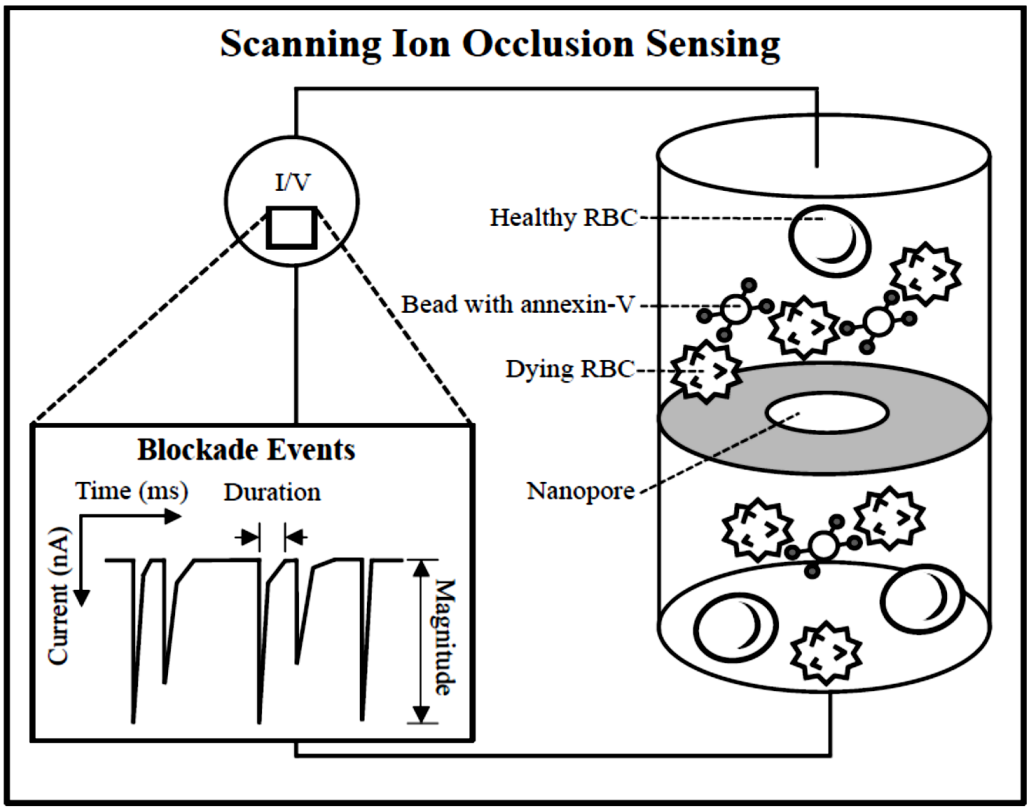

Fig. 5.2.2 Schematic diagram shows the SIOS experimental design.

5.2.2.6 Statistical Analysis

Results were expressed as mean ± SD of three to nine determinations from the blood of different donors of several (>3) independent trials. Data were compared using the Student's *t*-test; *p*-values less than 0.05 were considered statistically significant.

5.3Results

5.3.1 Size and blockade duration investigation by TRPS

PD is an anti-cancer agent which kills liver cancer cells with multi-drug resistance (MDR) with an IC50 around 5 μM [Cheung et al., 2005; Ong et al., 2008; Gao et al., 2012]. In the hemolysis assay, as shown in Figure 5.3.1, PD can lead to 100 % hemolysis at the concentration as 2.5 μM or above. The IC50 of PD in human RBCs is around 0.63 μM, much smaller than the IC50 from the cells with MDR.

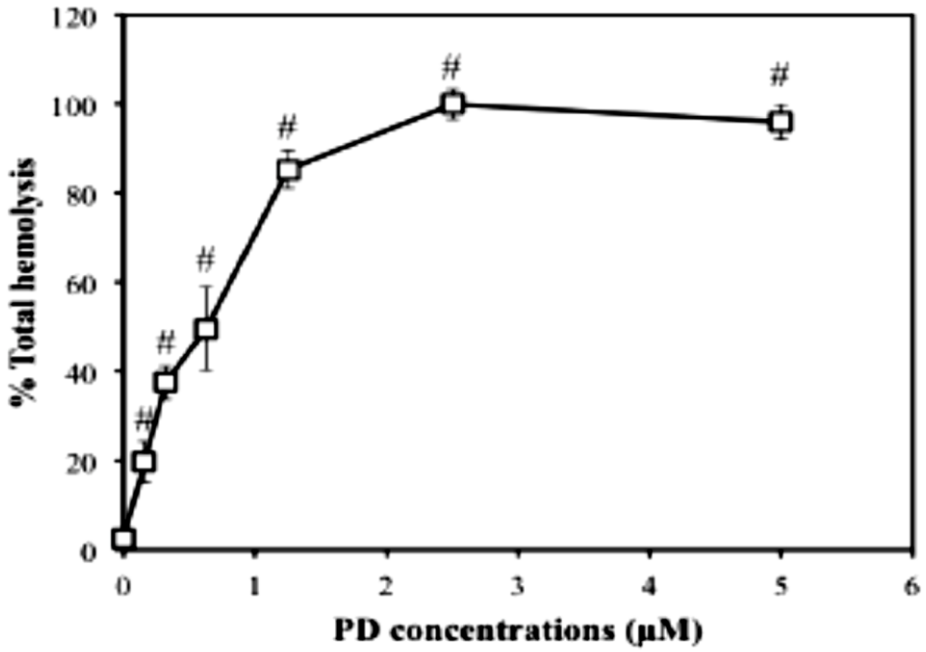

Fig. 5.3.1 Hemolysis assay of human RBCs 3 hr after PD treatment. Cells suspension after PD treatment was transferred to a 96-well plate, followed by measuring the absorbance at 415 nm. Total hemolysis was obtained by treating with Triton X-100. The percentage of hemolysis was expressed as the percentage of total hemolysis (mean±SD, n=3). (Anthony Cheung MPhil. CUHK Thesis, 2012).

Figure 5.3.2 is a typical example of a RT-TRPS trace using the NIST particle standards (mean size 4422 nm) (top) and human erythrocytes (bottom). It can be seen that a steady baseline was maintained at 103-109 nA after optimization. The baseline current is proportional to the size of nanopore, electrolyte conductivity and the voltage applied on the two sides of the nanopore. According to Ito et al. [2004a, 2004b], the magnitude of blockade event is proportional to the size of particles. Therefore by comparing the blockade event magnitude of erythrocytes to that of particle standards, the size of erythrocytes can be obtained.

As shown in Figure 5.3.3, the peak magnitude of erythrocytes in terms of current was about two times of that of particle standards. After normalization, the mean volume of erythrocytes was found to be 86 ± 12 fL, which was in line with the results from other studies [Canham, 1969; Evans and Fung, 1972; Tycho et al., 1985]. Abnormally small RBCs from patients with iron deficiency or thalassemia trait are called microcytes with a mean volume less than 80 fL [Van Vranken 2010]. Larger cells with a mean volume greater than 100 fL are called macrocytes. The most common etiologies for macrocytosis are alcoholism, folate and vitamin B12 deficiencies [Kaferle andStrzoda, 2012]. The mean volume size is therefore helpful in the diagnosis for microcytic and macrocytic anemia.

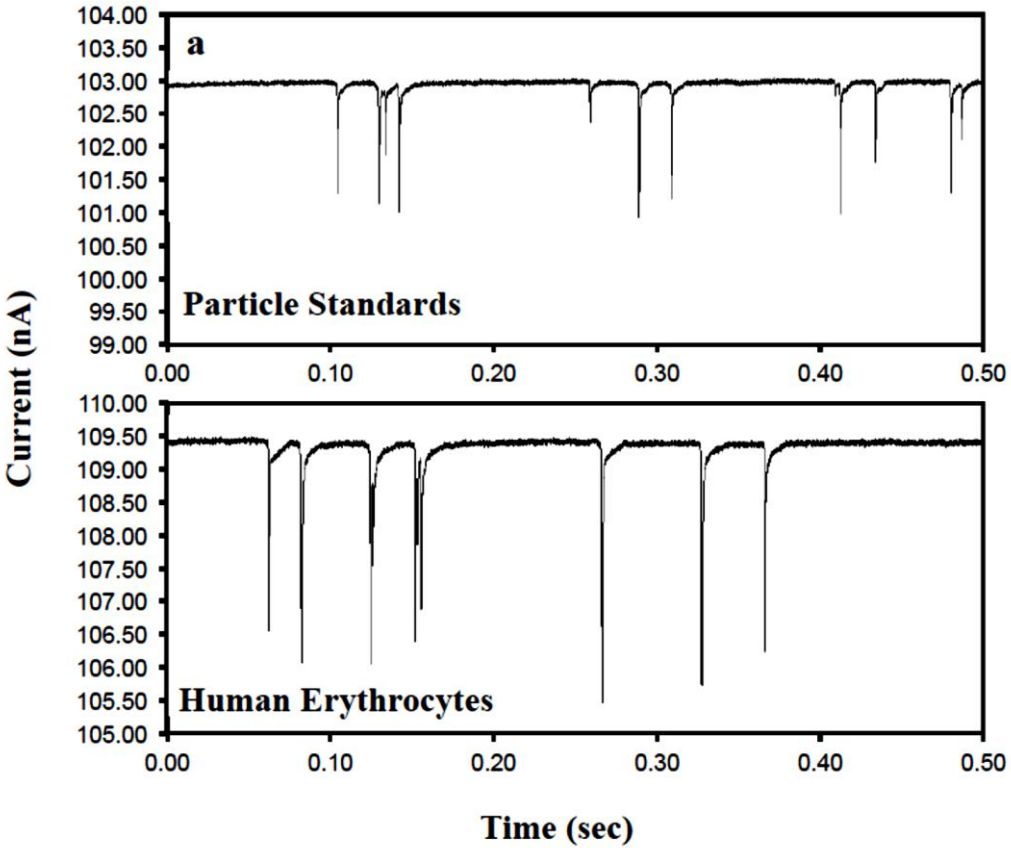

Fig. 5.3.2 Signal traced from TRPS system. The size of human erythrocytes was calibrated and quantified utilizing the NIST (mean size = 4422 nm) standard. Signal traces obtained in HEPES buffer.

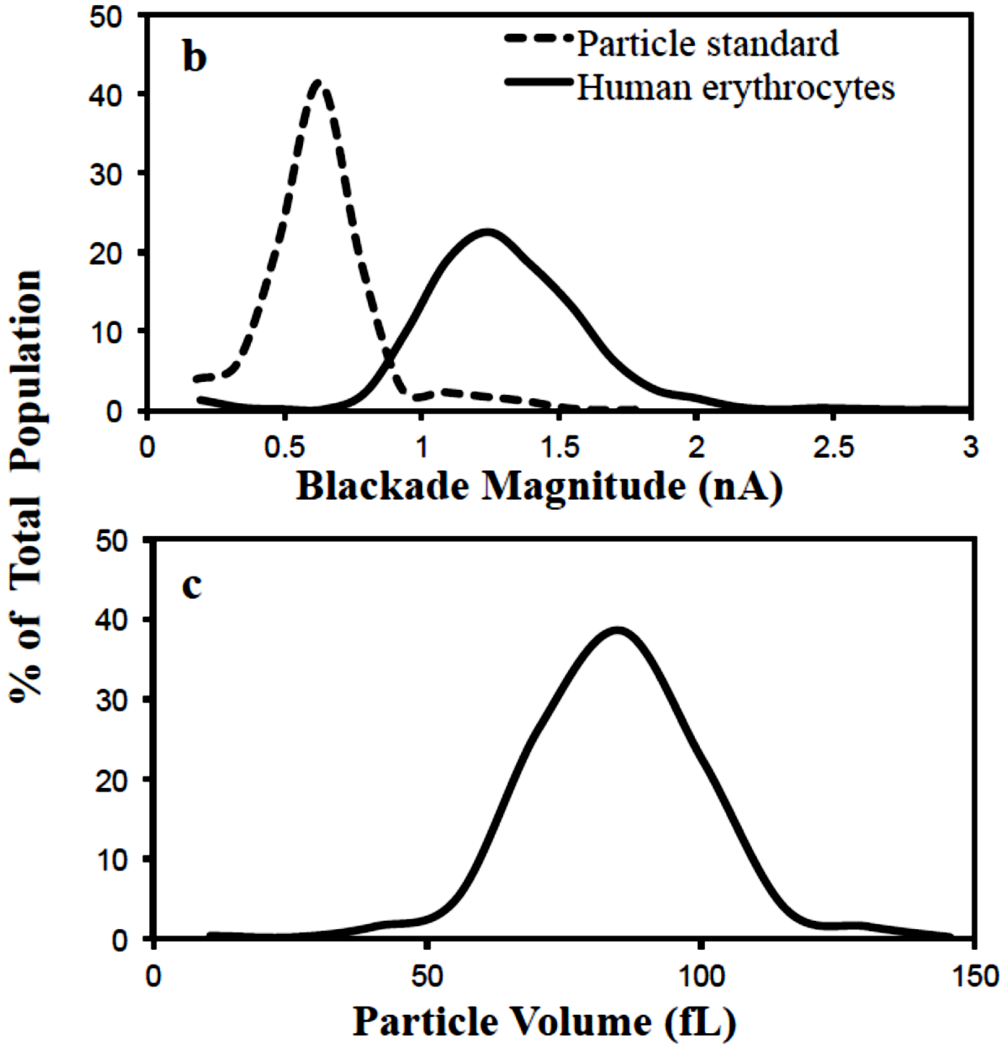

Fig.5.3.3 Signal obtained and recorded by using TRPS system for RBCs size measurement. The histograms of blockade magnitude for (Upper) standard particle and erythrocytes and (Bottom) cell volume of RBCs were obtained by using qNano software. (Anthony Cheung MPhil. CUHK Thesis, 2012)

5.3.2 RBCs cell shrinkage under PD treatment

Figure 5.3.4 showed the histogram showing the effect of PD on cell volume of human RBCs treated with PD of various concentrations. Significant size change to the whole cell population was observed with increasing PD exposure. An obvious cell shrinkage was observed in the group exposing to 2.5 μM PD.

At high dose of PD (e.g. 2.5 and 5.0 μM), few cells remain intact, with most of cells lysed. Assays were repeated and data are retrieved and presented in curves for comparison (Figure 5.3.5a, b). As expected, a dose-dependent decrease in the cell size was observed from 90 to less than 20 fL (Figure 5.3.4 and 5.3.5a). It seems therefore likely that the smaller particles less than 20 fL in the sets of RBCs treated with 5.0 μM PD should be the apoptotic bodies (confirmed by confocal microscopy, see below). Apoptotic bodies are smaller structures with sealed membrane vesicles detached from cell body during the process of eryptosis. In fact, formation of apoptotic bodies is another feature of eryptosis [Willekens et al., 2005; Bosman et al., 2005; Lang et al., 2006]. In Figure 5.3.5a, no significant difference between the mean and mode size was observed, indicating homogeneity in the cell size distribution. Likewise, the effect of PD on the duration time was in a dose-dependent fashion (Figure5.3.5b). As can be seen, the cells travelled through the sensing pore with

shorter duration times with increasing dose of PD treatment. This observation agrees well with the reduction in cell size. Also, the mean duration time was larger than that of its mode value (Figure 5.3.5b), indicating that a large proportion of cells did not travel with similar individual duration times but rather with a wide heterogeneous distribution of velocities.

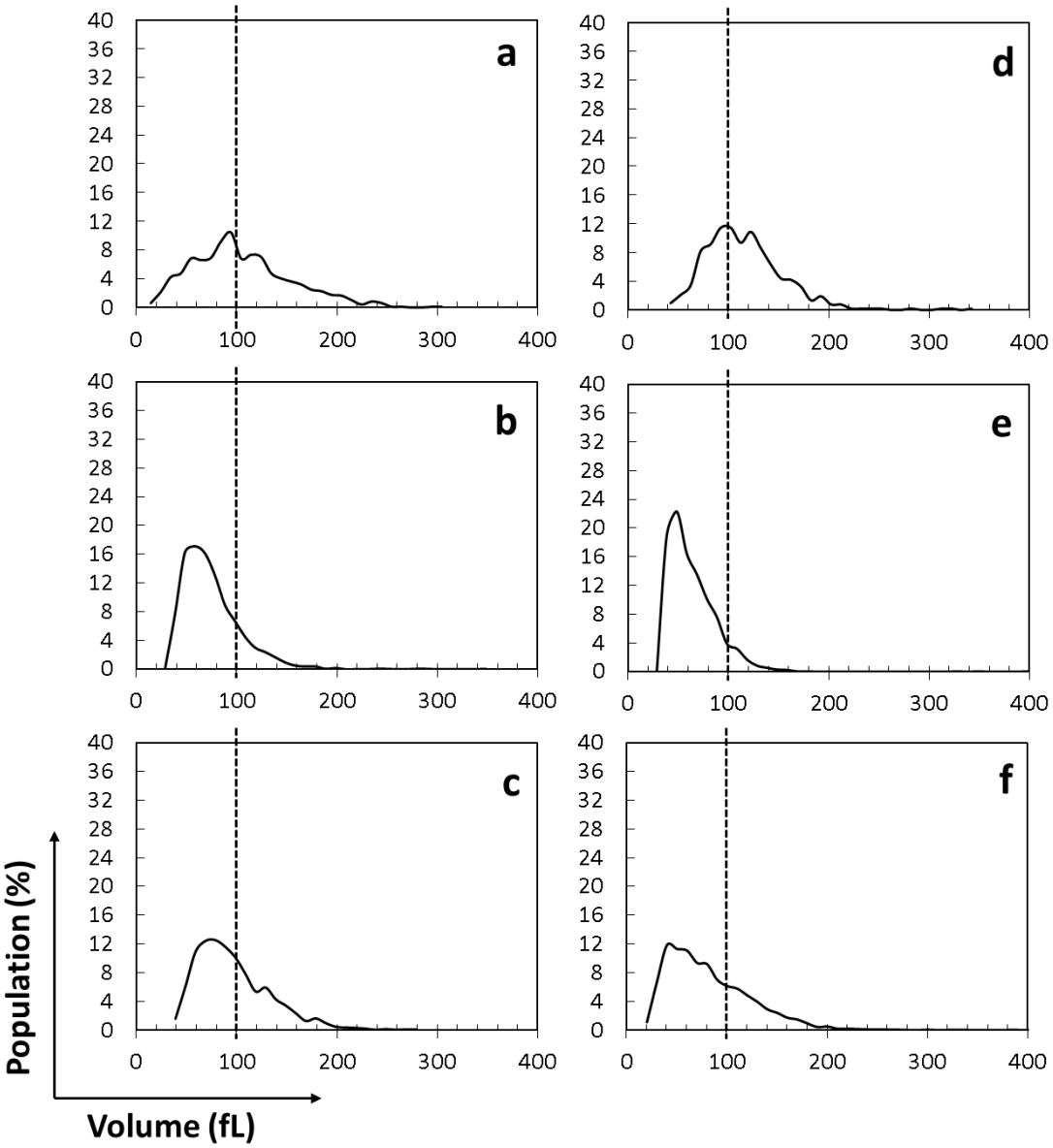

Fig. 5.3.4 RPS assay estimating the size of the RBCs. The RBCs were undergoing PD treatment for 24 hr at 37 ^{0}C. The final concentration of PD was (**a**) 0 µM, (**b**) 0.31 µM, (**c**) 0.63µM, (**d**) 1.25 µM, and (**e**) 2.5 µM. (**f**) RBCs was treated with 2 µM of ionomycin.

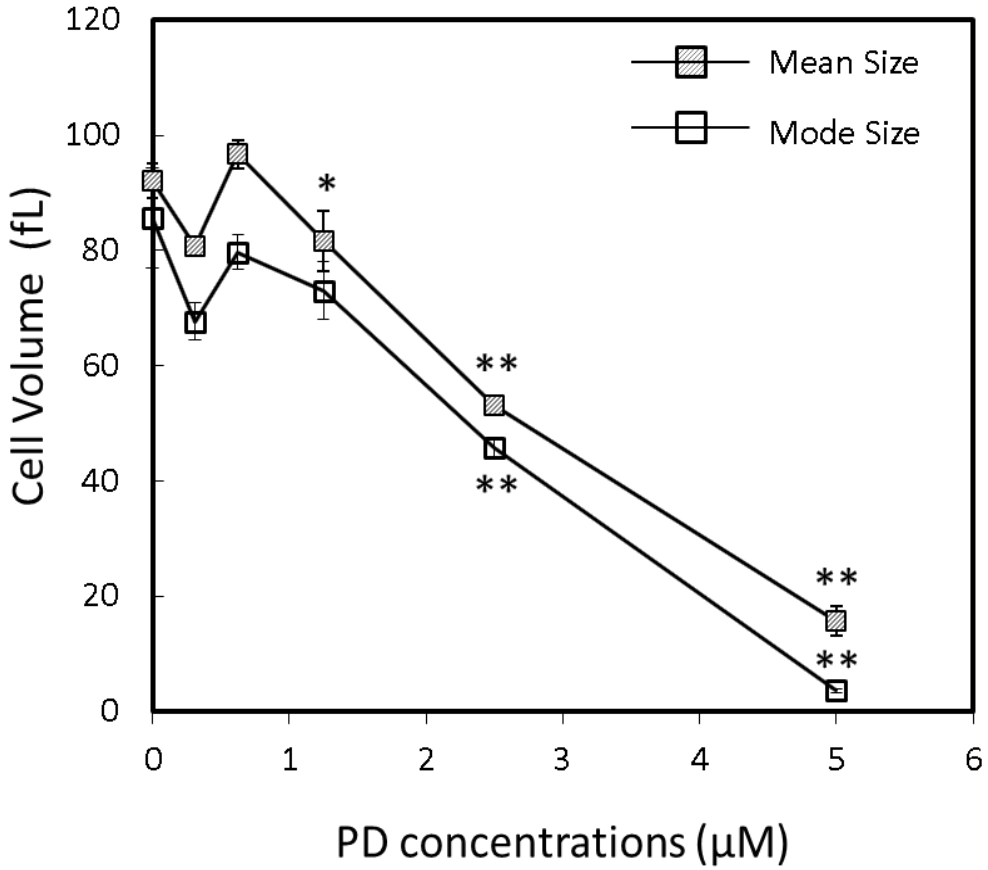

(a)

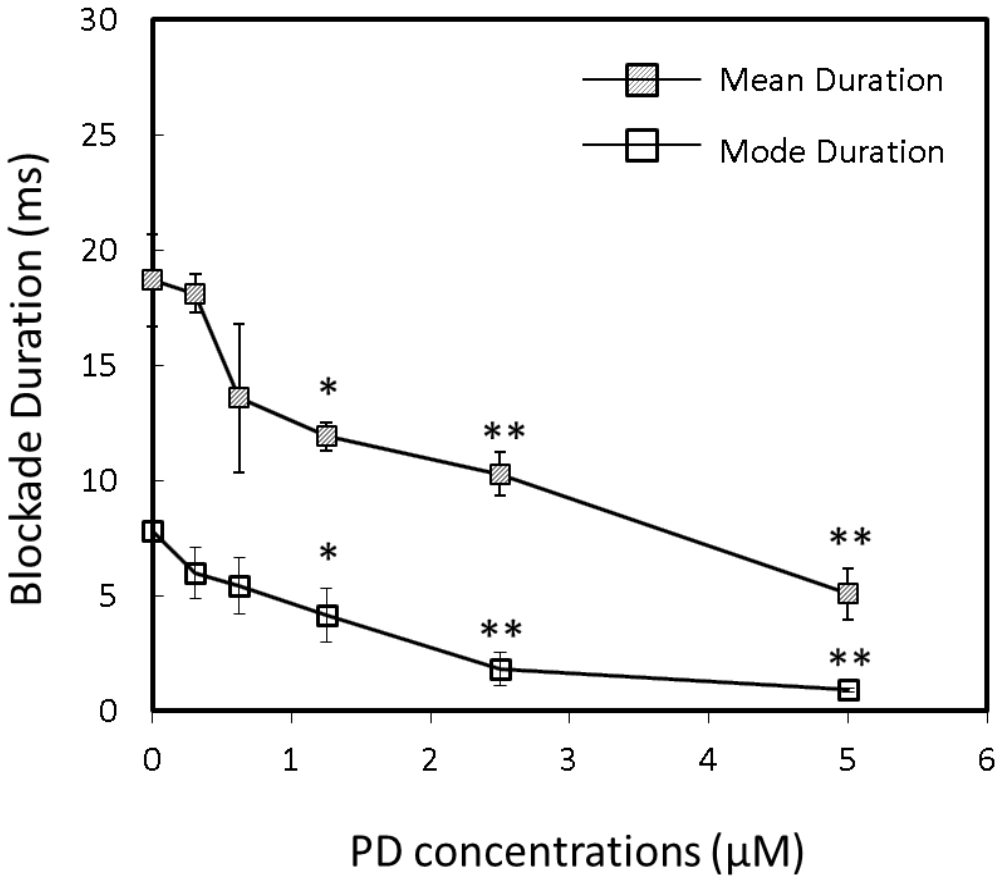

(b)

Fig. 5.3.5 Effect of PD on cell volume and blockade duration of human RBCs in solution of different osmolarities. Human erythrocytes (1.5 x 10^7/mL) were treated with HEPES buffer (control) or PD at the concentration as indicated for 24 hr at 37^{o}C and their cell volume and blockade duration were measured by TRPS. Assays were repeated and the mean and mode value of cell volume (fL) (**a**) and blocakade duration (ms) (**b**) were determined. Results are mean ± SD (n = 3), *p<0.05, **p<0.01 when compared to the corresponding control.

5.3.3 Confocal Imaging to prove the aggregations of eryptotic RBCs by the Annexin V-RFP functionalized beads

During the eryptosis, the externalization of lipid molecules phosphatidyl-serine (PS) from the inner to the outer leaflet of the plasma membrane marks the early phase of eryptosis. It serves as “eat-me” signal to invite macrophages to remove the defective RBCs [Foller et al., 2008]. Annexin V is a well-known probe which is commonly used for detecting cell death. Annexin V can be conjugated with fluorochromes such as green fluorescence protein (GFP) or red fluorescence protein (RFP), for fluorescence reporting in flow cytometry or confocal microscopy. In this study, we first to confirm the Annexin V-RFP modified beads can conjugate to the eryptotic RBCs. Confocal imaging was done with the Annexin V-RFP beads staining group.

Figure 5.3.6 shows the positive control group that RBCs were treated with ionomycin. The confocal images demonstrate that RBCs shrinked and formed apoptotic bodies (shown as arrow). Formation of echinocytes with spicules on the RBC surface was successfully stained with Annexin V-RFP. The RFP signal was localized at the cell periphery, as shown in the confocal photo. For the negative control, there was no RFP signal detected on the cell membrane, which indicated the

RBCs were not undergoing eryptosis in the absence of PS externalization.

Experiment was repeated by using bead-Annexin V-RFP. In the positive control group, a group of bead-Annexin V-RFP (positive in RFP signal) was sticking on the surface of RBCs, connecting numbers of RBCs to form a colony of cell cluster. In comparison, the Annexin V-RFP soluble solution stained onto the PS on RBCs without agglutination, indicating that binding of the soluble Annexin-V-RFP to the PS on the surface of apoptotic cells was insufficient to produce aggregates. On the other hand, there was no connection between RBCs and bead-Annexin V-RFP in the negative control group. RBCs were separated, without any beads sticking on the cell membrane. The results were matched with the Annexin V-RFP staining group. Hence, it is proved that the bead-Annexin V-RFP could successfully conjugate with the eryptotic RBCs.

Next, we performed the assays with PD and analyzed the RBCs with or without PD treatment. As expected, the PD-treated RBCs produced aggregates with the beads coated with the Annexin-V-RFP or stained with soluble Annexin V-RFP solution (Figure 5.3.7a-b). Also, apoptotic bodies were seen under microscope. With this groundwork and confirmation, we repeated the assays using the TRPS.

5.3.4 Detection of eryptosis by using Bead-Annexin V-RFP and TRPS

As shown in Figure 5.3.8, treatment of RBCs with PD reduced the averaged cellular volumetric size in a dose-dependent manner. In the presence of beads coated with Annexin-V-RFP, the histograms shifted to the right hand side indicating the formation of aggregates or assemblies with larger size (Figure 5.3.8a-c). Similar results were obtained from the positive control with ionomycin (Figure 5.3.8d). Experiments were repeated, data compared and significance found (p<0.05) (Figure 5.3.8e). In the delta graph where the percentage of particle population with beads were subtracted from the corresponding control without beads fraction by fraction (Figure 5.3.8), it can be seen that positive bars were obtained from the PD treated groups after 85 fL suggesting that assemblies were formed with eryptotic RBCs with a size larger than that of the normal RBC. It is noteworthy to mention that RPS was able to detect the number of assemblies of different sizes. This size variation indicates that apart from the eryptotic RBCs, apoptotic bodies were also attached to the beads.

Moreover, agreed with our previous observations that more cells were disintegrated in the 2.50 μM PD-treated group, more and larger positive bars were obtained from the 1.25 than the 2.50 μM PD group. On the other hand, more

negative bars were found before 85 fL in Figure 5.3.9 reveals that less small particles appeared in the preparation with PD and beads as most of them induced by the PD treatment (i.e. apoptotic bodies) had been absorbed by the Annexin-V functionalized beads.

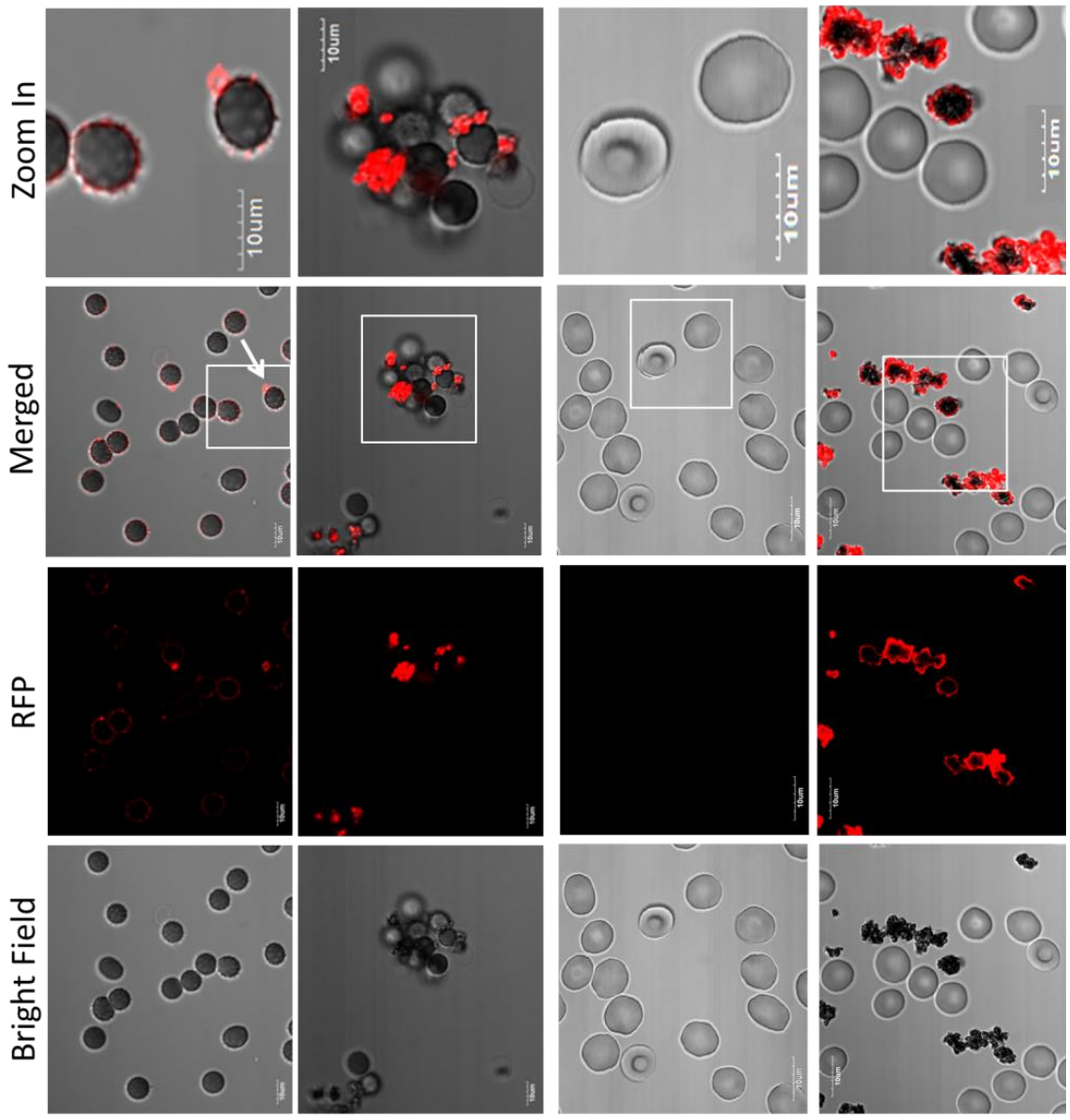
Zoom In
Merged
RFP
Bright Field
10um
Ionomycin (2 µM)
Annexin V- RFP
Ionomycin (2 µM)
Bead-Annexin V-
RFP
Control
Annexin V- RFP
Control
Bead-Annexin V-
RFP

Fig. 5.3.6 Confocal imaging of RBC staining with either Annexin V-RFP or Bead-Annexin V-RFP. RBCs were treated with HEPES buffer in the presence or absence (Negative Control) of 2 μM ionomycin for 24 hr at 37 ^{0}C.RBCs then were washed with HEPES buffer by centrifugation at 2,000 rpm for 5 min, followed by resuspensed in the Annexin V-RFP contained HEPES buffer (5 μL dye in 1 mL of cells). RBCs were incubated at room temperature in dark for 15 min, followed by washing with HEPES buffer. RBCs were resuspended in 1 mL HEPES buffer and transferred to a confocal dish for imaging. For the Ni-Mag-Annexin V-RFP groups, RBCs were directly resuspended in 1 mL HEPES buffer without the Annexin V-RFP dye and transferred into a confocal dish. Bead-Annexin V-RFP was injected into the sample at dilution in 800 X. Zoom-in image are the enlarged view of the inset in the merged images. Arrow: apoptotic body; scale bar, cell dimension in μm.

(a)

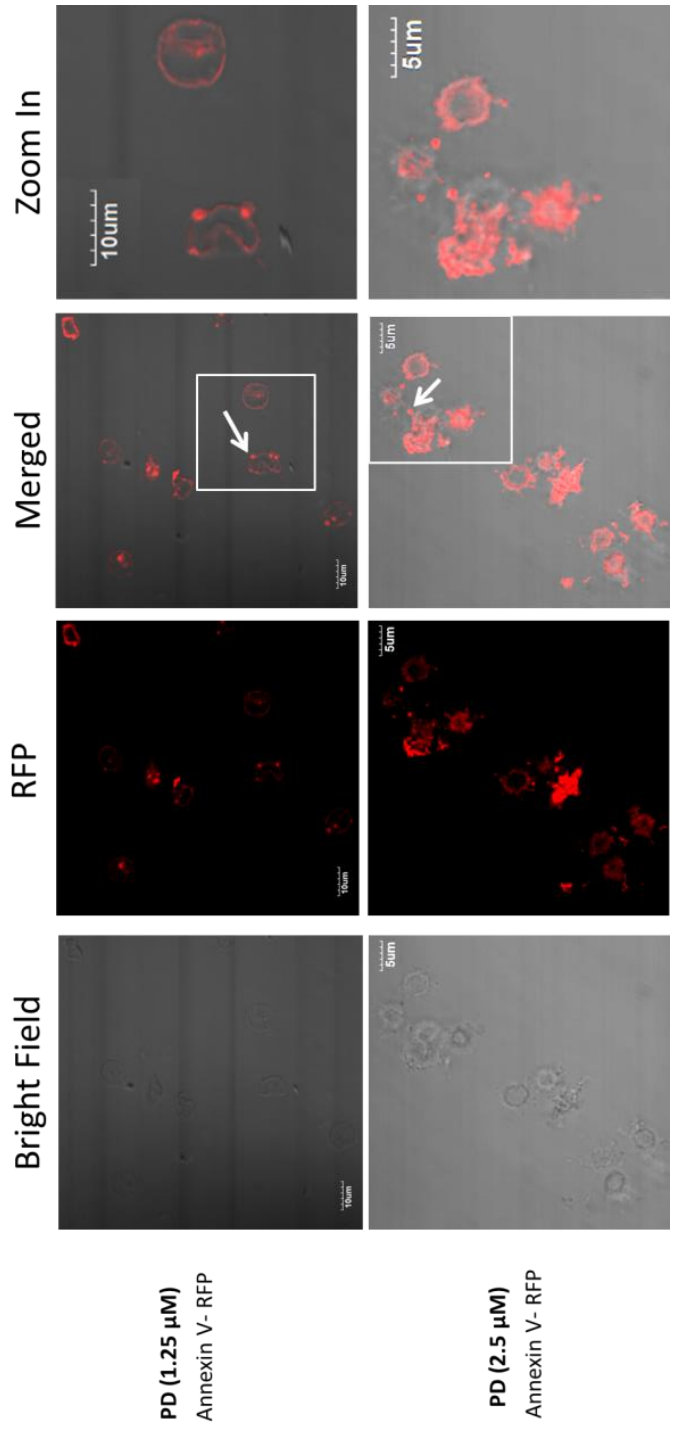
Bright Field
RFP
Merged
Zoom In
10um
5um
PD (1.25 µM)
Annexin V- RFP
PD (2.5 µM)
Annexin V- RFP

(b)

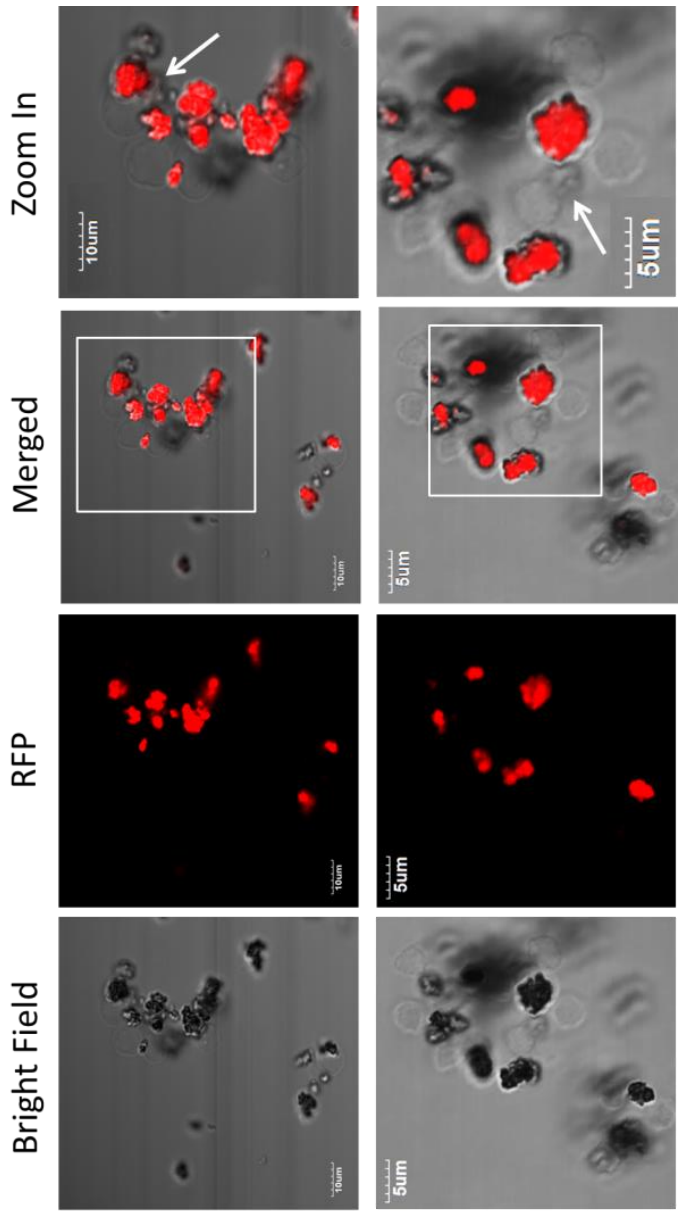
Bright Field
RFP
Merged
Zoom In
PD (1.25 µM)
Bead-Annexin V-RFP
PD (2.5 µM)
Bead-Annexin V-RFP
10um
5um

Fig. 5.3.7 Confocal imaging of PD treated RBC staining with either Annexin V-RFP or Bead-Annexin V-RFP. RBCs were treated with HEPES buffer containing 1.25 or 2.5μM PD for 24 hr at 37 ^{0}C. RBCs then were washed with HEPES buffer by centrifugation at 2,000 rpm for 5 min, followed by resuspended in the (**a**) Annexin V-RFP staining solution (5μL of dye in 1 mL cells) or (**b**) Annexin V-RFP beads (1:800 dilution). RBCs were incubated at room temperature in dark for 15 min, followed by washing with HEPES buffer. RBCs were resuspended in 1 mL HEPES buffer and transferred to a confocal dish for imaging. For the Annexin V-RFP beads groups, no washing step involved after incubation. Zoom-in image are the enlarged view of the inset in the merged images. Arrow: apoptotic body; scale bar, cell dimension in μm.

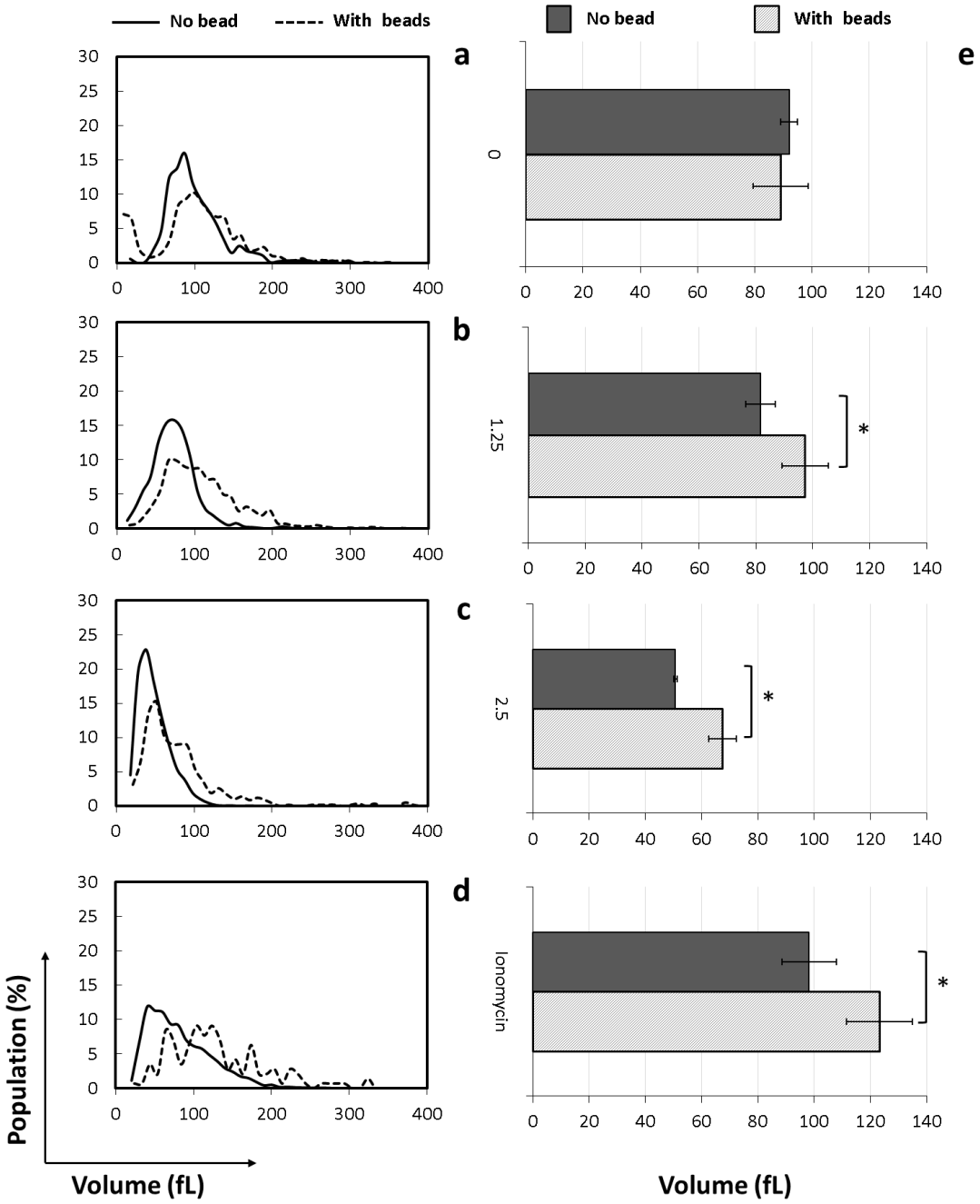

Fig. 5.3.8 TRPS assay for detecting eryptosis in the PD-treated RBCs with bead-Annexin V-RFP. RBCs were incubated with (**a**) 0 µM of PD, (**b**) 2 µM of ionomycin or (**c**) 1.25 µM of PD treatment for 24 hr. The solid line showed the cells populations before adding the bead-Annexin V-RFP, whereas the dotted line showed the cells population added with beads. The final concentration of Annexin V-RFP

beads was in 1:800 diluted. The beads were added into RBCs samples for 15 min before injecting to TRPS flow cell.

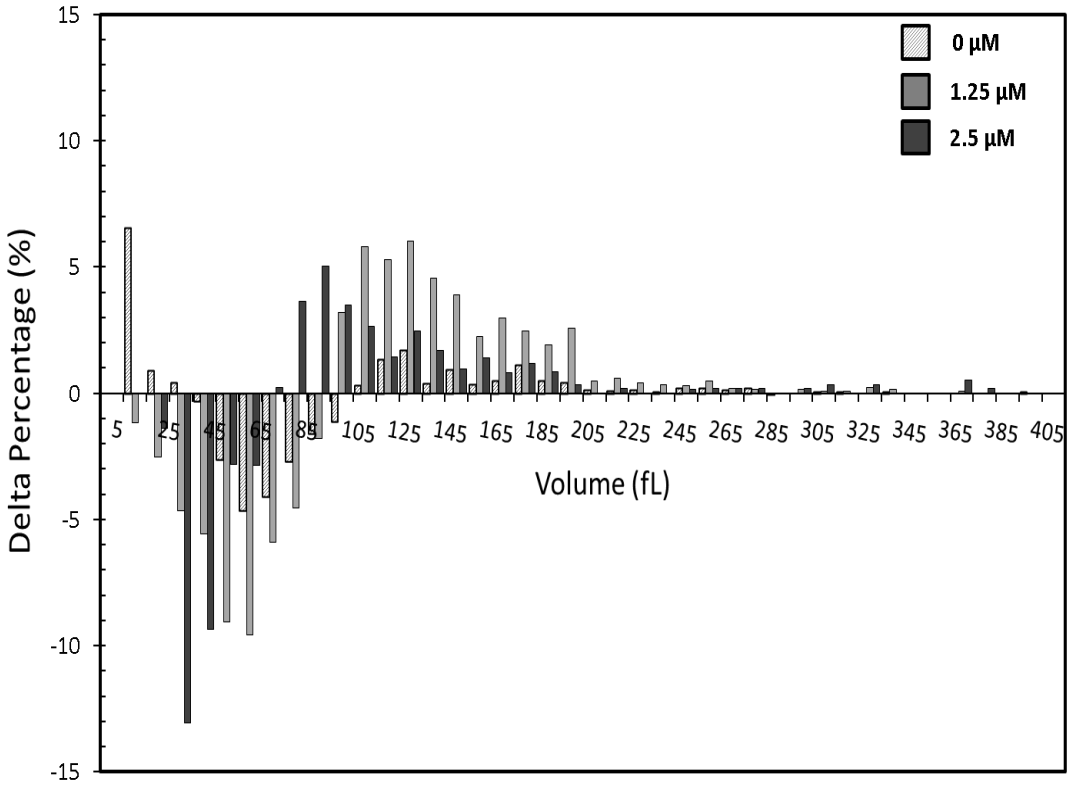

Fig. 5.3.9 Delta histogram (% of population against particle size) calculated by IZON software. The background populations of RBCs without bead-Annexin V-RFP were subtracted from the bead-Annexin V-RFP conjugated populations after PD treatment at the concentration as indicated (n=1).

5.3.5 Cytotoxicity of silver nanodecahedrons particles (AgNPs) to RBC

To show the toxic effect of AgNPs to human RBCs, hemolysis assay was done. RBCs were treated with different concentrations of AgNPs for 24 hr, followed by detection of the absorbance of supernatant at 415 nm. As shown in Figure 5.3.10, hemolysis occurred when RBCs were treated with AgNPs at the concentration higher than 0.5 x 10^{10} particles/mL. There was no obvious hemolytic effect in the range from 0 to 0.25 x 10^{10} particles/mL of AgNPs. On the other hand, RBCs were in low hemolysis rate when co-treated with AgNPs and anti-oxidizing agent NAC, maintained, at around 20 to 40% of the total hemolysis throughout the experiments. These observations indicate that NAC can rescue RBCs from the AgNPs toxicity.

5.3.6 Morphology study under confocal microscopic imagining

Under high concentration of AgNPs, RBCs underwent eryptosis as evidenced by the formation of ghosts and the Annexin V-RFP staining on the cell periphery (Figure 5.3.11). Early disco-echinocytes (white arrows) and ghosts were found in 1 x 10^{10} particles/mL of AgNPs treated RBCs (Figure 5.3.11). The presence of ghost cells in the confocal images supported the high hemolytic rate as the RBCs were devoid of Hb.

On the other hand, disco-echinocytes and echinocytes were found in the NAC AgNPs treated groups contained AgNPs of 2 x 10^{10} and 1 x 10^{10} particles/mL. Also, no or only a small number of ghost cells were found in these groups. Moreover, the Annexin V-RFP signals in the NAC containing groups were less than the one without NAC added (Figure 5.3.11).

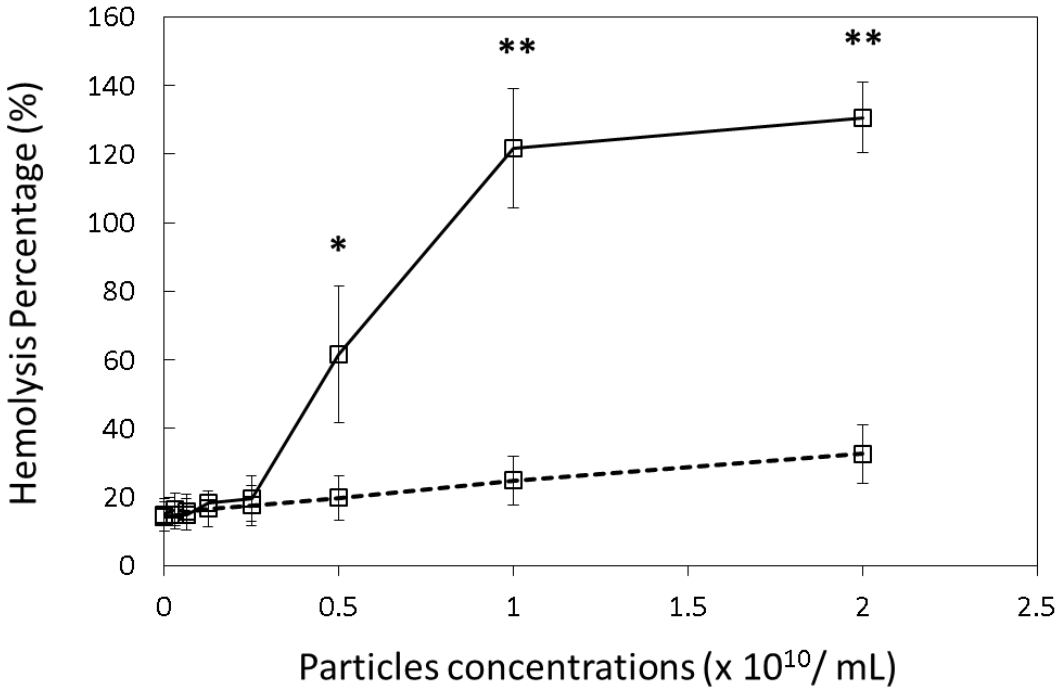

Fig. 5.3.10 Hemolysis assay of RBCs under the AgNPs treatement. RBCs were cultured in 12-well plates in the presence of 2.5 x 10^{9}, 5.0 x 10^{9}, 1.0 x 10^{10} or 2.0 x 10^{10} particles/mL AgNPs respectively; at 37 ^{0}C for 24 hr in the presence (1 mM) (dotted line) or absence of NAC (solid line).Results are expressed as mean±SD (n=3), * p< 0.05, ** p< 0.01.

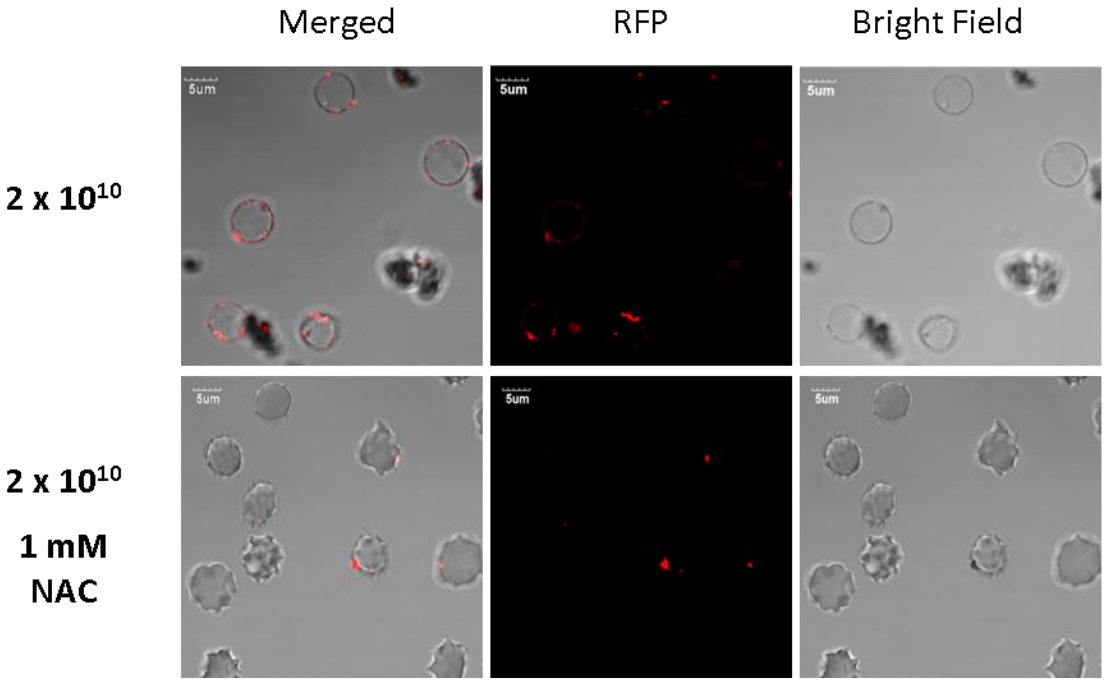
Merged
RFP
Bright Field
2 x 10^10
2 x 10^10
1 mM
NAC
5um

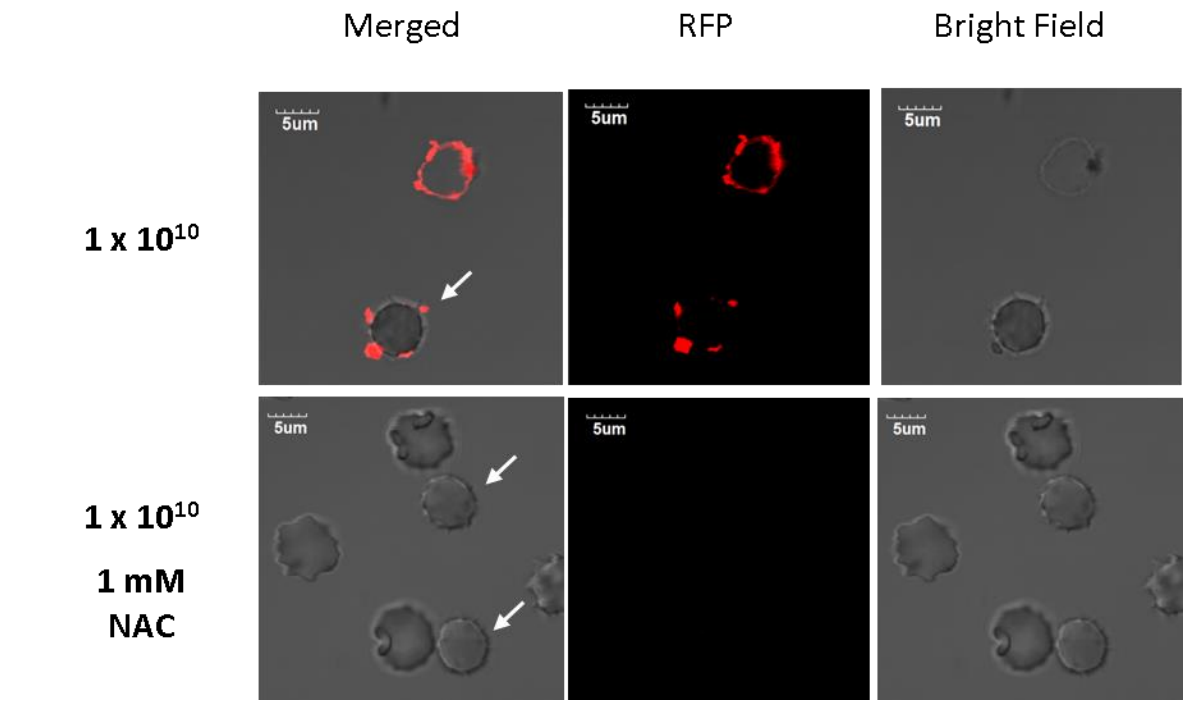

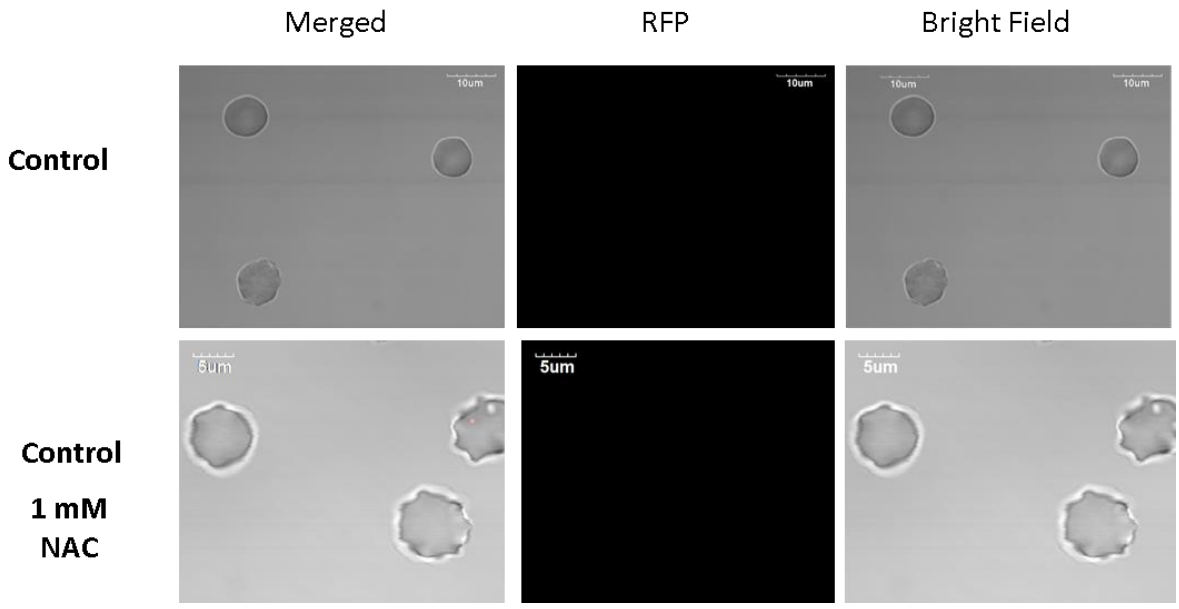

Fig. 5.3.11 Confocal images showing the morphology and Annexin V –RFP signal from the RBCs after AgNPs treatment. RBCs were cultured in the presence

of 2.0 x 10^{10} particles/mL AgNPs, at 37 ^{0}C for 24 hr. For the NAC treated group, 1 mM NAC was added into each well with AgNPs. RBCs were washed by HEPES buffer at 2,000 rpm, 5 min, followed by staining with Annexin V-RFP dye for 15 min at RT. RBCs were washed with HEPES buffer after staining. Then, RBCs were resuspended in 1 mL HEPES buffer in a confocal dish and observed under a confocal microscope.

5.3.7 Cells volume assay by TRPS

After the studies on the effect of AgNPs treatment in human RBCs, we applied the TRPS technique to investigate the change in cell volume and blockade duration, in order to link up the relationship between the death of RBCs and cells size after AgNPs treatment.

The first assay was done to identify the mean and mode cell volume of RBCs after treating with AgNPs. As shown in Figure 5.3.12a, there was a gradually increase of the cell volume from 90 to 155 fL when the concentration of AgNPs increased from 0 to 1 x 10^{10} particles/mL. At the highest concentration (2 x 10^{10} particles/mL), the RBCs shrinked, reducing the mean cell volume to around 60 fL. It is suggested the effect of AgNPs on RBC cells size was in a dose-dependent manner.

At the same time, there was no big different between the mode and mean size, except the one of the highest concentration treated group. These results indicate homogeneity in the cell size distribution under the treatment of AgNPs in the range from 0 to 1 x 10^{10} particles/mL.

Likewise, the effect of AgNPs on the blockade duration time was also in a dose-dependent fashion (Figure 5.3.12b). As can be seen, the cells took longer duration time to travel the nanopore after treatment with increasing dose of the AgNPs from 2.5 x 10^{9} to 1 x 10^{10} particles/mL. This observation agrees well with the increase in cell size. Also, the mean duration time was larger than that of its mode value (Figure 5.3.12b), indicating a wide heterogeneous distribution in terms of the travelling velocity.

According to the results from the hemolysis assay and confocal imaging, an obvious reduction of Hb leakage and Annexin V-RFP signal were observed in the treatment group with both the NAC and AgNPs. Hence, it was interesting to investigate the cell volume of RBCs under NAC and AgNPs treatment. As shown in the bar chats of Figure 5.3.13a, the control groups, no matter with or without NAC, the cells volume was around 90 fL. One mM of NAC did not affect the RBC cell

volume in control groups. In comparison, in the range between 0.25 to 2 x 10^{10} particles/mL of AgNPs, the RBC cell volume maintained relatively stable (~110 fL) among different dose of the AgNPs treatment groups when NAC was added. At the same time, in the dosage of AgNPs between 0 to 1 x 10^{10} particles/mL, the duration time for RBCs passing through the nanopore was shorter, compared with the groups without NAC. There was no obvious difference found among the groups with AgNP and NAC.

Our results therefore indicate that NAC can reduce the toxic effect of AgNPs in RBCs including the hemolysis rate, PS externalization and cells enlargement.

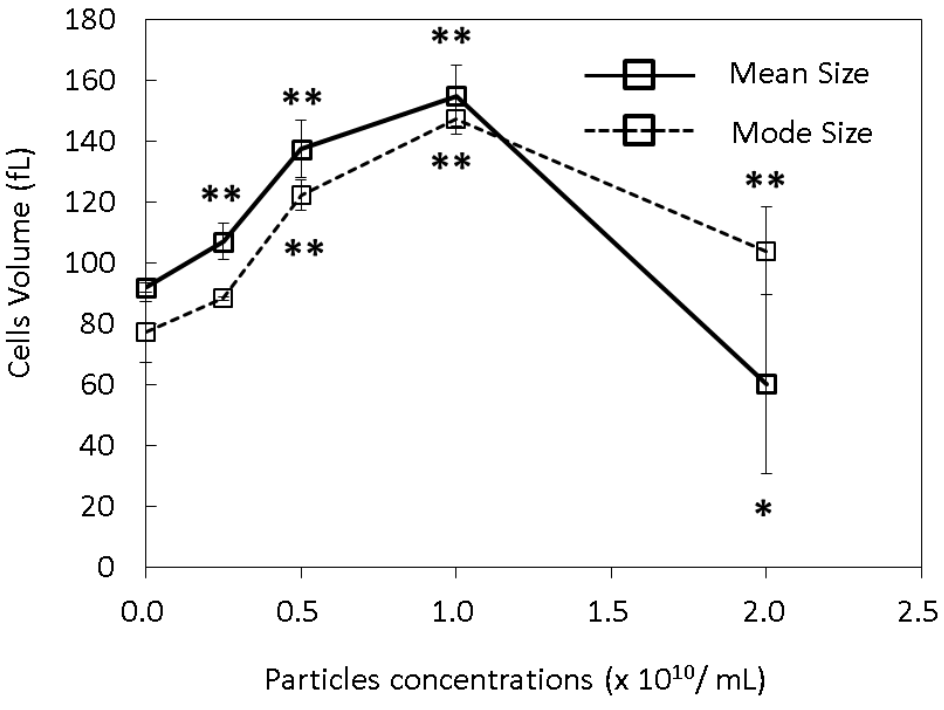

(a)

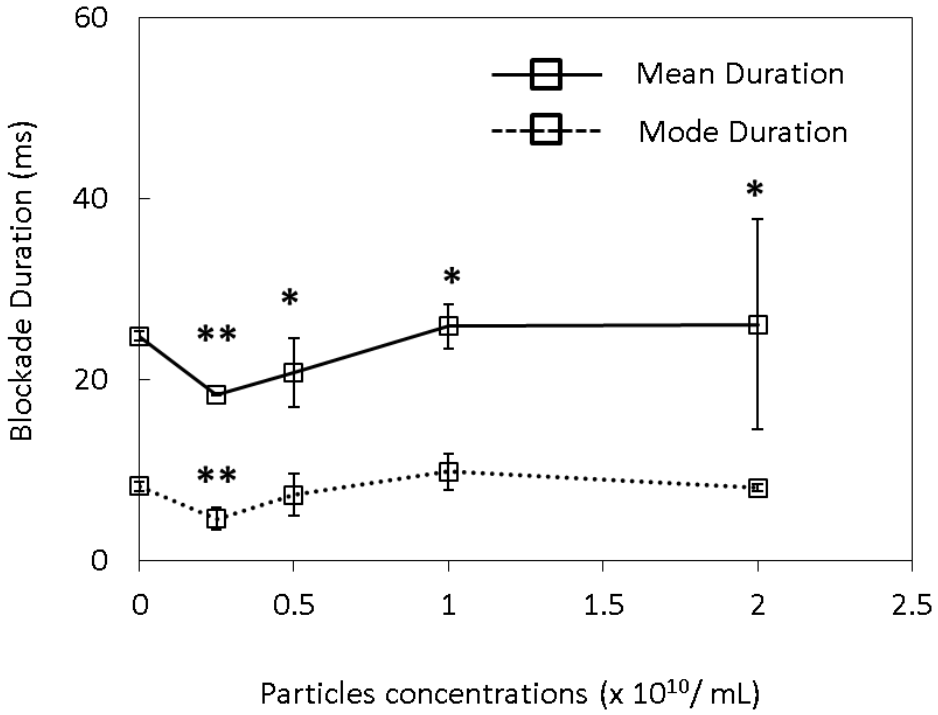

(b)

Fig. 5.3.12 Effect of AgNPs in RBCs on cell volume and blockade duration measured by TRPS. The RBCs were cultured in 12-well plates in the presence of 2.5 x 10^9, 5.0 x 10^9, 1.0 x 10^{10} or 2.0 x 10^{10} particles/mL AgNPs respectively, at 37 ^{0}C for 24 hr. The cell volume (**a**) and blockade duration (ms) (**b**) were determined. Results are mean ± SD (n = 3), * p<0.05, ** p<0.01 when compared to the corresponding control.

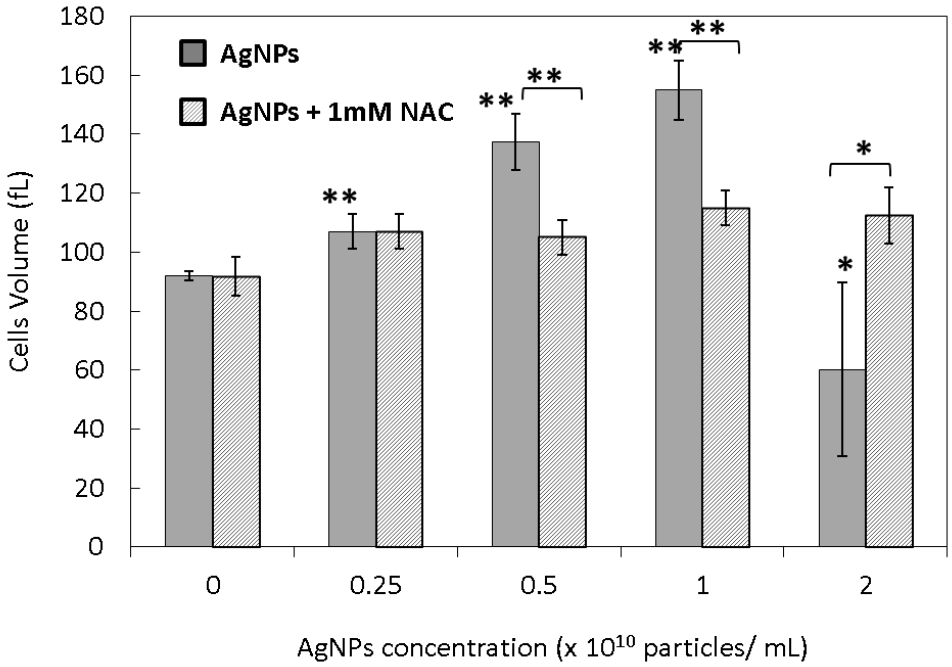
AgNPs
AgNPs + 1mM NAC
Cells Volume (fL)
180
160
140
120
100
80
60
40
20
0
0
0.25
0.5
1
2
AgNPs concentration (x 10^10 particles/ mL)

(a)

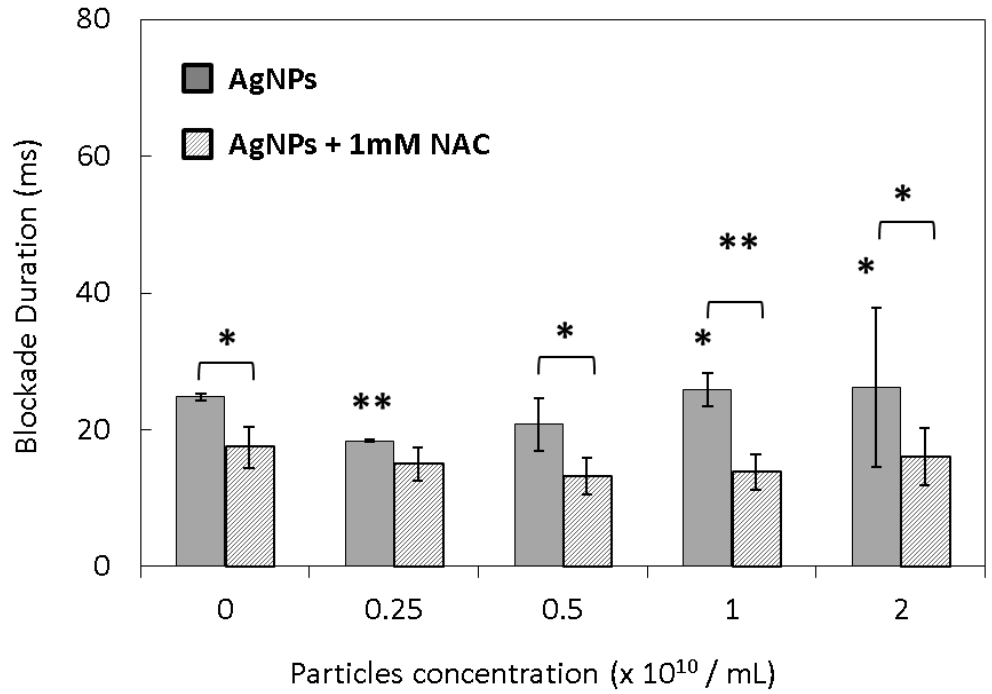
AgNPs
AgNPs + 1mM NAC
Blockade Duration (ms)
80
60
40
20
0
0
0.25
0.5
1
2
Particles concentration (x 10^10 / mL)

(b)

Fig. 5.3.13 TRPS assay on determining the effect NAC in AgNPs treated RBCs. Cells were incubated with AgNPs at 37 ^{0}C for 24 hr, in the presence or absence of 1 mM NAC. The cell volume (**a**) and duration time (**b**) were obtained. (Mean±SD, n = 3) (* p<0.05, ** p<0.01 when compared to the corresponding control).

5.4 Discussion

Results from our study indicate that TRPS is a sensitive and robust measurement method and it provides a new application in the cell-based study. In this regard, the TRPS platform required much smaller volume of suspension (35 μL) for sensing compared with that for microscopy (~ 0.5 mL) or flow cytometry (several mL). Using TPRS, our results show that PD is highly toxic to human erythrocytes leading to eryptosis based on our observation from the TRPS for cell shrinkage, apoptotic body formation and PS externalization. More work is needed to solve its side effect in RBCs if PD is to be used as an anti-cancer agent.

Also, data from our study show a dose-dependent size change in the RBCs and a high hemolysis rate when human RBCs were treated with AgNPs. RBCs enlarged in cell volume first followed by shrinkage as the concentration of AgNPs increased. At the same time, according to the results from confocal imaging, the RBCs treated with

2 x 10^{10} particles/mL of AgNPs became ghosts. These observations are similar to the one that RBCs were kept in hypotonic environment. Cell enlargement in hypotonic environment is due to the influx of water: the cells swell and the integrity of the cell membranes disrupt. As a result of this, Hb escapes from the RBCs. Under the treatment of AgNPs, the shape of the RBCs changed from discocytes to early dico-echinocytes [Oftedal et al., 2012], and to the ghosts. The geometric axial ratio (RP = thickness/diameter) of discocytes are 0.5, whereas RP = 0.5-0.9 in the dico-echinocytes [Milton and Frojmovic, 1979]. Diso-echinocytes were identified as discocytes which processed pseudopods and/or as swollen discocytes [Milton and Frojmovic, 1979]. It is believed that the high concentration of AgNPs leads to the pore formation on the RBC cell membrane, followed by the leakage of Hb. These results suggest that AgNPs have potential to affect the lipid component of RBC membrane. Also, ghost cell were found after the treatment with the AgNP suggesting that the RBC shape was maintained as a result of the balance between the intra- and outer-cellular pressure [Johnson et al., 1980; Oftedal et al., 2012].

Cell swelling is related to the anion permeability, and its increase may be due to the membrane oxidation or consequence of certain pathological conditions [Vitvitsky et al., 2000]. AgNPs have a strong antibacterial activity for the induction of oxidative

stress. In this connection, it has been proved that AgNPs can generate ROS leading to the degradation of cell membrane [Sanpui et al., 2011; Gurunathan et al., 2013]. RBCs were found to swell at the AgNPs concentration between 0.25 to 1 x 10^{10} particles/mL. This may be due to the production of ROS which led to cell swelling and then shrinkage eventually. NAC is a well-known and popular antioxidant which is supposed to reduce the oxidative stress. The role of NAC in minimizing oxidative stress is a result of its act to be the precursor for glutathione (GSH) synthesis [Romagnoli et al. 2013]. According to the confocal images and TRPS cells measurement, NAC demonstrated the effect on rescuing the RBCs from the AgNPs cytotoxicity. However, more work is needed to show the mechanism how NAC blocks the eryptosis in human RBCs.

References:

Borné, Y., Smith, J.G. et al. (2011). Red cell distribution width and risk for first hospitalization due to heart failure: a population-based cohort study. *Eur. J. Heart.Fail.*, 13(12), 1355-61.

Bosman, G.J., Willekens, F.L. and Were, J.M. (2005). Erythrocyte agng: a more than superficial resemblance to apoptosis?. *Cell. Physiol. Biochem.*, 16(1-3), 1-8.

Canham, P.B. (1969). Curves of osmotic fragility calculated from the isotonic areas and volumes of individual human erythrocytes. *J. Cell Physiol.*, 74(2), 203-11.

Chaloupka, K., Malam, Y. and Seifalian, A.M. (2010). Nanosilver as a new generation of nanoproduct in biomedical applications. *Trends Biotechnol.*, 28 (11), 580-88.

Cheung, J.Y., Ong, R.C. et al. (2005). Polyphyllin D is a potent apoptosis inducer in drug-resistant HepG2 cells. *Cancer Lett.*, 217(2), 203-11.

Ellsworth, M.L., Ellis, C.G. et al. (2009). Erythrocytes: oxygen sensors and modulators of vascular tone. *Physiology (Bethesda)*, 24, 107-16.

Evans, E. and Fung, Y.C. (1972). Improved measurements of the erythrocyte geometry. *Microvasc.Res.*, 4(4), 335-47.

Foller, M., Huber, S.M. and Lang, F. (2008). Erythrocyte programmed cell death. *IUBMB Life*, 60, 661-68.

Gao, M., Cheung, K.L. et al. (2012). Polyphyllin D induces apoptosis in human erythrocytes through Ca2+ rise and membrane permeabilization. *Arch Toxicol.*, 86, 741-752.

Gurunathan, S., Han, J.W. et al. (2013). Cytotoxicity of Biologically Synthesized Sliver Nanoparticles in MDA-MB-231 Human Breast Cancer Cells. *BioMed Research International*, 2013, Article ID 535796, 10 pp.

Henriquez, R.R., Ito, T. et al. (2004). The resurgence of coulter counting for

analyzing nanoscale objects. *The Analyst.*, 129, 478-82.

Ito, T., Sun, L. et al. (2004). A carbon nanotube-based coulter nanoparticle counter. *Accounts Chem. Res.*, 37, 937-945. (2004a)

Ito, T., Sun, L. et al. (2004). Comparison of nanoparticle size and electrophoretic mobility measurements using a carbon nanotube-based coulter counter, dynamic light scattering, transmission electron microscopy, and phase analysis light scattering. *Langmuir*, 20, 6940-45. (2004b)

Johnson, R.M., Taylor, G. and Meyer, D.B. (1980). Shape and Volume Changes in Erythrocyte Ghosts and Spectrin-Actin Networks. *J. Cell. Biol.*, 86, 371-76.

Kaferle, J. and Strzoda, C.E. (2012) Evaluation of macrocytosis. *Am. Fam. Phys.*, 79(3), 203-8.

Khairy, K., Foo, J. and Howard, J. (2008). Shapes of red blood cells: comparison of 3D confocal with the bilayer-couple model. *Bioeng.*, 2, 173-81.

Lang, F., Lang, K.S. et al. (2006). Mechanisms and significance of eryptosis. *Antioxid.Redox.Sign.*, 8(7-8), 1183-92.

Lang, E., Qadri, S.M. and Lang, F. (2012). Killing me softly - Suicidal erythrocyte death. *Int. J.Biochem. Cell Biol.*, 44(8), 1236-43. (2012a)

Lang, F., Qadri S.M. (2012). Mechanisms and significance of eryptosis, the suicidal death of erythrocytes. *Blood Purif,*. 33(1-3), 125-30. (2012b)

Low, M., Yu, S. et al. (2011). Investigative Study of Nucleic Acids-Gold Nanoparticles Interactions Using Laser-based Techniques, Electron Microscopy and Resistive Pulse Sensing with a Nanopore. *Aust. J. Chem.*, 64(9), 1229-34.

Milton, J.G. and Frojmovic, M.M. (1979). Shape-changing agents produce abnormally large platelets in a hereditary “giant platelets syndrome (MPS)”. *J.*

Lab. Clin. Med., 93(1), 154-61.

Oftedal, L., Myhren, L. et al. (2012). The lipopeptide toxins anabaenolysin A and B target biological membranes in a cholesterol-dependent manner. *Biochim. Biophys. - Biomembranes*, 1818(12), 3000-09.

Ong, R.C., Lei, J. et al. (2008).Polyphyllin D induces mitochondrial fragmentation and acts directly on the mitochondria to induce apoptosis in drug-resistant HepG2 cells. *Cancer Lett.*, 261(2), 158-64.

Roberts, G.S., Kozak, D. et al. (2010). Tunable Nano/Micropores for Particle Detection and Discrimination: Scanning Ion Occlusion Spectroscopy. *Small*, 6(23), 2653-58.

Romagnoli, C., Marcucci, T. et al. (2013). Role of N-acetylcysteine and GSH redox system on total and active MMP-2 in intestinal myofibroblasts of Crohn's disease patients. *Int. J. Colorectal.Dis.*, 28(7), 915-24.

Sanpui, P., Chattopadhyay, A. and Ghosh, S.S. (2011). Induction of apoptosis in cancer cells at low silver nanoparticle concentrations using chitosan nanocarrier. *ACS Appl. Mater. Inter.*, 3(2), 218-28.

Tycho, D.H., Metz, M.H. et al. (1985). Flow-cytometric light scattering measurement of red blood cell volume and hemoglobin concentration. *Appl. Opt.*, 24(9). 1355-65.

Van Vranken M (2010) Evaluation of microcytosis. *Am. Fam. Phys.*, 82(9),1117-22.

Vitvitsky, V.M., Frolova, E.V. et al. (2000). Anion permeability and erythrocyte swelling. *Bioelectrochemistry*, 52(2), 169-77.

Vogel, R., Willmott, G. et al. (2011). Quantitative Sizing of Nano/Microparticles with a Tunable Elastomeric Pore Sensor. *Anal.Chem.*, 83(9), 3499-506.

Willekens, F.L., Were, J.M. et al. (2005). Liver Kupffer cells rapidly remove red

blood cell-drived vesicles from the circulation by scavenger receptors. *Blood*, 105, 2141-45.

Willmott G.R., Parry B.E.T. et al. (2011). Resistive pulse asymmetry for nanospheres passing through tunable submicron pores. *J. Appl. Phys.*, 109, 094307, 13 pp.

Chapter 6 Conclusions

In this thesis, the use of LAMP assay to detect the MRSA *PVL* gene as a proof-of-concept model, by using traditional DNA binding dyes, optical method such as fluorescence or SPR, and a novel approach combining AuNPs and TRPS was demonstrated. On the other hand, the use of NPs carrying plasmid DNA for transfection, and probes against PS for measuring the cytotoxicity of drugs in RBCs were also described. To sum up, chapters in this thesis tried to demonstrate an integration of different biochemical methods, kinds of NPs and electrochemical analysis such as TRPS for different biomedical applications

Biosensor is a device for detecting analytes including proteins, enzymes, antigens, nucleic acids and cells etc., based on their biological and physiochemical features [Turner et al., 1987]. Biosensor requires a sensitive detector system reflecting the true status of target signals in the sensing system. As demonstrated in Chapter 2, the traditional DNA binding dyes exhibit inhibitory effects in both qPCR and the RT-LAMP. This indicates that the current detection/signal generation methods based on the use of fluorescent DNA-binding dyes for quantifying DNA are not suitable for the next-generation biosensor.

The platform demonstrated in Chapter 3 presents an integrating approach for the detection of MRSA or other pathogens. First of all, in the AuNP-Lamplicons section,

specificity was enhanced in the LAMP-based AuNP TRPS platform, which is a result of the combined use of both the capturing and reporting AuNPs. The double-targeting AuNPs work like the primary and secondary antibodies in the sandwich ELISA and Western blot to recognize the targets and amplify the signals for detection. Moreover, the LAMP-based AuNP TRPS platform involves DNA amplification which can be finished within 30 min to generate more copies of targets. In particular, LAMP is able to amplify a small amount of target DNAs into abundant amount of large sized DNA stem-loop structures in one single temperature without the need of thermal cycling. It allows the employment of the for capturing and reporting AuNPs to form large aggregates for TRSP sensing despite there are only a few hundreds of target DNAs initially. The *sensitivity* is enhanced by this approach and the LOD was found to be 208 copies of the MRSA *PVL* template in our experimental setting. Besides the testing of the presence or absence of target DNAs (positive/negative), the TRPS is able to provide a *quantitative measurement* for LAMP products (qLAMP) without using any DNA binding dyes thus overcoming the shortcoming of the inhibitory effects from the DNA binding dyes during the LAMP process.

As a good biosensor for detection, *speed and user-friendly* are also important According to our experience, the detection of MRSA *PVL* genes by our platform,

including the extraction of gDNA, can be completed within two hours. To compare with the conventional PCR, the time spending for DNA amplification and signal acquisition is minimized in our LAMP-based AuNP RPS system. At the same time, the volume of DNA sample required for sensing is only 35-40 μL after mixing with the AuNPs mixture. It indicates that a small amount of reagents and sample obtained from patients are sufficient for target detection. Additionally, the mechanism of electrochemical based detection method is *easy and robust* to perform. The signals generated from the TRPS can be acquired by setting an optimal threshold and/or stretching the elastic nanopore membrane to provide flexibility for assays. As shown in the individual signal tracings (Figure 3.3.8), each of the particles can display a numeric signal. Therefore, our LAMP-based AuNP RPS platform matches most of the criteria of a good bionsensor, which are user-friendly, time and reagent saving, sensitive and specific for DNA detection and convenient for DNA quantification. For the flexibility of the platform from the other angle, the DNA probes on the AuNPs can be replaced by other pathogen-specific genes or drug resistance genes, which allows the platform to detect other pathogens. With a better design, *multiplexed assay* can be performed. The DNA profile of MRSA and other pathogens from patients can be obtained easily in a short period of time in clinical setting.

The approach of using NFs to carry plasmid DNA is proved to be successful in

transfecting human cell lines in Chapter 4. The advantages of using NFs as carriers are two-fold. First, we can see a high transfection rate has been seen by using NFs as DNA carriers. Second, the cytotoxicity is low when the NFs were used for transfection. Comparing with other AuNPs, the NFs have a large surface area which can carry more DNA strands thus enhancing the transfection rate. Also, the NFs are obviously less toxic than the AuNPs and therefore they have potentials to be used in human [Sarker et al., 2013]. The application of NFs can be extended by surface functionalization with antibodies or apoptotic proteins for targeting cancer cells, so that the transfection specificity and anti-cancer efficiency can be increased.

In this thesis, we have introduced the application of TRPS for the development of novel biosensor. In fact, based on our trial, application of TRPS can be extended from the field of nanotechnology to cell-based assays when combined with appropriate designs with NPs or microparticles (beads). As demonstrated in Chapter 5, through the change of the cell size or enlargement after conjugating with detection beads, TRPS can quantify and distinguish the death of RBCs form the viable counterpart. This is a new biosensor which combines TRPS and functionalized beads with molecular probes for cell-based assays. Taken together, this thesis shows an approach to integrate and refine different aspects of science and technologies to achieving superior R&D for new applications. This approach is an important key

turning great research into great applications and products for biosensing.

References:

Turner, A., Wilson, G. and Kaube, I. (1987). Biosensors: Fundamentals and Applications. Oxford, UK, *Oxford University Press*, 770.

Sarker, S.R., Aoshima, Y. et al. (2013). Arginine-based cationic liposomes for efficient *in vitro* plasmid DNA delivery with low cytotoxicity. *Int. J. Nanomedicine*, 8, 1361-75.